NASA CONTRACTOR REPORT

N.A.S.A. CR-866


NASA CR-866

# RESEARCH AND DEVELOPMENT ON AN ELECTRON-SENSITIVE SOLID STATE MATRIX

*Prepared by*
WESTINGHOUSE DEFENSE AND SPACE CENTER
Baltimore, Md.
*for Goddard Space Flight Center*

NATIONAL AERONAUTICS AND SPACE ADMINISTRATION • WASHINGTON, D. C. • SEPTEMBER 1967

# RESEARCH AND DEVELOPMENT ON AN ELECTRON-SENSITIVE SOLID STATE MATRIX



Prepared under Contract No. NAS 5-3446 by
WESTINGHOUSE DEFENSE AND SPACE CENTER
Baltimore, Md.

for Goddard Space Flight Center

NATIONAL AERONAUTICS AND SPACE ADMINISTRATION

For sale by the Clearinghouse for Federal Scientific and Technical Information
Springfield, Virginia 22151 – CFSTI price $3.00

## ABSTRACT

In response to a Proposal Request issued by the National Aeronautics and Space Administration, the Aerospace Division of the Westinghouse Defense and Space Center initiated a study to show feasibility of an electron-sensitive solid state matrix. This matrix was to detect electrons with energies between 20 and 50 keV, and in addition, it was to determine the lateral position at which these electrons hit the matrix.

This device then is to be used in an electron tube to detect ultraviolet images of extremely low intensity. The conversion of the ultraviolet photons to low energy electrons is achieved by a sensitive photocathode and the suitable accelerating and focusing voltages. This arrangement is the most sensitive and fastest detector of ultraviolet (and possibly other) photons known. Its signal-to-noise ratio is large since the semiconductor element does detect a 20 keV electron unambiguously without any noise contribution to the system.

After completion, this system is to be used to detect faint astronomical images from a satellite platform. It will be trained onto regions of space with suspected faint ultraviolet sources for longer periods of time. Upon expiration of a sufficient time, the image will slowly, but definitely, emerge from its environmental noise, and its resolution will improve with the accumulation of counting statistics. New sources of ultraviolet (or other) energy will be discovered and a new dimension in depth will be added to the explorable space. This continuous underlying thought concerning the accomplishments of this system made the day-by-day tedious and painstaking investigation somewhat more bearable.

During the course of the investigation, a variety of composite surface barrier diodes were made and tested. The front surface of these diodes consisted of a p-type inversion layer on high resistivity n-type silicon. The insensitive side (the back) of these units had a grid-like arrangement of contacts

on them with up to 32 lines running in each of the two perpendicular directions. The horizontal and vertical sets of these lines were insulated from each other.

The units having 32 lines per 1/2 inch on their insensitive side were tested with a radioactive source and with an electron-beam setup built for this purpose. It was found that the area above some lines was extremely sensitive to 35 keV electrons and that some of these lines were completely noiseless.

An electronic tube was constructed with one of the surface barrier units in it. This tube has an S-11 (cesium-antimony) photocathode in it and the electrons emitted from this layer then are focused and accelerated toward the anode. As of the time of writing this report; that is, after over 1 month of operation, the tube is still working with an output level of about 30 percent of its original yield for a specified amount of incident ultraviolet and visible light intensity.

In actual use, the photocathode and the semiconductor element will not be enclosed together in a vacuum envelope, but they will be exposed to the vacuum of space. This will eliminate the contamination of the photocathode by the semiconductor element and vice versa. The decay of the photocathode described above will then be prevented since the vapors and ions will be free to leave the detecting area instead of mixing and migrating in a closed envelope. In this manner then, the feasibility of the detecting system will be increased and the working life of the arrangement will be extended for at least several years.

TABLE OF CONTENTS

## LIST OF ILLUSTRATIONS

# 1. INTRODUCTION AND APPROACH TO THE PROBLEM

In response to Request For Proposal No. PC39476, issued by the National Aeronautics and Space Administration, Goddard Space Flight Center, Greenbelt, Maryland, calling for research and development on an Electron-Sensitive Solid State Matrix, the Aerospace Division of the Westinghouse Defense and Space Center undertook an effort to show feasibility of such a mosaic.

It was understood at the outset of this experiment that the semiconductor mosaic will be part of a larger detecting system capable of seeing extremely faint ultraviolet images. The system was to consist of an ultraviolet photocathode and a semiconductor mosaic element enclosed in a vacuum envelope and provided with the suitable accelerating and focusing voltages. Upon ultraviolet light incident on the photocathode, electrons are emitted from this photocathode and are accelerated and focused upon the semiconductor matrix (figure 1-1). These electrons maintain a position correspondence between the photons incident onto the photocathode and the electrons incident onto the mosaic element. In this manner, for each electron emitted from the photocathode, a pulse will be obtained from the mosaic signifying the position of the impinging electron. An electron image then is obtained instead of the incident photon image. Since the photocathode is almost 100 percent efficient in the far ultraviolet, this system will give one electron for each five incident photons. Upon completion, this photon counter then will be the most sensitive ultraviolet light (or other light depending on the photocathode and cooling) sensor available.

At the outset of this effort, a brief study was initiated to determine the types of solid-state detectors suitable for detecting electrons between 20 and 50 keV. Also of interest were the specifications requiring maximum system efficiency, low interaction between elements, low noise level channels, and

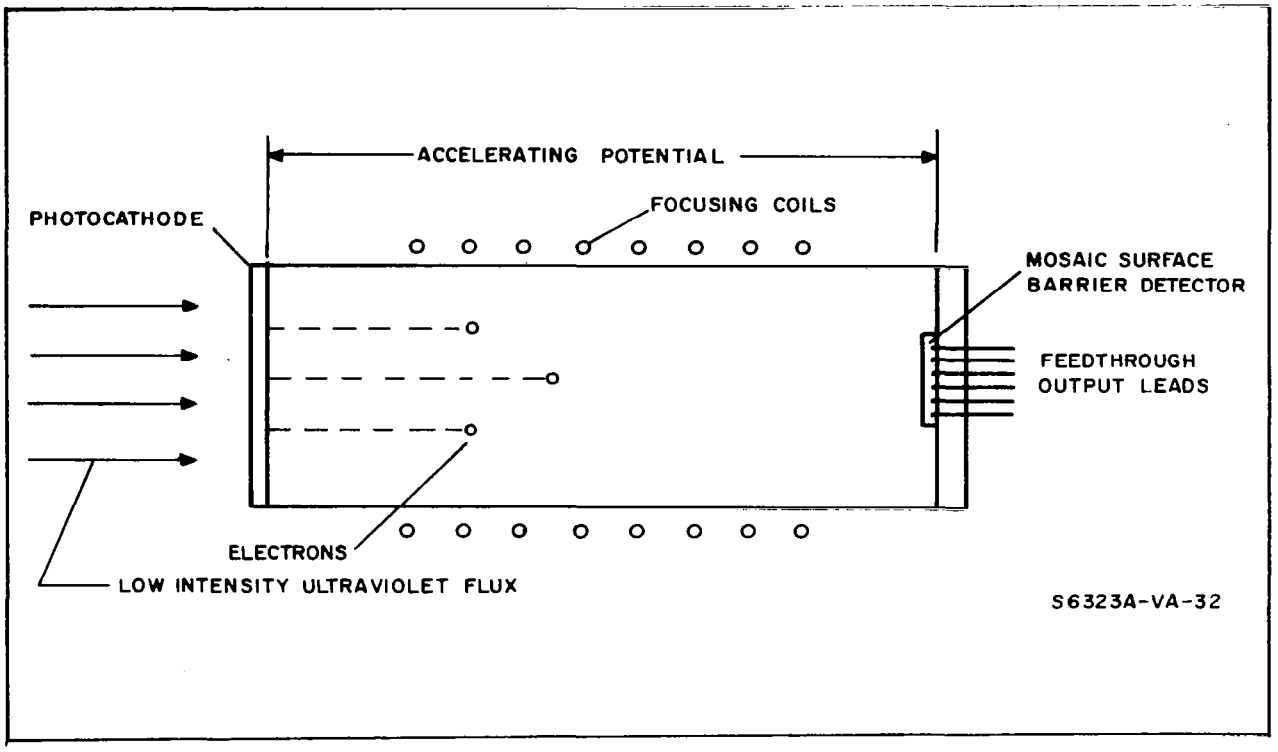


Figure 1-1. The Ultraviolet Detecting System

detector uniformity over large matrix areas. As a result of this survey, it was decided that surface barrier diodes are the most suitable type units to satisfy the above requirements. For this reason, they were chosen as the basic unit for this program.

The characteristics of diffused or lithium drifted detectors closely approximate those of the surface barrier units; however, the temperatures involved when diffusing or lithium drifting are somewhat higher than the temperatures encountered when making surface barrier diodes. This causes diffusion of the carrier gas molecules into the lattice, which together with the frozen disorder, characteristic or diffusion (or drift) temperatures, causes a reduction of lifetime, reduction of collection time, and a corresponding increase in the noise level.

In order to obtain a position sensitive mosaic, the front surface of this unit was designed to have a continuous electron-sensitive surface. At the

same time, the insensitive (the back) side of the detector had a multitude of contacts on it to facilitate position readout. These contacts on the insensitive side of the diode consisted of two sets of parallel lines, one set perpendicular to the other, with each line insulated from all other lines. Each individual line in this grid pattern formed a diode with the gold-coated front surface. This diode when backbiased produces an output signal when an electron hits the front surface above the line forming the respective diode. In this manner, outputs from two mutually perpendicular lines localized an impinging electron sufficiently and gave position information on the location of the electron impact. A schematic diagram of this diode design is shown in figure 1-2.

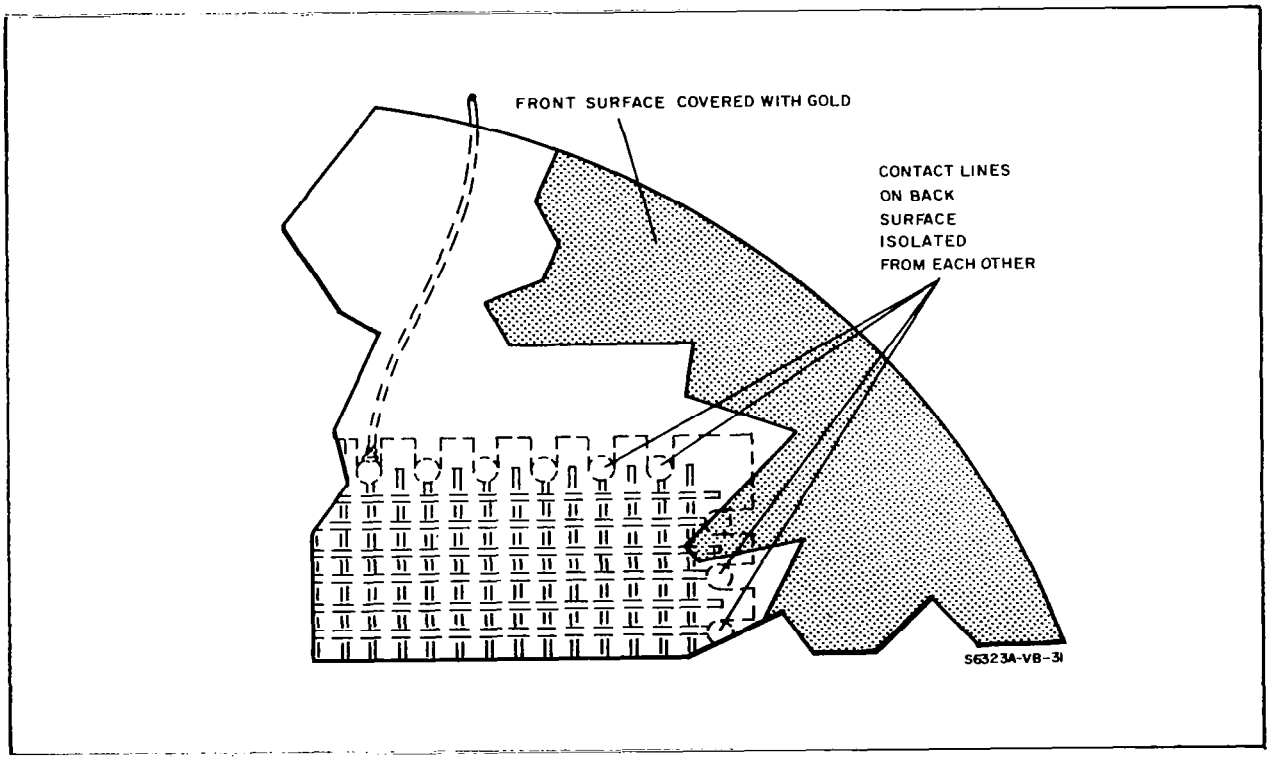


Figure 1-2. Schematic Diagram of the Position Sensitive Detector

Following the decision to use a surface barrier diode the establishment of fabrication procedures for the above design was attempted. The bulk of the effort then revolved about the improvement of this procedure to yield the satisfactory, noiseless, efficient diode able to operate under a reverse bias

of about 50 volts without an increase in noise level. It is needless to say that the fabrication procedure was closely coupled with cleaning procedures and that these procedures by themselves accounted for a large fraction of the time spent on fabrication. The fabrication procedures are described in detail herein following the mechanism and analysis section.

The fabricated unit required testing in order to ascertain its working condition. For this reason, certain amounts of test equipment for evaluating was acquired and a certain amount of it was built. The test equipment for evaluating the fabricated units consisted of an Ortec 101-201 preamplifier system together with an Atomic Instrument Company pulse height analyzer and a Berkeley counter. This apparatus performed satisfactorily, and pulse counting was reliably performed with this apparatus.

First, a radioactive source was used as the electron supply, but later, in order to test the units with various electron energies and intensities, an electron gun test setup was built. This unit consisted of a vacuum chamber, an electron gun, a variable power supply (up to 50 keV) to accelerate the electrons, and the sample holder with its multiple feedthroughs. Using this setup, electron beams with variable velocities and intensities could be made to impinge on the samples. This apparatus was useful when testing the diodes and it is described thoroughly in the section on test equipment.

The readout circuitry was later transistorized in order to demonstrate the inherent possible size reduction of the circuitry. The preamplifier, amplifier, and the counter were built up using separate solid state components; that is, unipolar and bipolar transistors, resistors, and capacitors. The input to the counter was obtained from self-triggering multivibrators. The output of the counter yields a number corresponding to the channel which originated the input pulse. This system was constructed in a 5- x 5- x 6-inch enclosure, exclusive of the power supply, and showed satisfactory performance.

A controlled humidity and temperature room and enclosures within this room also were set up to condition the front surface of the diodes at various

combinations of humidity and temperature. After completion of the surface barrier unit, an electron tube containing both the semiconductor element and an ultraviolet photocathode was constructed. This tube has an S-11 (cesium antimony) photocathode in it, and the electrons emitted from this layer then are accelerated and focused onto the anode. The tube was constructed approximately one month ago, and it is still working with an output level of about 30 percent of its output measured immediately after construction.

The last section will deal with the results and conclusions obtained during the contractual period. It describes the operation of the multiple contact units, the operation of the tube constructed with a unit in it, and the transistorized readout circuitry. In closing, some recommendations will be made as to the improvement of the units, construction of the tube, and molecularizing the readout.

Finally, a comparison of the hybrid tube approach (the semiconductor element and photocathode in a vacuum envelope) with the electronographic method (film used in conjunction with a photocathode) is given. This paragraph outlines the advantages and disadvantages of both systems and shows that the advantages of the hybrid tube definitely outweigh those of the electronographic method.

# 2. MECHANISM OF OPERATION AND ANALYSIS OF THE SURFACE BARRIER DIODE

## 2.1 GENERAL

The principle of operation of a surface barrier diode is well understood to investigators involved in this field, and it is briefly described below.

Consider a slice of high resistivity n-type silicon with a thin p-type layer at its surface (figure 2-1). When an incoming charged particle having sufficient energy impinges on the surface barrier detector it will go through the thin front p-type layer of the diode and decay in the depleted n-type material. Upon imbeding itself into the material, the particle will lose its energy by repeated collisions with the lattice and with electrons. During this process, it will create a cloud of electron hole pairs along its trajectory. These electrons and holes then are drifted out of the depletion zone with the help of an applied field and will enter the contact electrodes. When these charges traverse an appropriate electrical impedance outside of the diode material, they give rise to a detectable pulse. Essentially then, the incoming particle gives rise to a burst of generation current in the depletion region of a diode which at other times has a rather low reverse leakage current.

It is of interest in connection with surface barrier diodes to evaluate the width of the depletion layer, the electric field and potential in the layer, and the speed (collecting time) of the diode. Attention will be paid to each one of these quantities and their size, and other characteristics of interest will be evaluated analytically.

## 2.2 PROPERTIES OF BARRIER LAYERS

Before attempting to evaluate the above quantities a brief review of some of the more elementary properties of barrier layers will be given.

An understanding of the properties of such a junction is most readily achieved by thinking of two separate pieces of semiconductor being brought

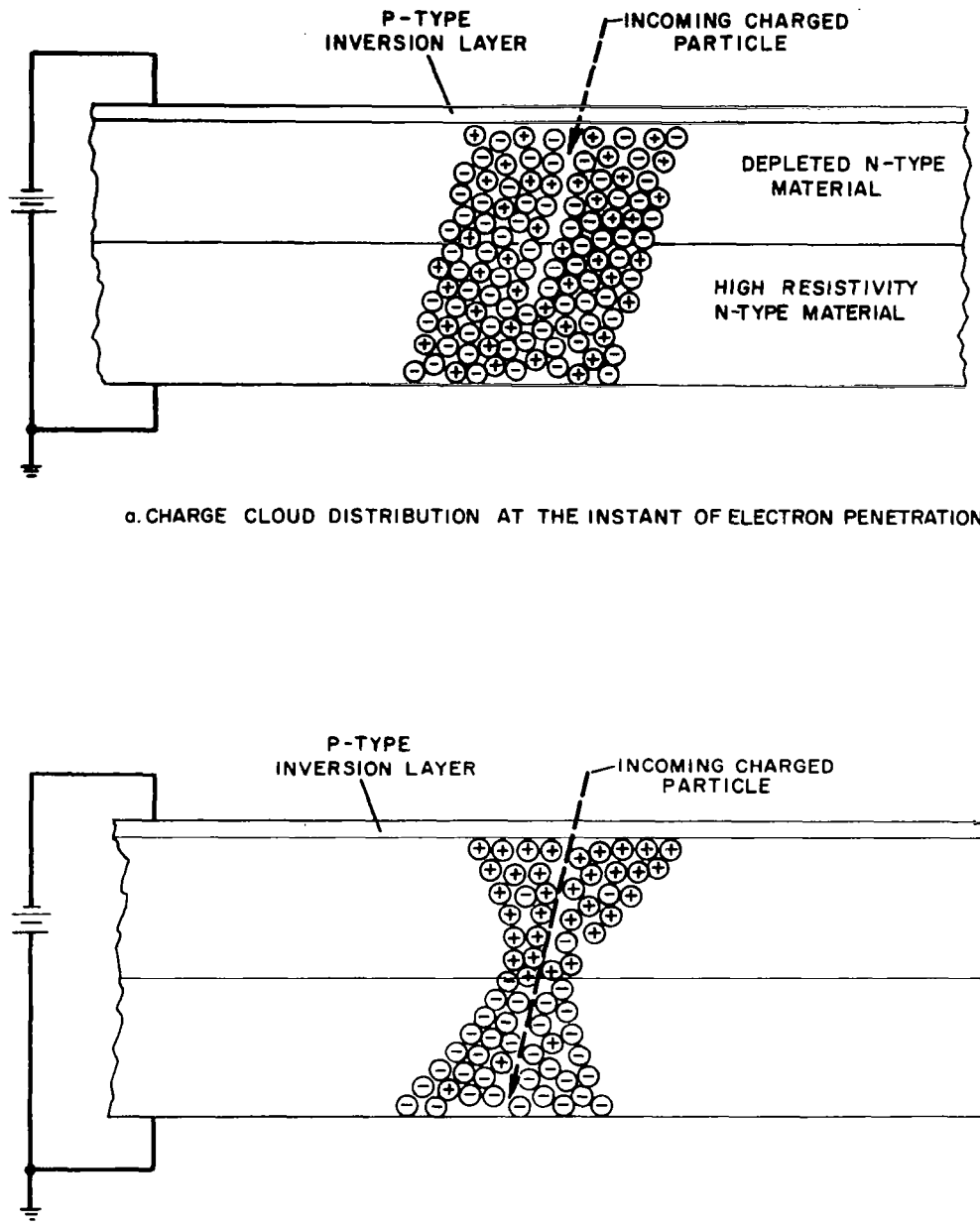


Figure 2-1. A Simplified Structure of a Surface Barrier Detector and the Impinging Charged Particle

together and joined. The two conduction bands are now in electrical contact, one containing electrons and the other nearly empty (figure 2-2a). Under the influence of diffusion, electrons flow from the n-type material to the p-material, as indicated in figure 2-2b. The p-type crystal therefore acquires a negative charge and the n-type material is positively charged. (It now contains a number of ionized donors whose charges are not balanced by an equal number of free electrons.) In the valence band, an exactly similar process occurs with some of the holes moving from the p-material into the n-material. These holes leave behind a negative charge due to ionized acceptors. There is, therefore, upon joining these materials, a transient flow of carriers from one type of material into the other. This flow establishes a positive charge on the n-side and an equal negative charge on the p-side of the material, as indicated in figure 2-2c. Such a potential difference (Q) does exist across all pn junctions in equilibrium, the magnitude being such that the net flow of carriers across the junction due to diffusion pressure is brought almost to zero by the opposing potential gradient.

As seen in figure 2-2c, after Fermi levels are matched and the charges are adjusted, only electrons with energies larger than the bandgap energy in electronvolts are able to make the transfer from the n- to the p-side. Similarly, for holes moving across the barrier from the p- to the n-side, the energy for a successful transfer has to be larger than the bandgap measured in electronvolts. At the junction of the two types of materials, the Fermi potentials adjust to the same level (a fundamental rule of all solids) with the corresponding adjustment of the electron population.

The physical origin of the barrier in itself is necessarily a consequence of the structure of the material. At equilibrium, the p-side, since it acquired some additional negative charge, is somewhat negative with respect to the n-side. For this reason, the free majority carriers of both types near the junction are somewhat repelled, and they (on both sides of the junction) withdraw away from the junction leaving a net charge due to the donors and acceptors respectively (figure 2-3). The volume of material

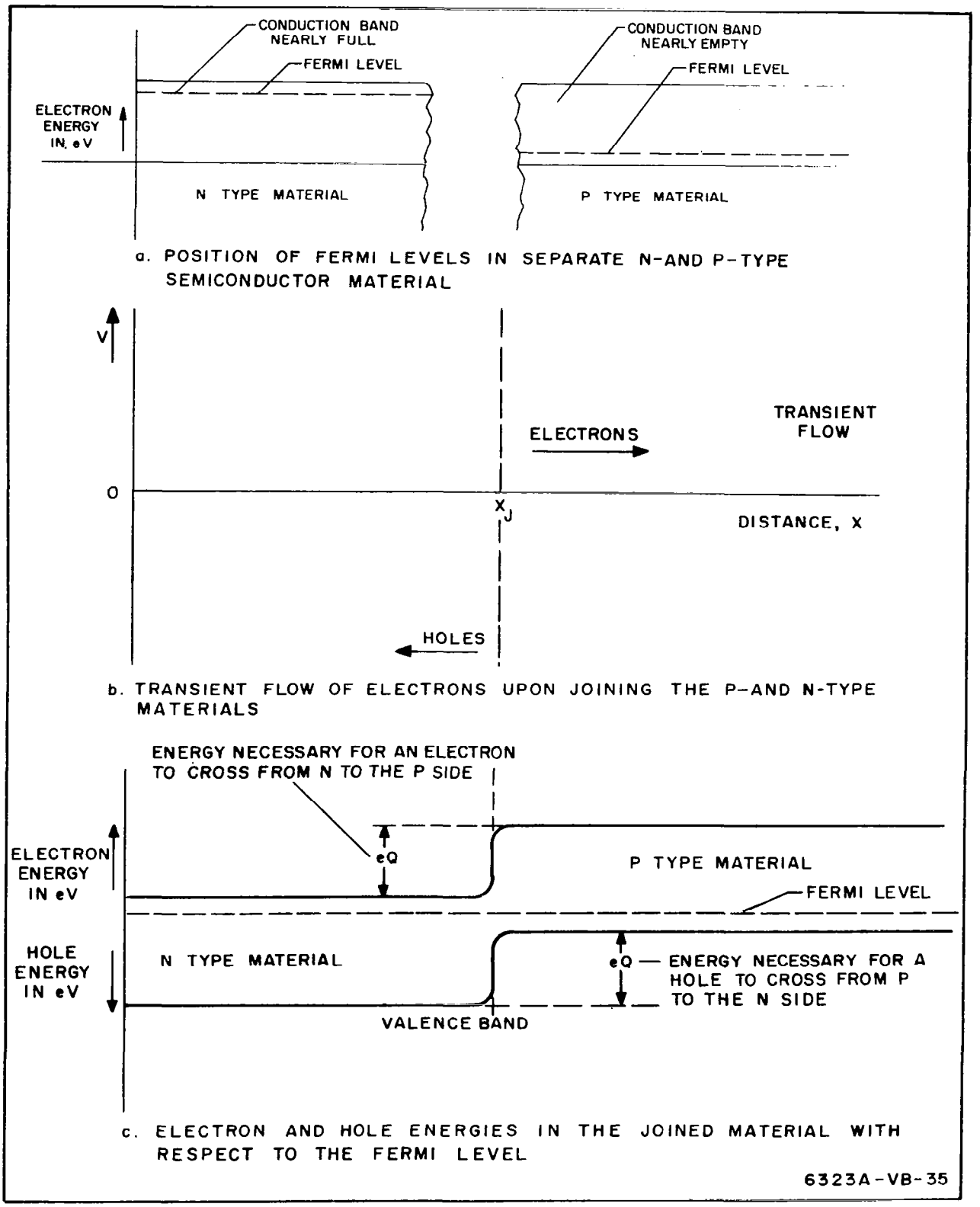


Figure 2-2. Illustration of Electron and Hole Energies With Respect to the Fermi Level

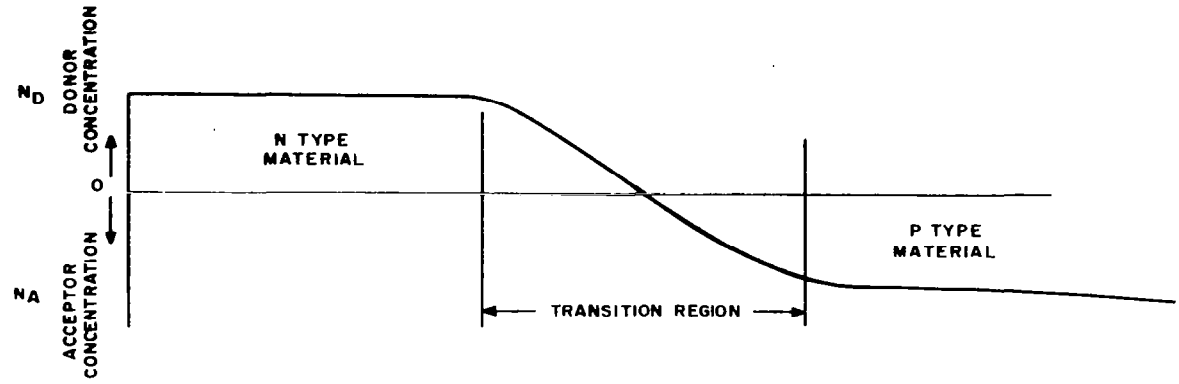


a. CONCENTRATION OF DONORS AND ACCEPTORS IN THE VICINITY OF THE JUNCTION

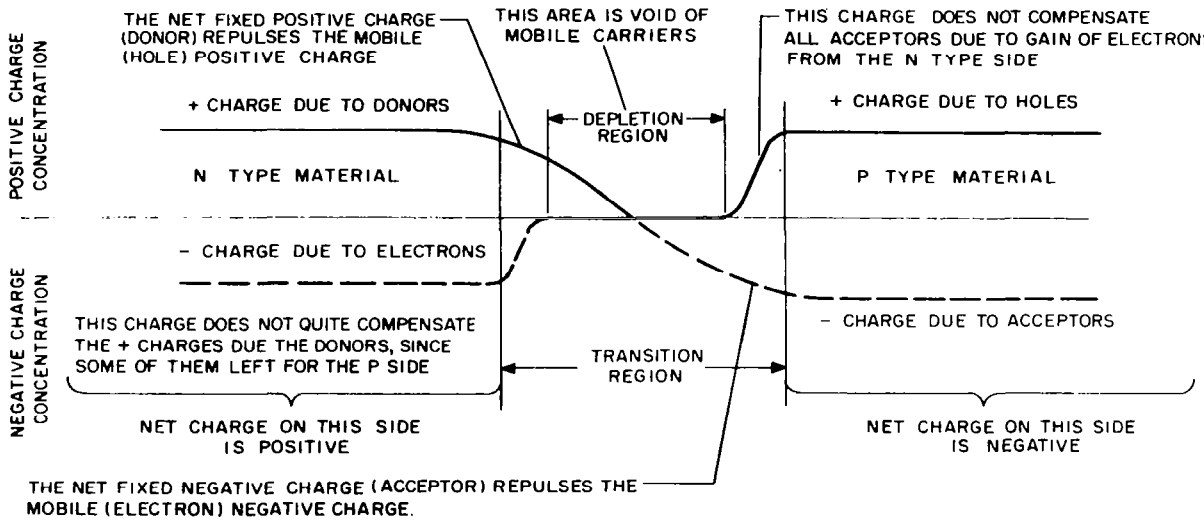


b. CONCENTRATION OF DONORS, ACCEPTORS, ELECTRONS AND HOLES IN THE VICINITY OF THE JUNCTION

6323A-VB-33

Figure 2-3. Illustration of Charge Concentrations in the Vicinity of the Junction

containing only donors and acceptors is termed the depletion region. An electron then, for example, upon crossing the junction to the p-type material experiences no force until it gets into the depletion region. In the depletion zone, however, the donors attract it towards the n-type material and the acceptors repel it toward the n-side. This force on the electron due to the built-in charges is the physical origin of the barrier.

At usual operating temperatures, there exists residual diffusion current. That is, some majority carriers acquire enough energy to overcome the repulsion of the barrier and to cross it. In order to maintain equilibrium, this forward current has to be balanced by a reverse current of equal magnitude. This reverse current is due to the minority carriers near the junction, which are swept across by the attracting field for the minority carriers to cross the junction, and due to carrier generation in the depletion zone. These generated carriers then also are swept out by the favorable field for the minority carriers.

When considering diodes and transistors made out of relatively low-resistivity material, the major contribution to the reverse current is due to the minority carriers near the junction, since the depletion layer is narrow. These carriers, unlike the majority carriers, are not retarded by the barrier at the junction but accelerated across it by the built-in potential and cause a reverse leakage current denoted by $I_s$. This current will be described subsequently. The reverse current due to generation is predominant only in low-resistivity, wide-depletion-layer devices such as nuclear particle detectors. The magnitude of this current per unit area is given by

$$I_g = 2gXq$$

where

$g$ = the generation rate of the carriers

$X$ = the width of the depletion region

$q$ = the electron charge

The current balance in equilibrium is then given by

$$I_f = I_s + I_g$$

## 2.3 THE BARRIER WITH AN UNBALANCED CURRENT THROUGH IT UNDER APPLIED POTENTIAL

In the paragraph above, it is shown how a depletion layer void of mobile charges is formed by the built-in potential. When this potential is increased externally, that is when a diode is backbiased, most of this increase appears across the depletion layer. Since the concentration of the space charge in this volume is limited by the donor and acceptor concentration, the necessary increase of space charge to absorb the potential gradient can be obtained only by widening the depletion region. The relation between the field gradient and space charge is given by Poisson's equation

$$\frac{d^2V}{dX^2} = - \frac{4\pi\sigma}{K}$$

where

$\sigma$ = charge density (donor or acceptor concentration)

K = dielectric constant (12 for Si)

Upon increasing the reverse bias, the depletion layer will widen due to the retreat of the majority carriers from the junction. This widening is not necessarily symmetrical on both sides of the junction but depends on the concentration of the impurities on the two sides. A brief derivation will show the width of the depletion layer, its variation with voltage, and the capacitance associated with it.

Consider the somewhat idealized picture of impurity concentration (figure 2-4), since charges are equal on both sides

$$qN_D x_n = q g N_A x_p$$

It follows then that

$$x_n = x_p \frac{N_A}{N_p}$$

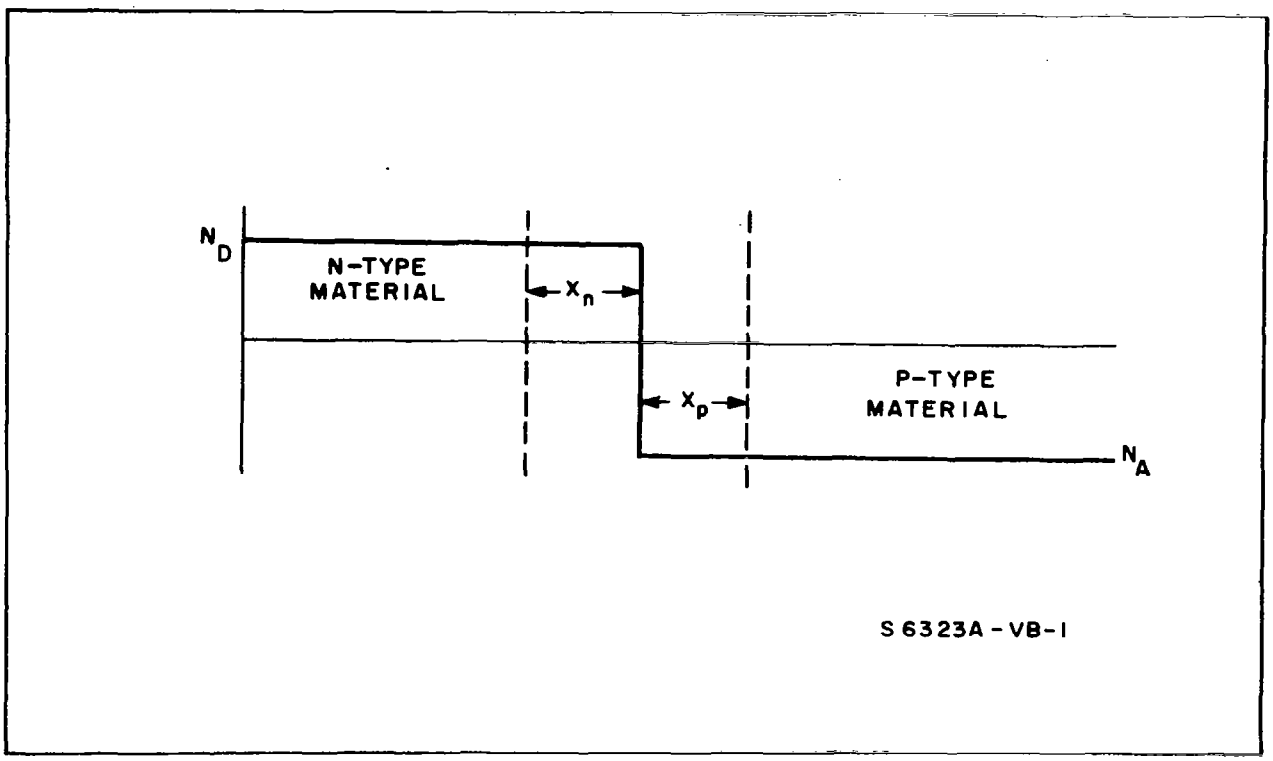


Figure 2-4. Idealized Impurity Concentration in a pn Junction

and

$$x_p + x_n = X = x_p \left(\frac{x_p}{x_n} + 1\right) = x_p \left(\frac{N_A + N_D}{N_D}\right)$$

similarly

$$x_n + n_p = X = x_n \left(\frac{N_A + N_D}{N_A}\right)$$

adding the two expressions and multiplying by 1/2 the following expression is obtained:

$$x_n + x_p = X = 1/2 \left(\frac{N_A + N_D}{N_A \cdot N_D}\right) (x_n N_D + x_p N_A)$$

The capacitance of a capacitor is $C = \frac{\epsilon}{4 \pi D}$, and it is reasonable to approximate the actual charge distribution by an effective charge distribution

with the total charge concentrated at $1/2\ x_n$ and $1/2\ x_p$ respectively. D, the distance between the two charge sheets, is then $\frac{X}{2}$ and $C = \frac{\epsilon}{2\pi X}$.

Applying $Q = CV$ where Q is the effective surface charge concentration of the capacitor and V the applied potential

$$Q = \frac{eV}{2\pi X}$$

From above

$$Q = g N_D x_p = g N_A x_p = 1/2\ g\ (x_n N_D + x_p N_A)$$

Substituting into the expression for X, it becomes

$$X = \frac{N_A + N_D}{N_A \cdot N_D} \frac{Q}{g} = \frac{eV}{2\pi X g} \frac{N_A + N_D}{N_A \cdot N_D}$$

and simplifying

$$X = \left( \frac{eV}{2\pi g} \frac{N_A + N_D}{N_A \cdot N_D} \right)^{1/2}$$

In case $N_D >> N_A$ (as in the surface barrier diode)

$$X = \left( \frac{eV}{2\pi g N_A} \right)^{1/2}$$

and the barrier is for all practical purposes in the p-region.

This expression then gives the depletion layer width as a function of the bias voltage.

$$X = \left( \frac{eV}{2\pi g N} \right)^{1/2}$$

which reduces to $4.2 \times 10^{-7}\ (e\ V\ \rho\ \mu)^{1/2}$ if use is made of the equation

$$g N \mu = \sigma = \frac{1}{\rho}$$

If $\rho$ is in ohms-cm and $\mu$ is $cm^2/V$ sec, this will give the width of the depletion layer in cm.

The other important parameter, the electric field F, can be obtained using Poisson's equation

$$\frac{d^2\phi}{dx^2} = - \frac{4\pi g N}{\epsilon} \quad (esu)$$

since F is equal to

$$\frac{d\phi}{dx} = - \frac{4\pi g N X}{\epsilon} + C$$

Using the boundary condition

$$F = 0 \text{ at } x = x_p$$

$$F = \frac{4\pi g N}{\epsilon} (x_p - x)$$

Approximating $x_p = X$ (the whole barrier width)

$$F = \frac{4\pi g N}{\epsilon} (X - x)$$

$$F_{max} = \left(\frac{8\pi g N V}{\epsilon}\right)^{1/2}$$

Substitution of

$$\left(\frac{eV}{2\pi g N}\right)^{1/2} \quad \text{for X}$$

$$F_{max} = \left(\frac{8\pi g N V}{\epsilon}\right)^{1/2}$$

This expression at higher bias volts can reach the order of $10^4$ V/cm.

The potential (V) is given by the following expression:

$$V = \phi = d\phi = \frac{4\pi g N}{\epsilon} (X - x)\, dx$$

and

$$\phi_0^x = \frac{4\pi g N}{\epsilon} \left[X x - \frac{x}{2}^2\right]_0^x = \frac{4\pi g N}{\epsilon} \frac{x}{2}^2$$

The potential in the depletion layer is of quadratic form (figure 2-5).

The field depletion depth and capacitance are of importance when designing surface barrier units, and for this reason, a nomograph relating these quantities was prepared so that the above considerations do not have to be repeated for each unit fabricated. This nomograph is reproduced in figure 2-6.

One of the most important parameters of the barrier diodes besides the above-mentioned ones is their collecting time; that is, the time a charge cloud

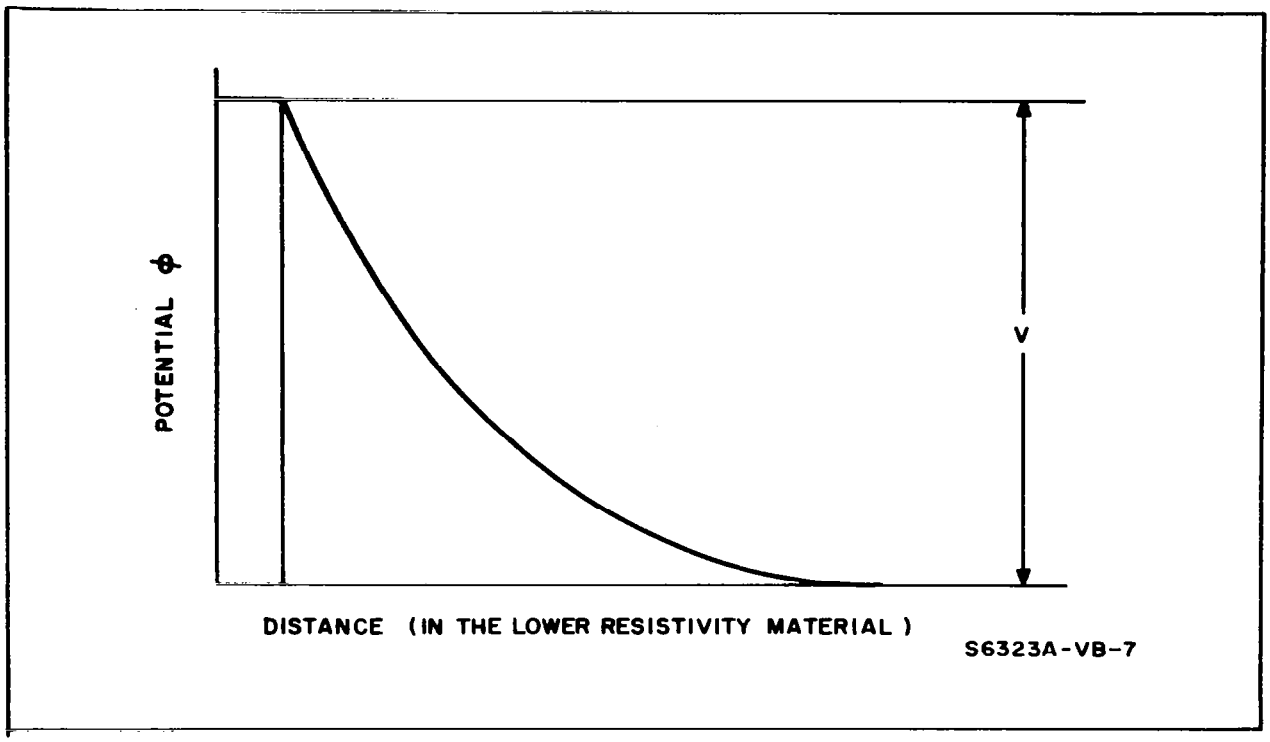


Figure 2-5. Potential vs Distance in the Depletion Region

due to a single incident particle can be drifted out of the depletion zone and the depletion zone can be made ready to accept the next particle. To stay on the conservative side, it will be assumed that the material is made up of holes (their mobility is lower than the electron mobility) and that they have to traverse the full width of the depletion zone.

The hole drift velocity is given by

$$V_d = \frac{dx}{dt} = \mu F$$

then

$$dt = \frac{dx}{\mu F} = \frac{dx}{\mu a} (X - x)$$

where

$$a = \frac{4 \pi g N}{\epsilon}$$

$$t = \frac{1}{\mu a} = \int \frac{dx}{X - x} = \frac{1}{\mu a} - \ln \left[ X - x \right]_{x=0}^{X}$$

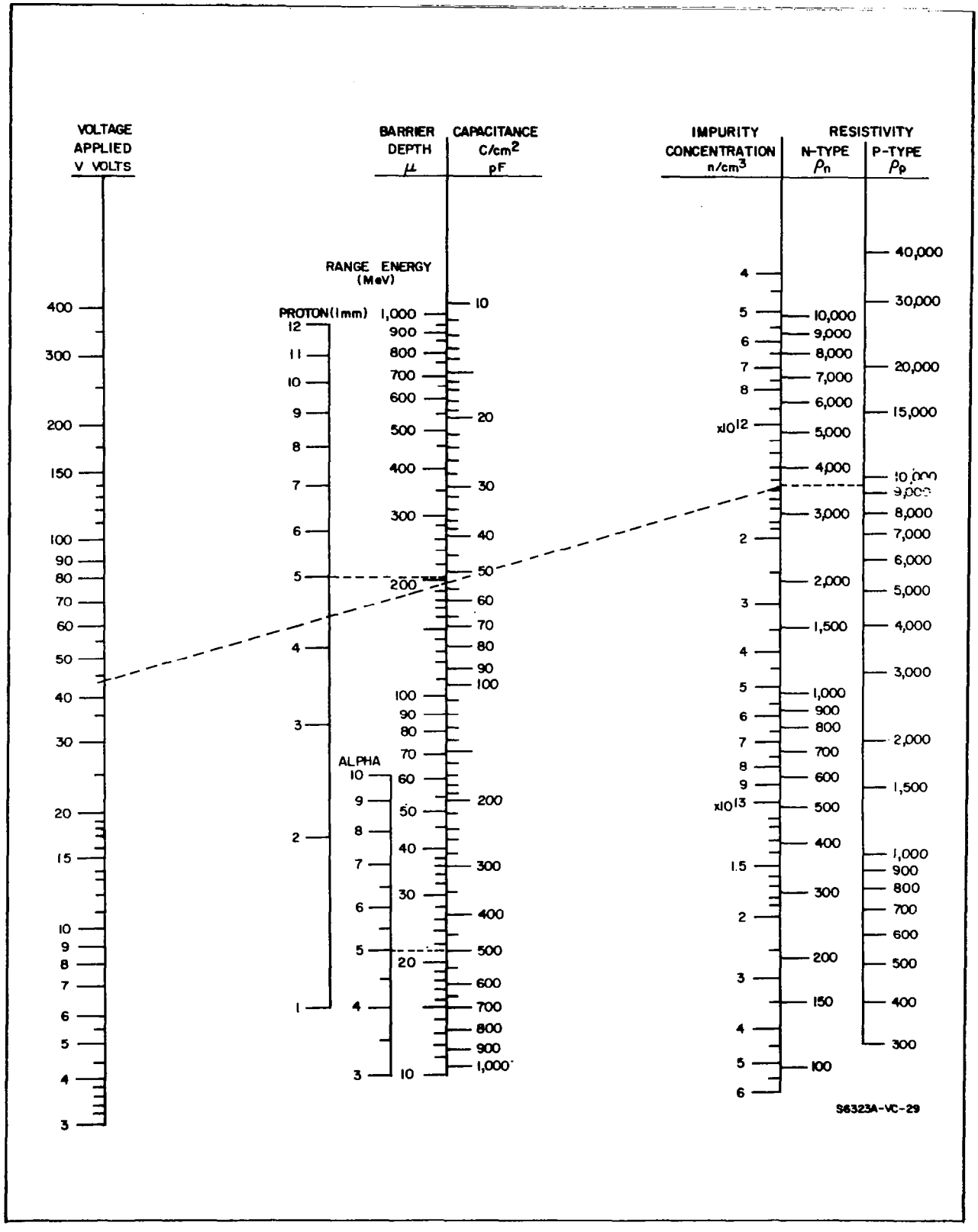


Figure 2-6: Nomograph for Silicon Barrier Diodes

The value of the integral evaluated between these limits is infinite since the field is zero at $x_p$. For this reason, the integration is carried out over 99 percent of the zone assuming that the width of the region is somewhat graded (an approximation fitting conditions to a fair degree). On this basis then, K = kX

$$t_c = \frac{1}{\mu a}\left[\ln x - \ln (1-k)\, x\right] = \frac{1}{\mu a} \ln \frac{\dot{1}}{1-R}$$

if k = 0.99

$$t_c = 4.6/\mu a = 4.6\, \epsilon/4\pi g N \mu = 4.6\, \epsilon \rho/4\pi$$

Converting from electrostatic to practical units

$$t_c \sim \frac{e\rho}{8\pi}\ 10^{-11}\ \text{sec}$$

For a p-type silicon ($\epsilon = 12$) detector of about 1000 ohm-cm resistivity to $t_c = 5 \times 10^{-9}$ sec. Actually, owing to the conservative nature of the starting assumptions, this collecting time is reduced by a factor of 3 in actual practice, and collecting times in the low nanosecond region can be obtained using these units.

Above, the variation of depletion width, capacitance, electric field, and potential were described due to an applied potential. As to the flow of currents through the barrier, these also will be necessarily disturbed and shifted from their state equilibrium due to the bias voltage. The minority drift current $I_s$ is uneffected by change of bias since it mainly depends on the concentration of the carriers in the vicinity of the depletion zone. The generation current $I_g$ will also stay constant to a first approximation. However, the flow of the majority carriers across the barrier is effected significantly by the applied potential, since the applied potential will directly add (or subtract) from the barrier height. The total reverse current now becomes

$$I_r = I_s + I_g - I_f$$

with the bias dependent majority carrier flow $I_f$ briefly evaluated below.

The number of charge carriers having an energy in excess of $E_b$ can be obtained from the statistical distribution of these particles. The carriers in the semiconductor obey the Fermi Direct Distribution

$$f = \frac{1}{1 + e^{\frac{E - E_F}{KT}}}$$

If E is larger than $E_F$ by several times (T), then the value of the exponential is large (E is inherently negative) compared to unity, and the unity in the denominator can be neglected in comparison with the exponential. For non-degenerate material, this indeed is the case and the governing statistics becomes the Maxwell Boltzmann distribution

$$f = e^{\frac{E_F - F}{KT}}$$

By integrating this expression between proper limits, it can be shown that the number of carriers having energies larger than $E_b$ is proportional to

$$e^{-\frac{E_b}{KT}}$$

In case the pn junction is biased an additional potential, the built-in potential alters the height of the potential barrier between the n- and p-regions and gives rise to a current flow. This flow according to the above will be

$$I_f' = I_f e^{-\frac{Vg}{KT}}$$

where

$$V = E_b - Q$$

is the applied potential and is equal to the difference between the total and built-in potentials.

Assuming $I_s = I_f$ (neglecting $I_g$ in the equilibrium case) the total reverse current becomes

$$I = I_s \left(e^{-\frac{Vg}{KT}} - 1\right) - I_G'$$

This expression is also valid for forward current with V becoming negative. This curve is indeed well obeyed in practice, and the equation describing it is a basic design expression. Graphical representation of the above equation is shown in figure 2-7.

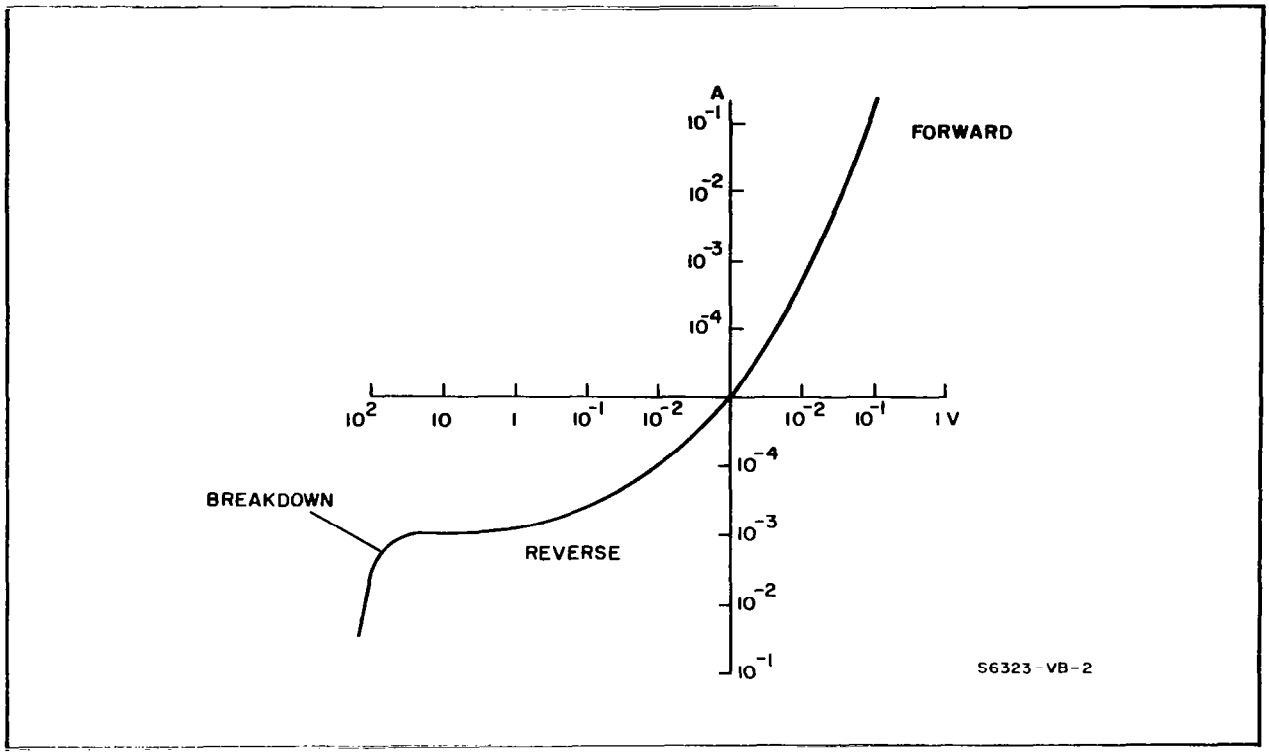


Figure 2-7. A Typical Characteristic of a Junction Diode (The Diode Equation is not Obeyed at or Past the Breakdown Region)

## 2.4 THE EFFECT OF RADIATION ON DETECTOR PERFORMANCE

There is extensive literature available on radiation effects of silicon and germanium.[1,2] In general, radiation of any kind induces lattice defects causing a reduction in carrier lifetime and an increase in resistivity. Prolonged radiation will occasionally convert the material to opposite type by creating specific levels in the material.

In case of moderate flux, the detector will show acceptable stability for a long time, since there is usually a substantial margin between the available and the necessary collecting time. Upon exposure to a substantial dose, the

reduction in lifetime will manifest itself first by a reverse current increase, then by an increase in the noise level, and finally by a loss of resolution due to incomplete collection.

Deterioration of particle resolution generally becomes evident after $5 \times 10^{11}$ neutrons/cm$^2$. After $10^{13}$ neutrons/cm$^2$, the pulse is reduced in height, it is broadened, and multiple peaks appear.[3] X-rays usually cause an effect at about $10^{14}$/cm$^2$.

Usually the initial loss of resolution and decrease in pulse height can be remedied by increasing the bias of the detector, since this enhances collection and thus somewhat balances the effect of radiation damage. In case the radiation dose exceeds substantially the above-mentioned limits, loss of the favorable diode characteristics will inevitably follow.

# 3. FABRICATION PROCEDURE

## 3.1 GENERAL

Fabrication procedures, cleaning procedures, and improvement of these techniques were the most time, consuming parts of the contractual effort. As the project proceeded, it became apparent that extreme care and extreme cleanliness are required to make these units successfully. This necessitated special apparatus such as an evaporator, sink, etc, used only in connection with this project. Although the cleaning procedure was developed through many trials and errors, only the final process will be described in this report. All operations connected with the fabrication were performed in a clean room atmosphere.

## 3.2 LAPPING AND POLISHING

The material used for fabrication was 2000-ohm-cm n-type uncompensated silicon and it was obtained from Dow Corning Corporation, Midland, Michigan. The slices obtained were approximately 0.022 inch thick and about 1 inch in diameter. Radial resistivity and resistivity along the ingot with exception of the extreme ends were within 20 percent of nominal value. These slices then were lapped on both sides in a circular lapping machine (made by Dallons Labs, Los Angeles, California) down to about 18 mils. A 12-micrometer grit compound of alumina obtained from Micro Abrasives Corporation in Westfield, Mass., was used for this purpose. The wafers to be lapped were then put into holders placed previously in the lapping machine (figure 3-1). Pella Oil (obtained from Shell) served as the lubricating vehicle. In this circular lapper, 0.002 inch was taken off each side of the wafer. When the slice thickness got down to about 0.018 inch, the wafers were unloaded and thoroughly cleaned. The cleaning consisted of first dipping the slices into a mixture of 1/2 methanol and 1/2 acetone, then swabbing the wafers while they were attached to a vacuum platform, and finally rinsing the discs using

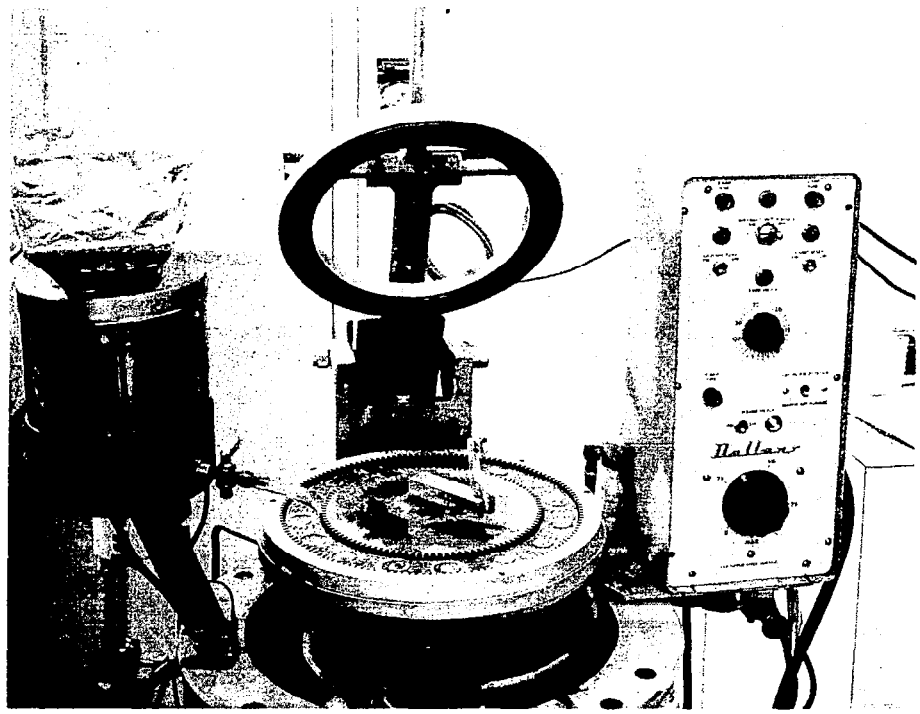

Figure 3-1. Circular Lapping Machine With Wafers in the Holders

a trichloroethylene spray. Usually, after this treatment there was no 12-micrometer grit left on the wafers.

Next, 8 slices were cemented onto a 5-inch diameter, 1-1/2-inch thick steel block using parafin (figure 3-2) and set onto a Lapmaster (figure 3-3). The Lapmaster (made by Crane Packing Co., Chicago) lapped an additional 0.001 inch of the wafers using a 3-micrometer compound. The wafers then were washed using Joy detergent, followed by a thorough scrubbing with cotton balls and running water. They were then put onto so-called ball polishers, figure 3-4 (made by Robinson Houghin Inc., Columbus, Ohio). This machine mirror polished the front side of the wafers in about 2 hours using pitch impregnated Morris pads from J.R. Morris Co., Southbridge, Mass. and 1-micrometer alumina compound (2 teaspoons/liter). The slices now had only a very few faults and scratches.

The steel block was then heated up in an oven and the wafers were taken off. They were turned around and cemented down, with apiezon wax, since the parafin will not hold down the polished slices. Starting with the Lapmaster,

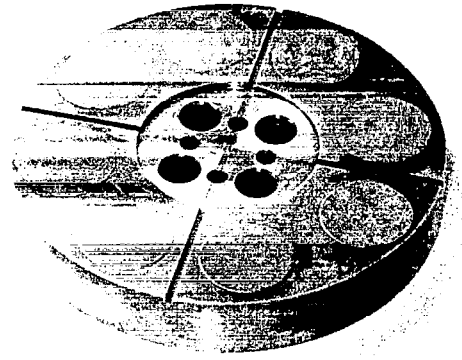

Figure 3-2. Steel Block Ready for Lapping

all procedures were repeated until a mirror finished surface was obtained on the other side of the wafer. All slices were then taken off the block and cleaned in trichloroethylene followed by trichloroethylene vapor degrease lasting 1/2 hour in a Sachslit Extractor (figure 3-5). The slices were rinsed in acetone, rinsed five times in deionized water, boiled for 10 minutes in sulfuric acid in individual pyrex beakers, and rinsed six times with distilled water.

At this point, the wafers were mirror polished on both sides, they were cleaned, and ready for the next step - the contact evaporation. The wafers however, were not flat, neither were the two sides parallel. The flatness profile varied up to 0.002 inch and the sides were out of parallel to within 0.001 inch (figure 3-6). However, these geometrical limitations of the slice did not affect the device design and the wafers made satisfactory devices.

## 3.3 PREPARATION OF THE GRID STRUCTURE ON THE INSENSITIVE SIDE OF THE DIODE

The grid structure serving as the contact on the insensitive side of the device was evaporated onto the back surface of the silicon through a series

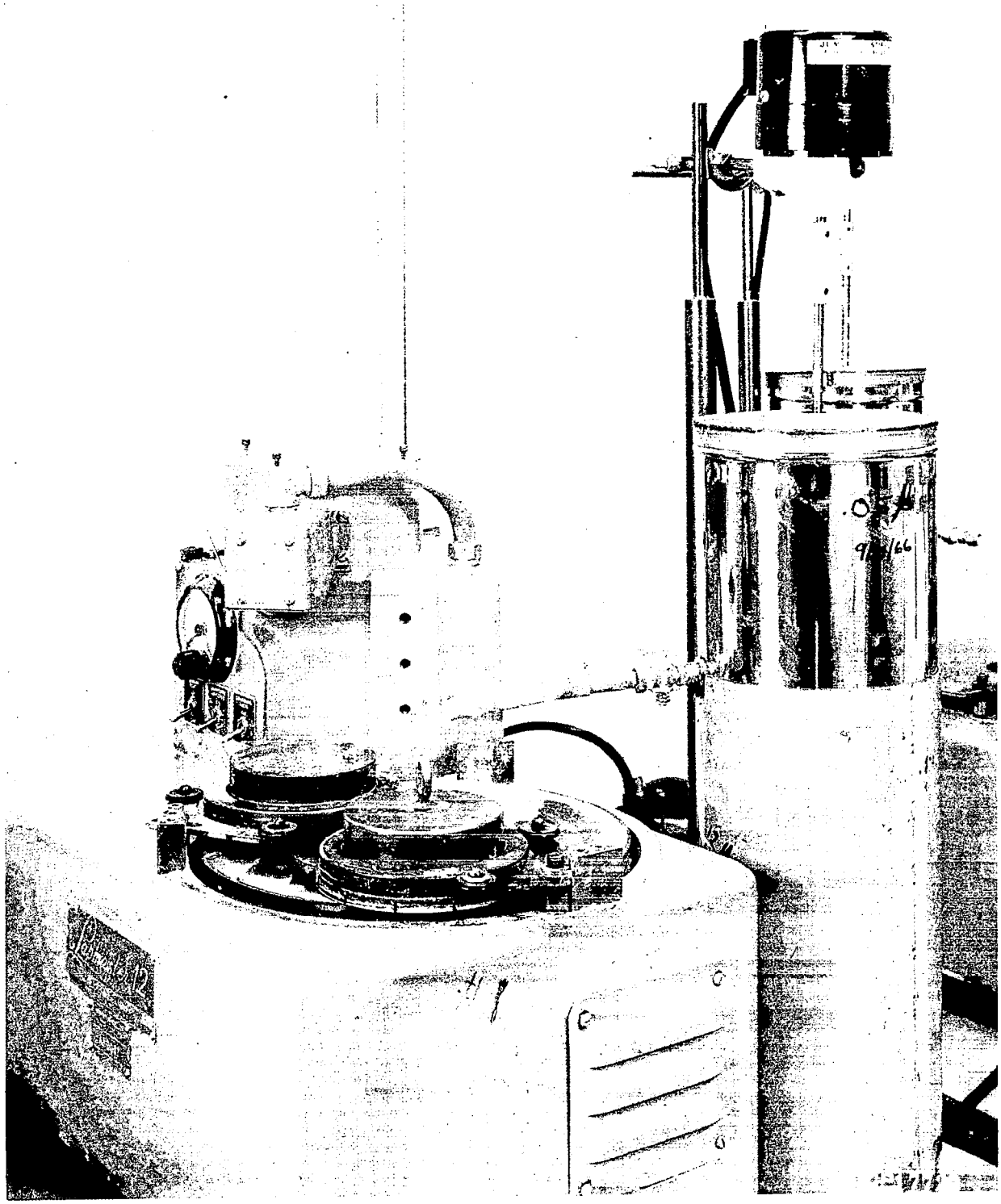

Figure 3-3. Steel Block on the Lapping Machine

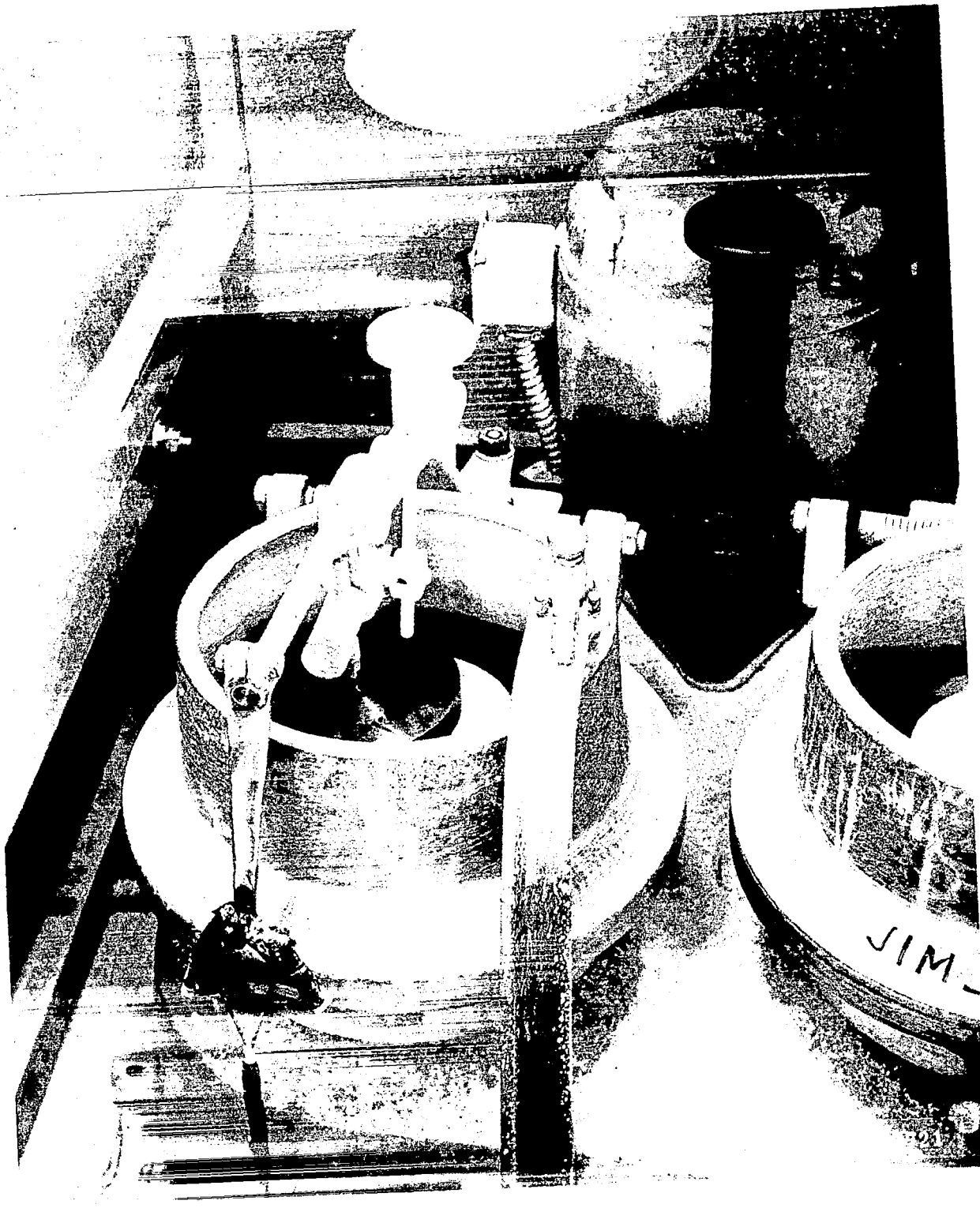


Figure 3-4. Steel Block Polished With the Ball Polishers

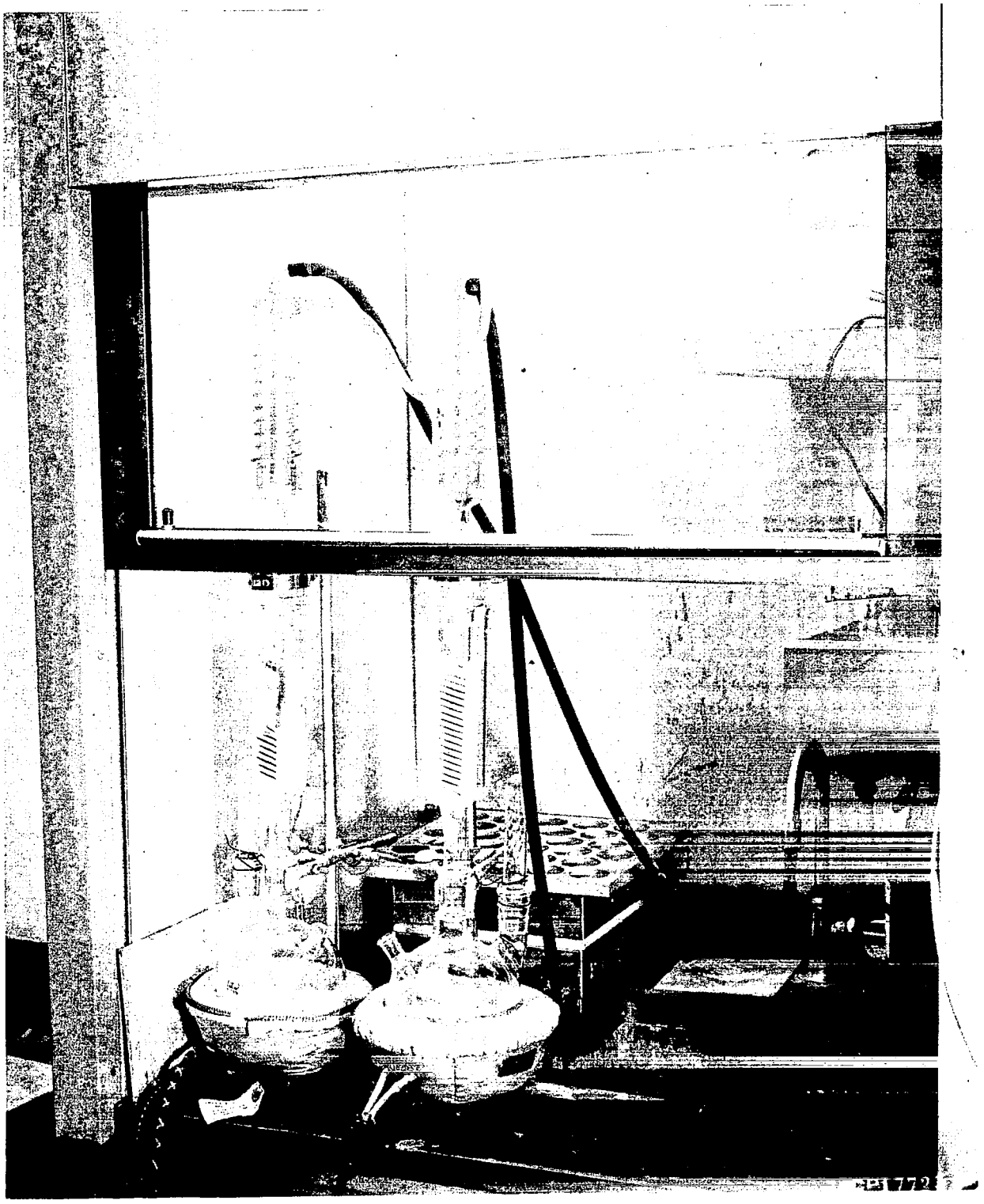

Figure 3-5. Wafers in the Sachslit Extractor

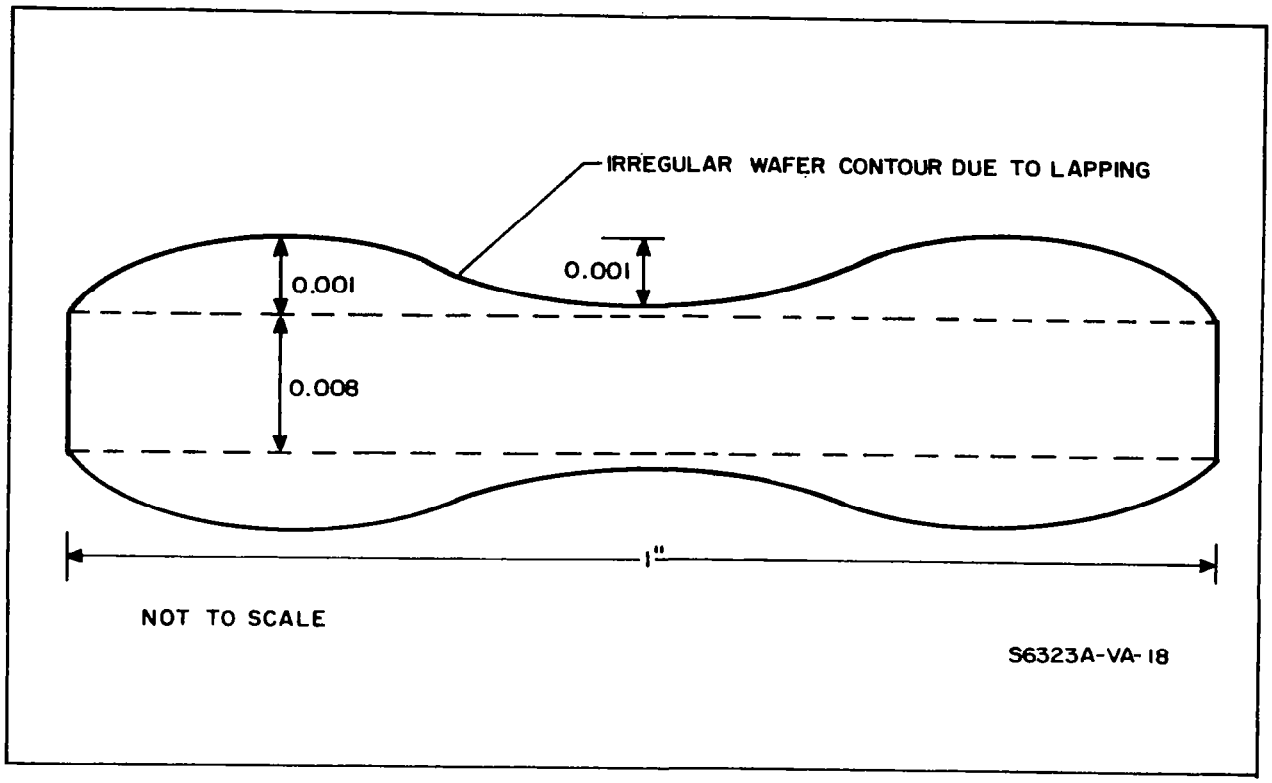


Figure 3-6. Wafer Shape After Polish

of metal masks. These masks were optically aligned and attached to the slice held in a holder. Once the optical alignment was completed, the assembly was fastened rigidly together. It was then put into the evaporator where it could be heated, ion bombarded, and subjected to vapor deposition. Upon completion of a particular evaporation, the assembly was taken out of the evaporator, the metal mask was changed to another one, and the second mask was optically aligned with the pattern left by the previous one. The assembly then was again fastened together under the microscope and the previous process steps were repeated.

## 3.4 PREPARATION OF THE METAL MASKS AND HOLDERS

The metal masks were made from oxygen free high conductivity copper foil. The 0.002-inch thick foil was first cut into 2- by 2-inch pieces and the required pattern was put on it using Kodak Metal Etch Resist (KMER) using the standard photolithographic procedure. This procedure consisted of

coating the metal foil with KMER and spinning the material at about 3000 rpm in order for the coating to flow outward from the center. In this manner, a thin and uniform coating was obtained. Next, the coating was baked for about 1 hour at 90°C in order to harden it. The foil was then put under a microscope and a glass plate with the required pattern on it was put onto the foil. The coating on the foil was then exposed using a Sylvania Sun Gun type lamp for about 10 seconds from a distance of about 18 inches from the coating. This polymerized the KMER under the open areas of the plate but left the coating soft under the masked black areas of the plate. The unexposed soft KMER coating was then sprayed and washed off with the KMER thinner. The copper foil was then baked for at least 2 hours at 190°C to firm the thin coating to the metal foil. As a next step, the foil was electroplated using a nickel sulfamate solution to cover the open areas with about 0.001 inch of nickel. This nickel plate was well adherent to the copper and it was pinhole free. During this plating procedure, the electrolyte did not attack the baked-on KMER mask. The KMER was then swabbed off and the foil was thoroughly cleaned off the KMER. To ensure cleanliness, the foil was dipped into hot T-100 solution, a proprietary KMER stripper obtained from Industrial Chemical Laboratory, Richardson, Texas. After thorough rinsing of this metal, a clean nickel-plated copper foil was obtained with the copper showing through in spots where the KMER previously masked the nickel plate. The foil was then immersed into a proprietary etch (M-V etchant obtained from McDermid Inc., Waterbury, Conn.) and the copper openings in the nickel were etched through with it. While etching the copper through, this etchant did not attack the nickel. The edge of the holes and lines after completing the etch did not display a ruggedness of more than 1/2 mil. This was considered to be a fair definition considering that the foil itself was 0.002 inch thick. Mask prepared in this manner was then successfully used throughout the project.

Masks were made using this process with a 0.015 inch center-to-center pattern distance corresponding to 32 lines per 0.5 inch. These masks were used when fabricating active devices and they are displayed in figures 3-7,

3-8, and 3-9. Masks having a pattern center-to-center distance of about 7 mils (64 lines per 0.5 inch) were also made and they are shown in figures 3-10, 3-11, and 3-12, but active devices were not made using these masks. The masks were then clamped between metal frames, figure 3-13, to prevent bending or tearing when handled.

In order to align the wafers with the masks, they were put into the center part of a holder shown in figure 3-14. The opening in the middle of the holder is used to pull the slice tightly against the holder with the help of a vacuum arrangement provided by a motor, hose, and a base block. The base block fitted tightly into the bottom of the wafer holder (figure 3-15). This fastening of the wafer onto the holder was necessary to prevent motion of the wafer and the holder with respect to each other during alignment, since this motion would make it impossible to register the mask to the underlying pattern on the wafers. The metal frame holding the mask was then inserted under the jaws of the wafer holder, and using a microscope to monitor it, the metal frame was moved around until the proper registered position was found (figure 3-16). The frame was then clamped to the holder using three screws and the protruding jaw of the holder. The assembly was then taken off the vacuum chuck. The mask holder, wafer, and wafer holder were then one rigid piece (figure 3-17) and could be put into the evaporator, heat treated, ion bombarded, and vapor deposited.

## 3.5 EVAPORATION PROCEDURE AND BONDING

After alignment of the wafers the assembly was put into the evaporator and the vacuum chamber was pumped down to $10^{-6}$ torr or less. The aligned assembly was then heated to 200°C for 1-1/2 hours using radiant heaters in quartz tubes. The heater was then shut off and the wafer was ion bombarded. Nickel was then evaporated out of a tungsten filament followed by a gold evaporation from a molybdenum boat. An overall view of the evaporator and a top view of the evaporation chamber are shown in figures 3-18 and 3-19. In addition, some of the evaporation tools are shown in figure 3-20. The

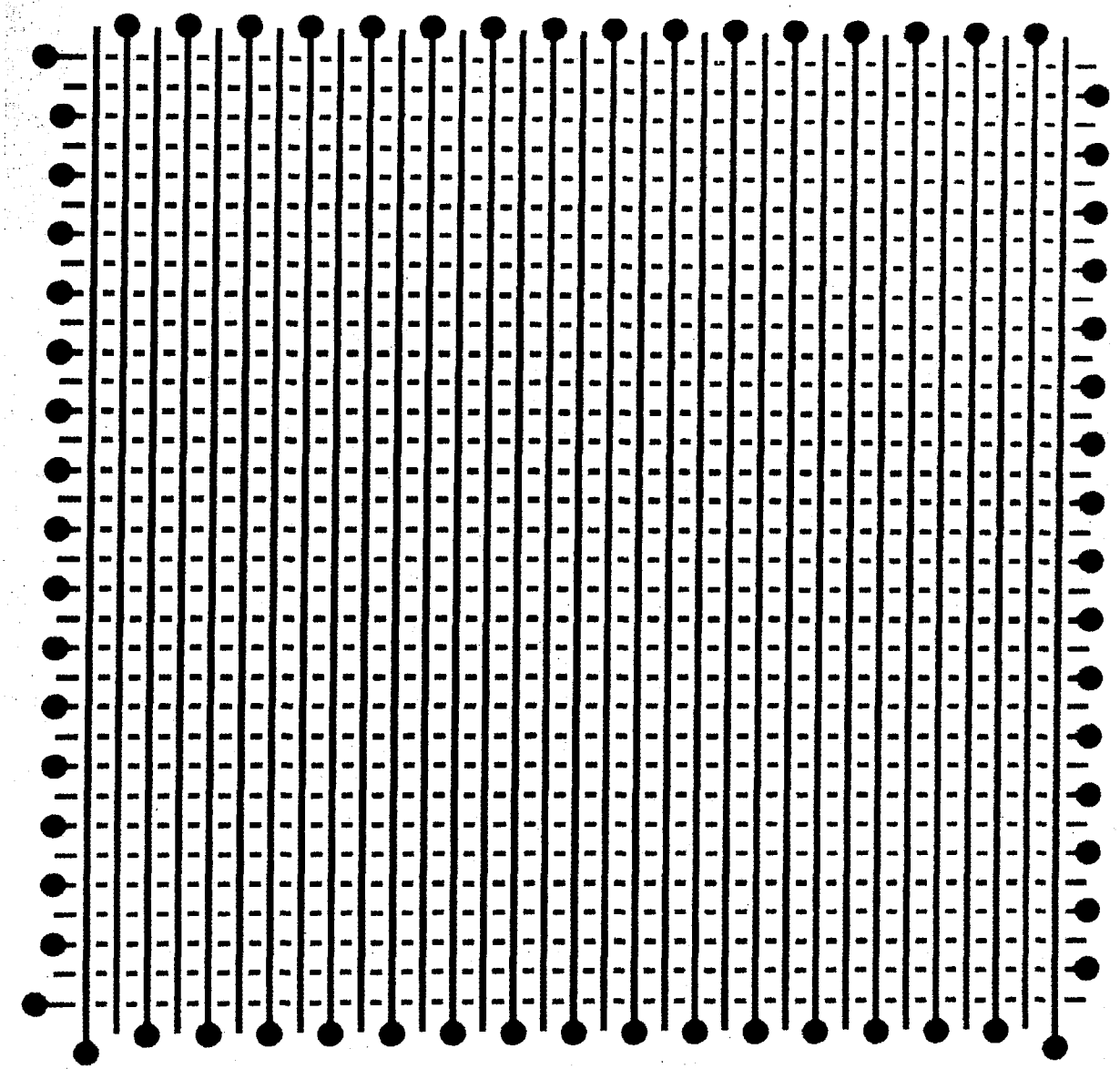

Figure 3-7. Mask No. 1 - Used for Evaporation of Nickel and Gold to Define Ohmic Contacts on the Insensitive Side of the Wafer (Center-to-Center Distance 0.015 Inch)

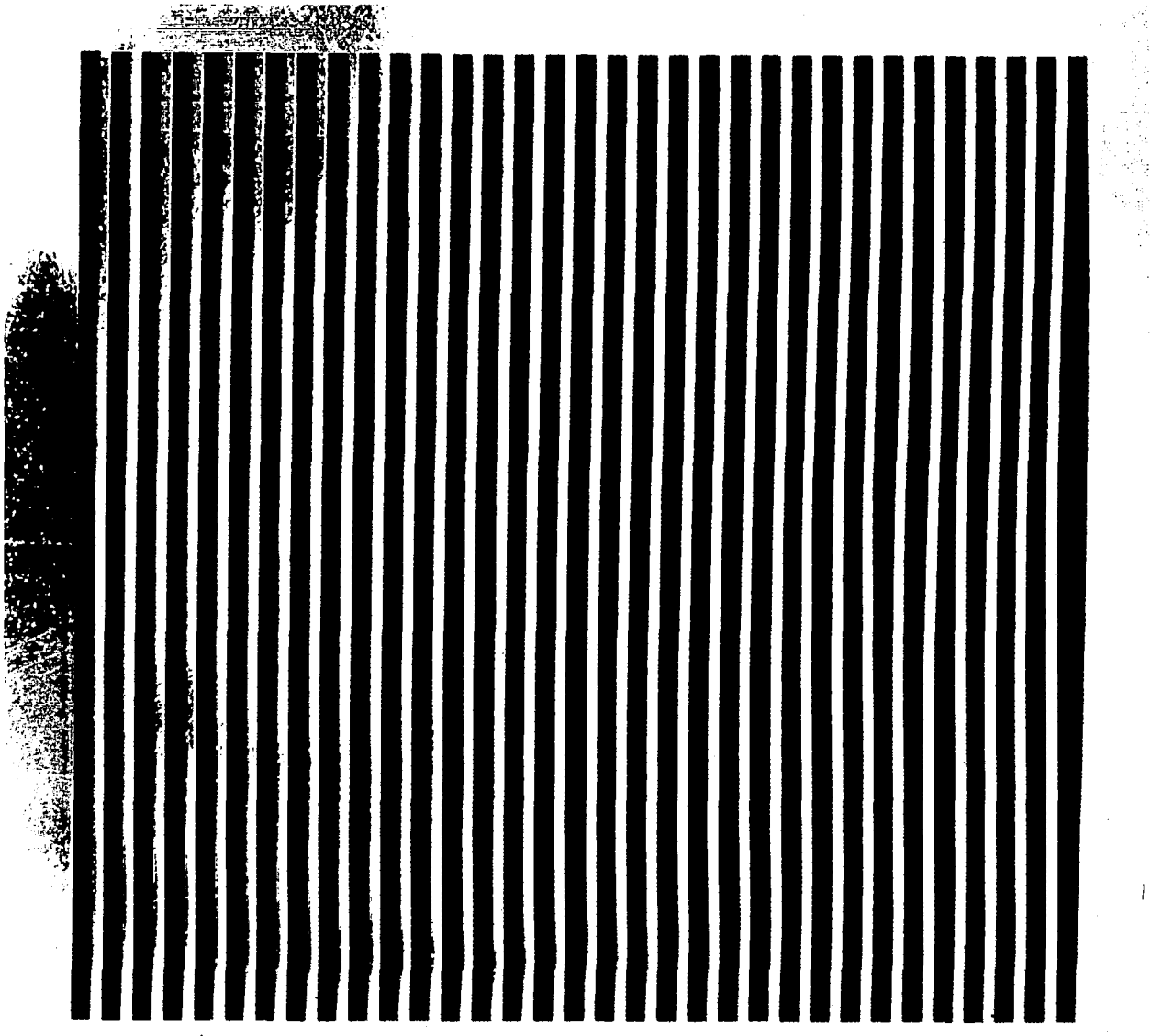

Figure 3-8. Mask No. 2 - Used for Evaporating Silicon Monoxide for Insulation Purposes (Center-to-Center Distance 0.015 Inch)

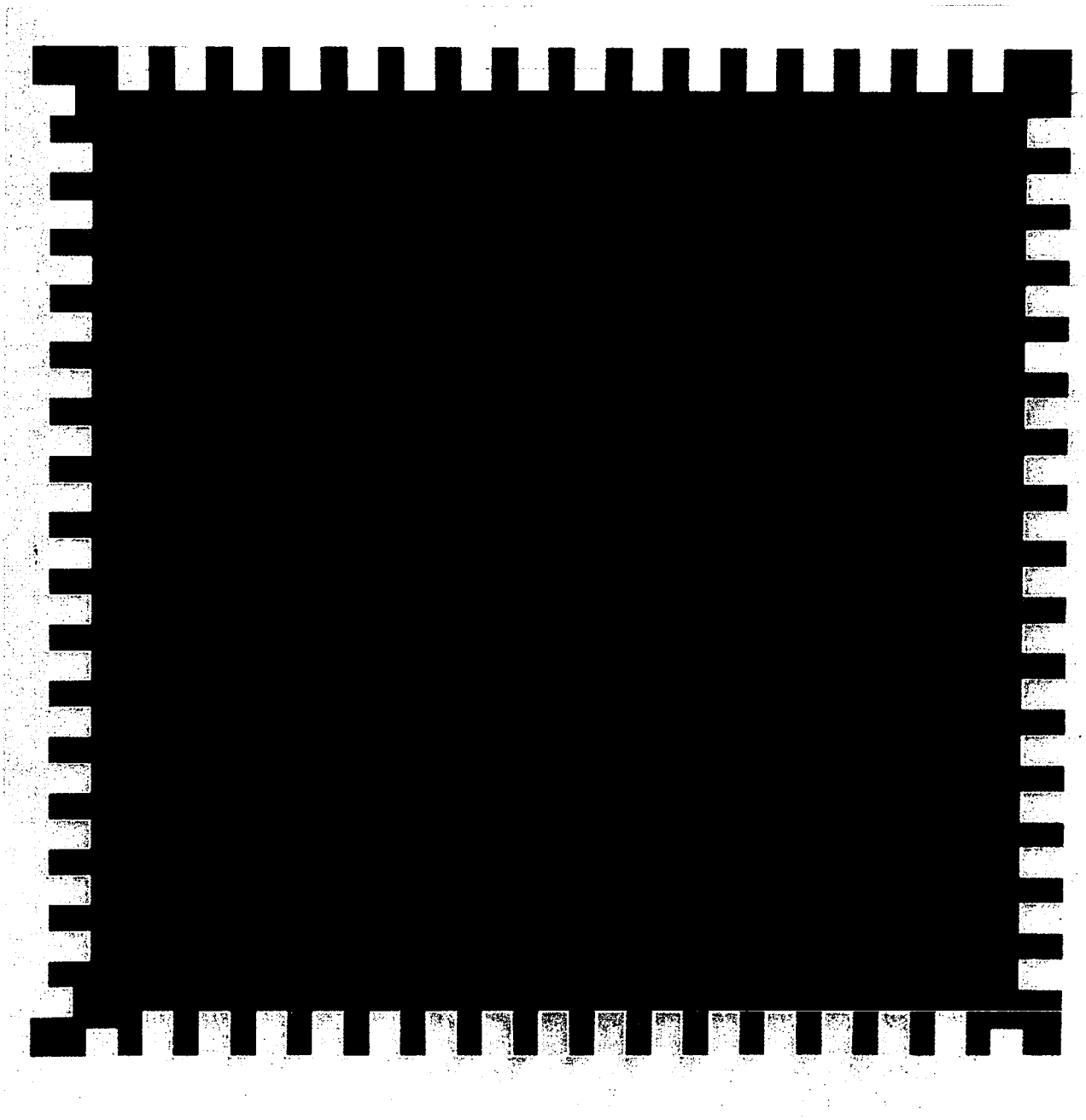

Figure 3-9. Mask No. 4 - Used for Silicon Monoxide Evaporation to Insulate the Grid Network (Center-to-Center Distance 0.015 Inch)

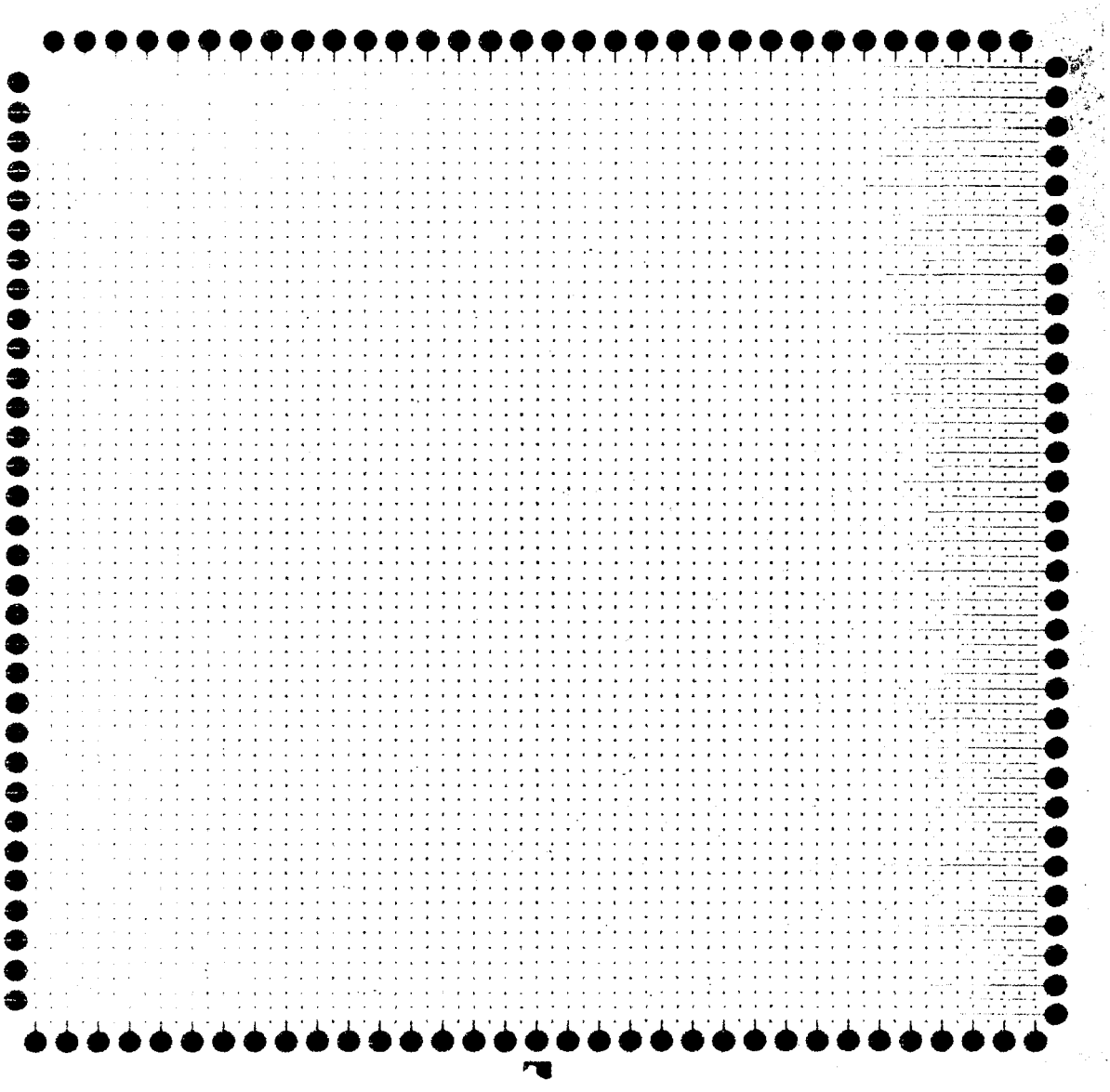

Figure 3-10. Mask No. 1 - Used for Evaporation of Nickel and Gold to Define Ohmic Contacts on the Insensitive Side of the Wafer (Center-to-Center Distance 0.0075 Inch)

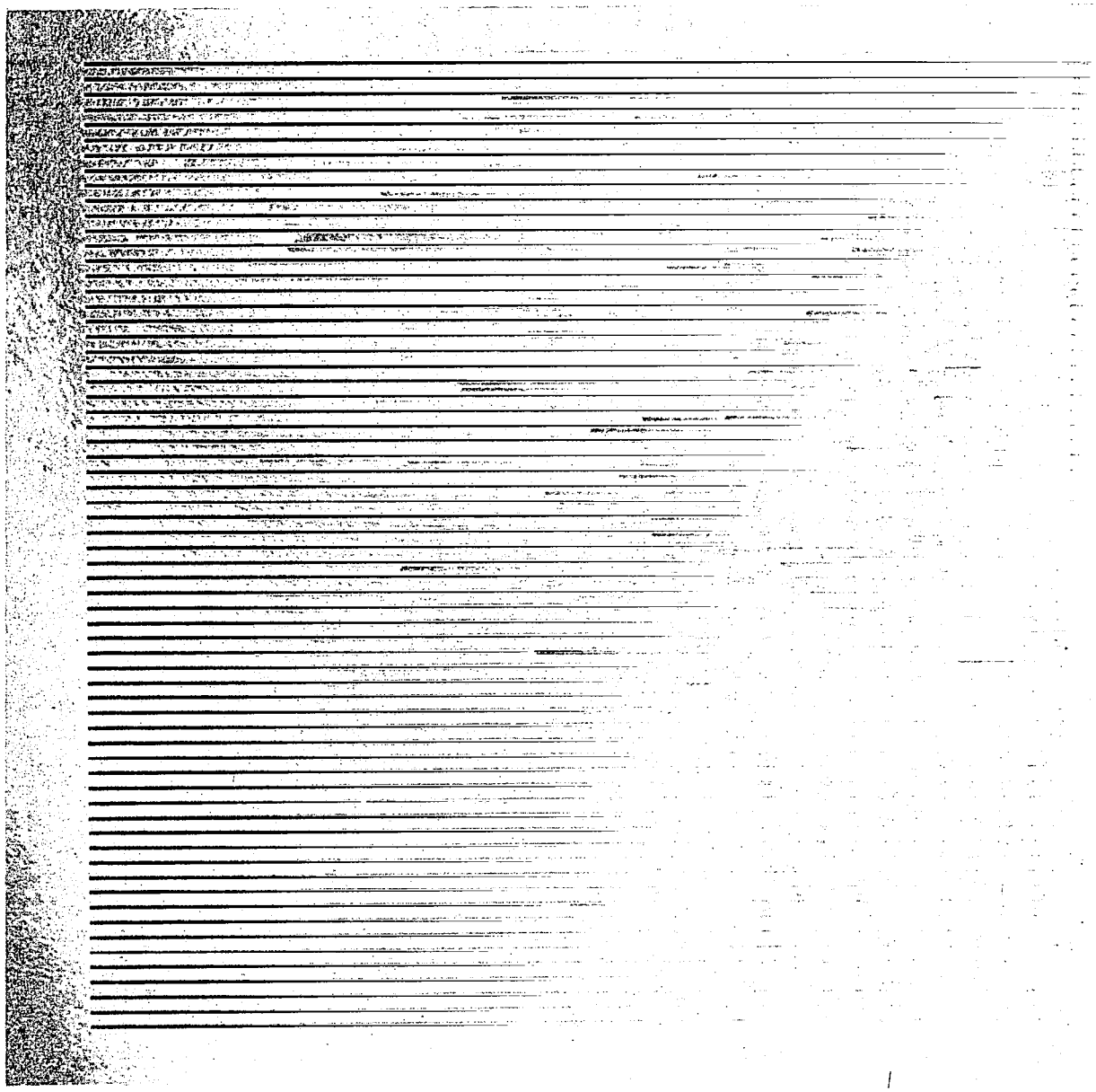

Figure 3-11. Mask No. 2 - Used for Evaporating Silicon Monoxide for Insulation Purposes (Center-to-Center Distance 0.0075 Inch)

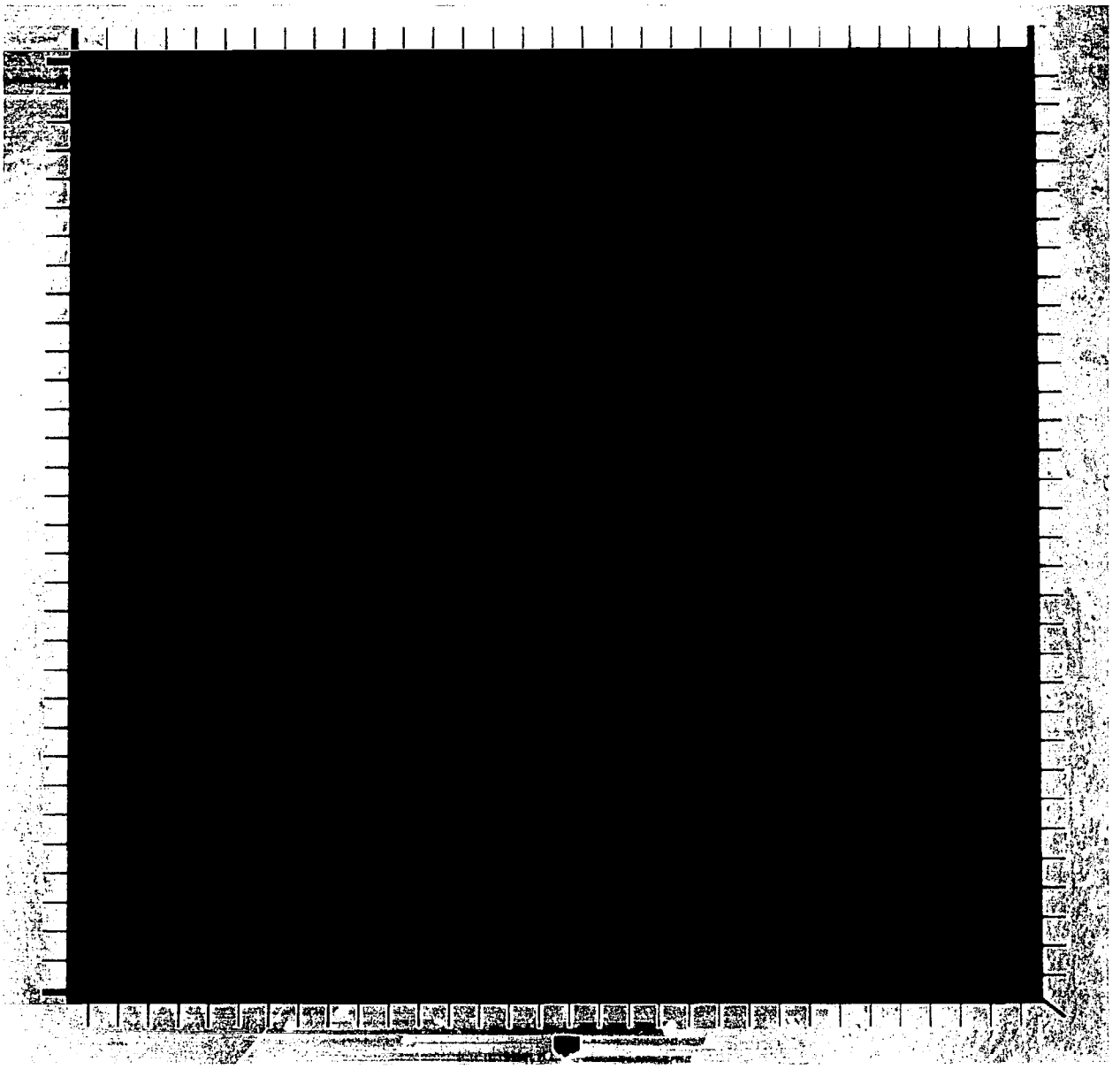

Figure 3-12. Mask No. 4 - Used for Silicon Monoxide Evaporation to Insulate the Grid Network (Center-to-Center Distance 0.0075 Inch)

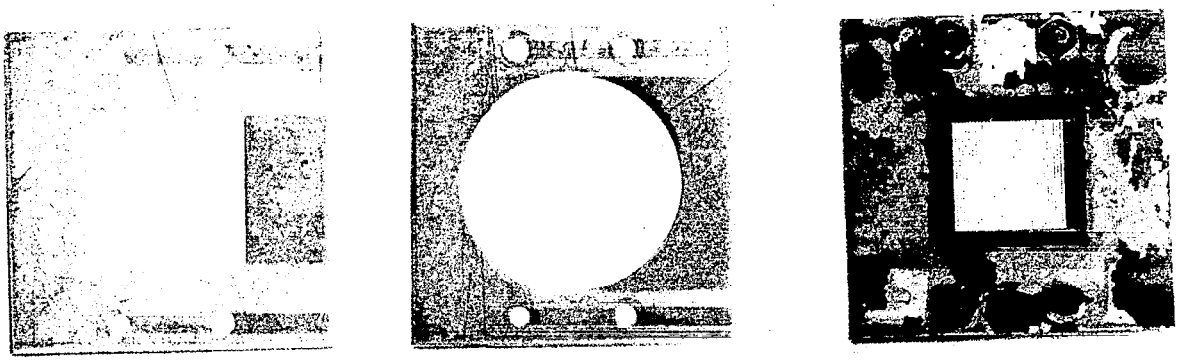

Figure 3-13. Metal Frame Top, Metal Frame Bottom, and Clamped Metal Frame With Mask in Between Them

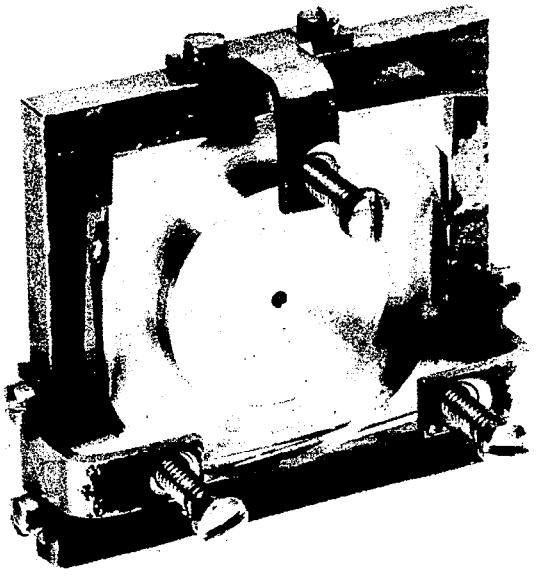

Figure 3-14. Wafer Holder

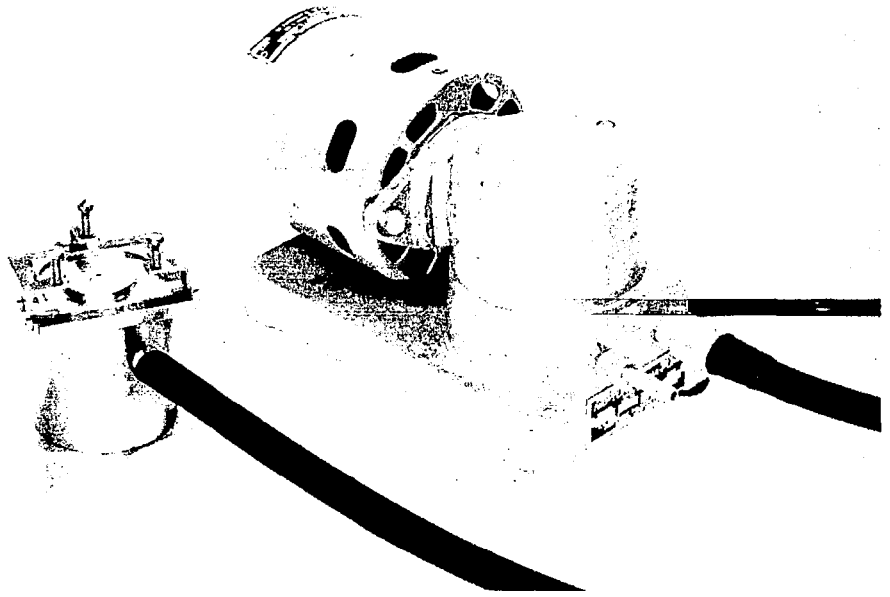

Figure 3-15. Motor, Hose, and Base Block Fitting into the Bottom of the Wafer Holder

total resistivity of the 1/2-inch long, 0.025-inch wide line was about 25 ohms after completion of the evaporation. A picture of the first evaporated pattern on the wafer is shown in figure 3-21.

Following the nickel-gold evaporation, the second mask was aligned with the first pattern on the wafer. The assembly was fastened together and again placed into the evaporator. The holders and wafers were heated to 200°C for 30 minutes and 800 Å of silicon monoxide, obtained from Kemet Corporation, and was then evaporated onto the wafer from a specially designed boat (obtained from Matheson Company). Following an anneal at 200°C for 30 minutes, the wafers were cooled and unloaded. Figure 3-22 shows the wafer after this step and it is apparent that the long continuous gold lines are covered with silicon monoxide.

After another mask change the third evaporation followed. The assembly was first heated to 100°C for 15 minutes and then the temperature was dropped to 75°C. At this temperature a heavy nickel layer was evaporated

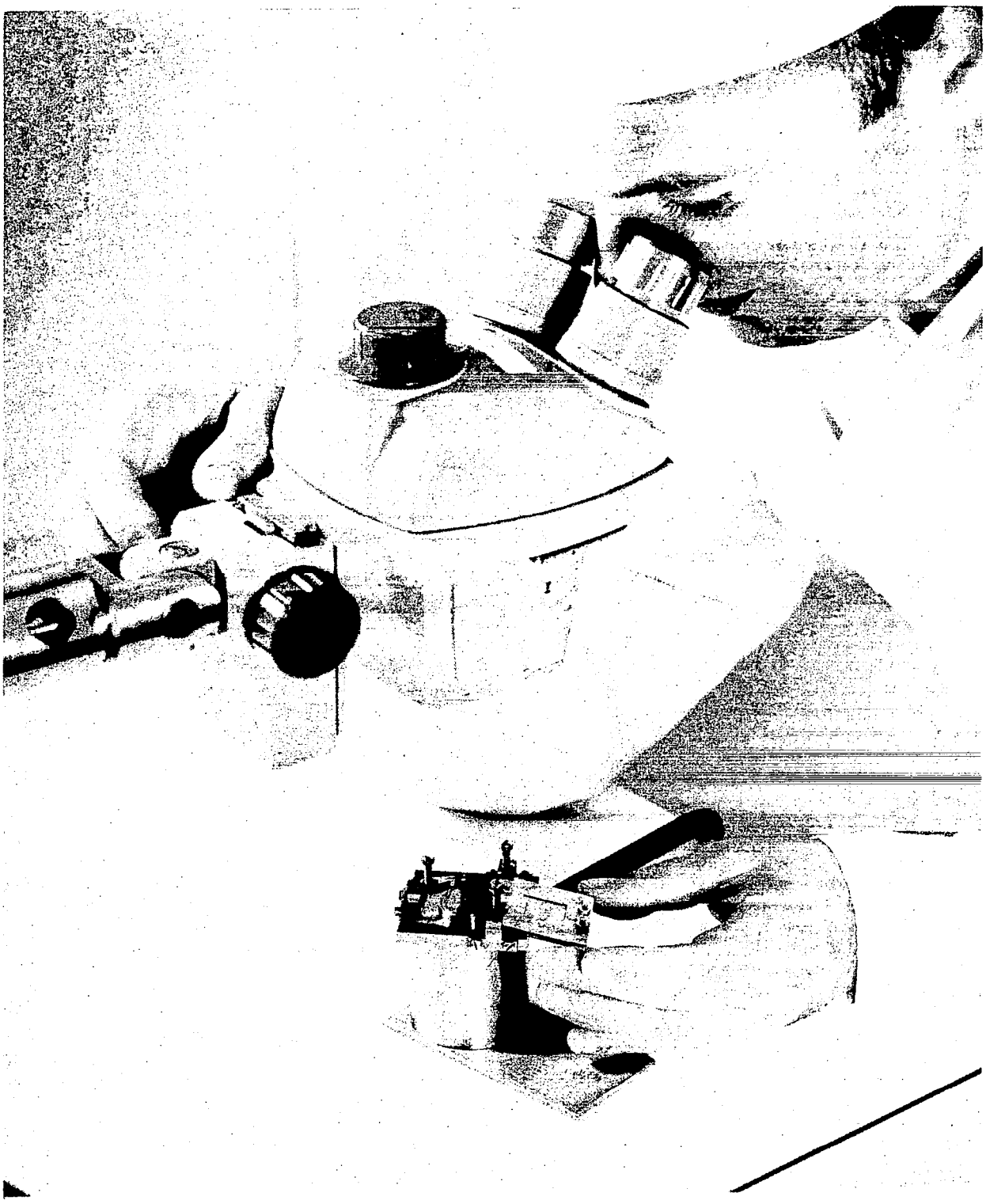

**Figure 3-16. Alignment of the Mask With the Wafer Under the Microscope**

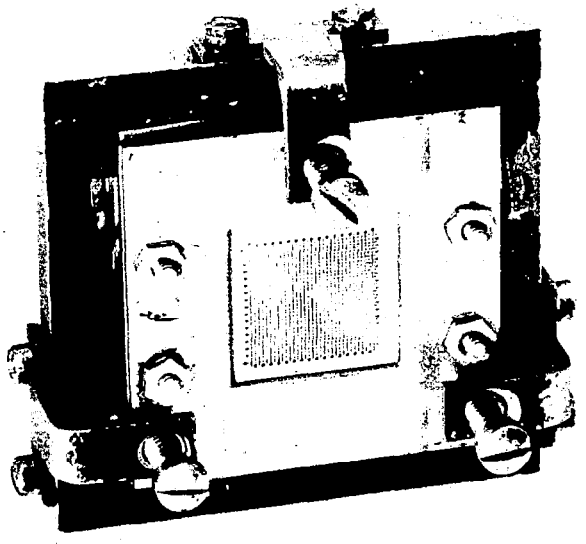

Figure 3-17. Wafer Holder, Wafer, and Mask Holder Clamped into One Rigid Assembly

onto the silicon followed by a heavy layer of gold. As can be seen from figure 3-23, this operation joined the discontinuous nickel-gold lines over the silicon monoxide and formed continuous conductors over the insulating strip.

A fourth silicon monoxide evaporation then covered up and passivated the grid pattern leaving only the bonding pads open.

Connections to the bonding pads were made by thermal compression bonding. Instead of the usual 0.0008-inch diameter gold wire used for standard thermal compression bonding, 0.005-inch diameter gold wire was used. It was easier to keep the heavier wire straight, preventing the formation of loops and kinks. This helped to reduce the noise level of the units somewhat, since the gold wire used was about 1 inch long and several kinks and knots were eliminated by going from the 0.0008-inch to the 0.005-inch wire. In all other aspects, the bonding procedure was the same as in the case of standard gold bonding.

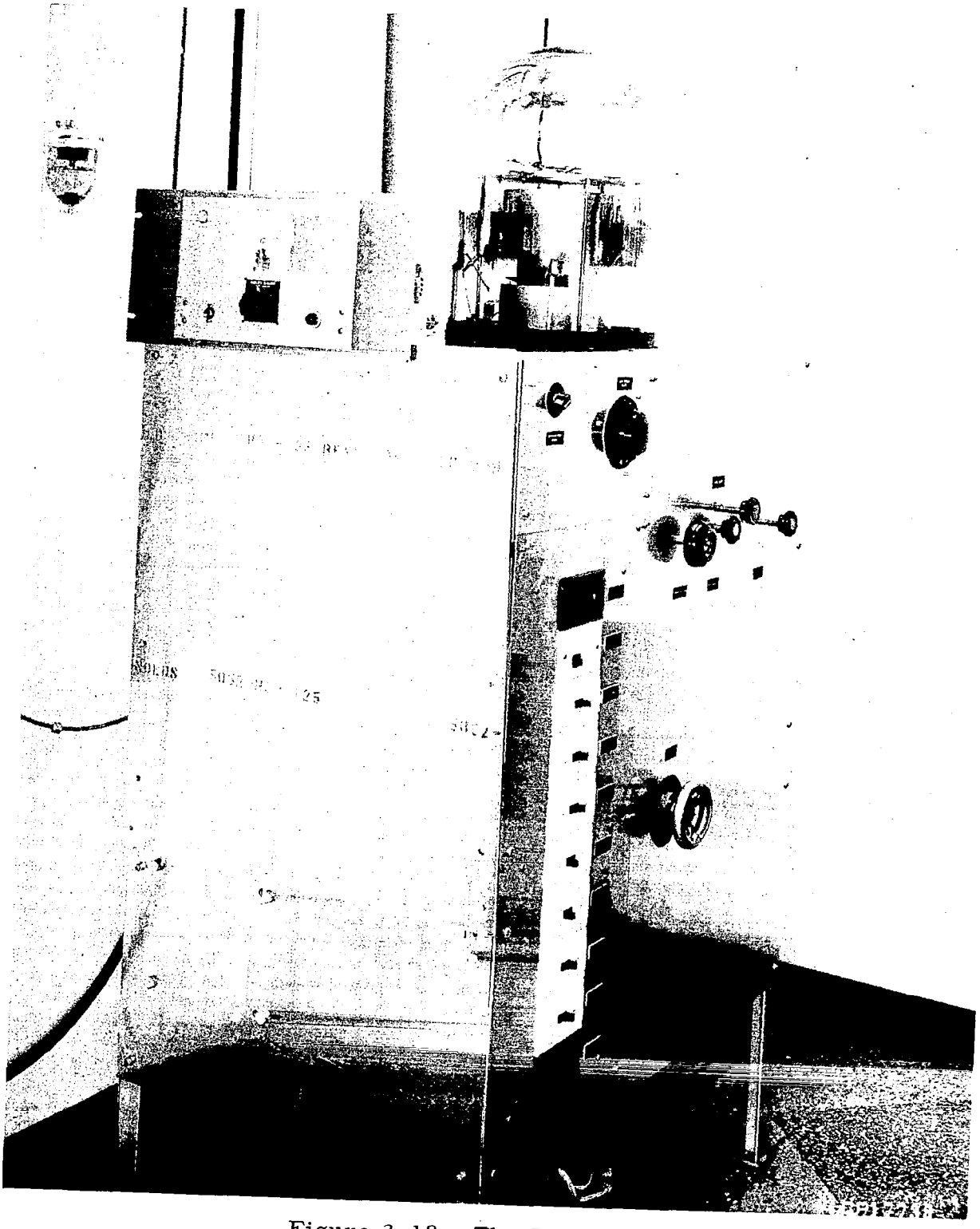

Figure 3-18. The Evaporator

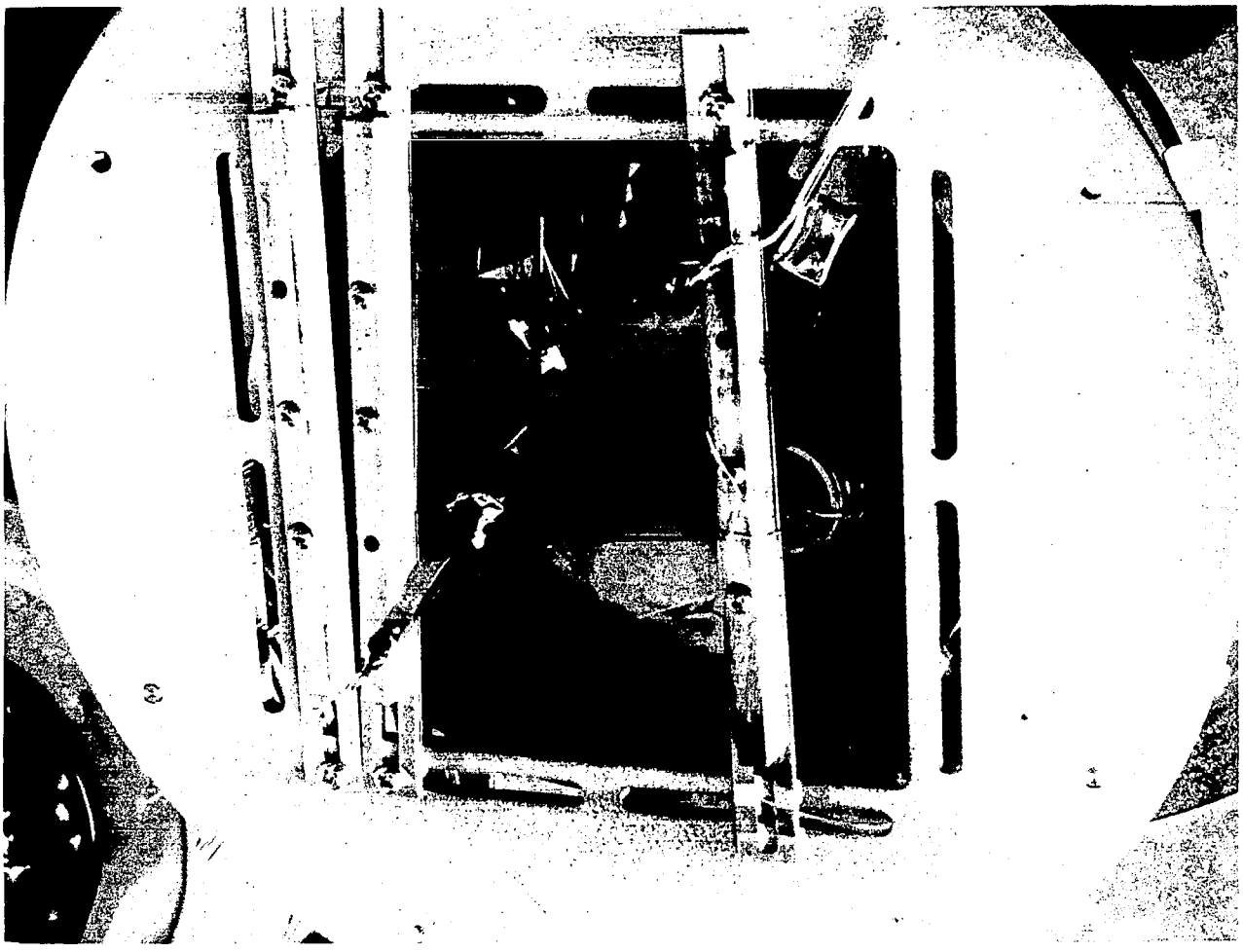

Figure 3-19. Top View of the Evaporation Chamber Showing the Molybdenum Shield

In order to review briefly, the bonding process is summarized below. The wafer to be bonded was heated to about 330°C using a small hotplate. The gold wire was then pressed with a capillary into the gold bonding pad on the wafer. Since this wire was balled up at its lower end it could not slip through the capillary and it was flattened and alloyed to the underlying gold pad. Upon lifting the bonding head the capillary slid up along the gold wire, since the gold wire was now attached to the silicon. A miniature hydrogen torch was then used to burn the wire into two pieces leaving the appropriate length

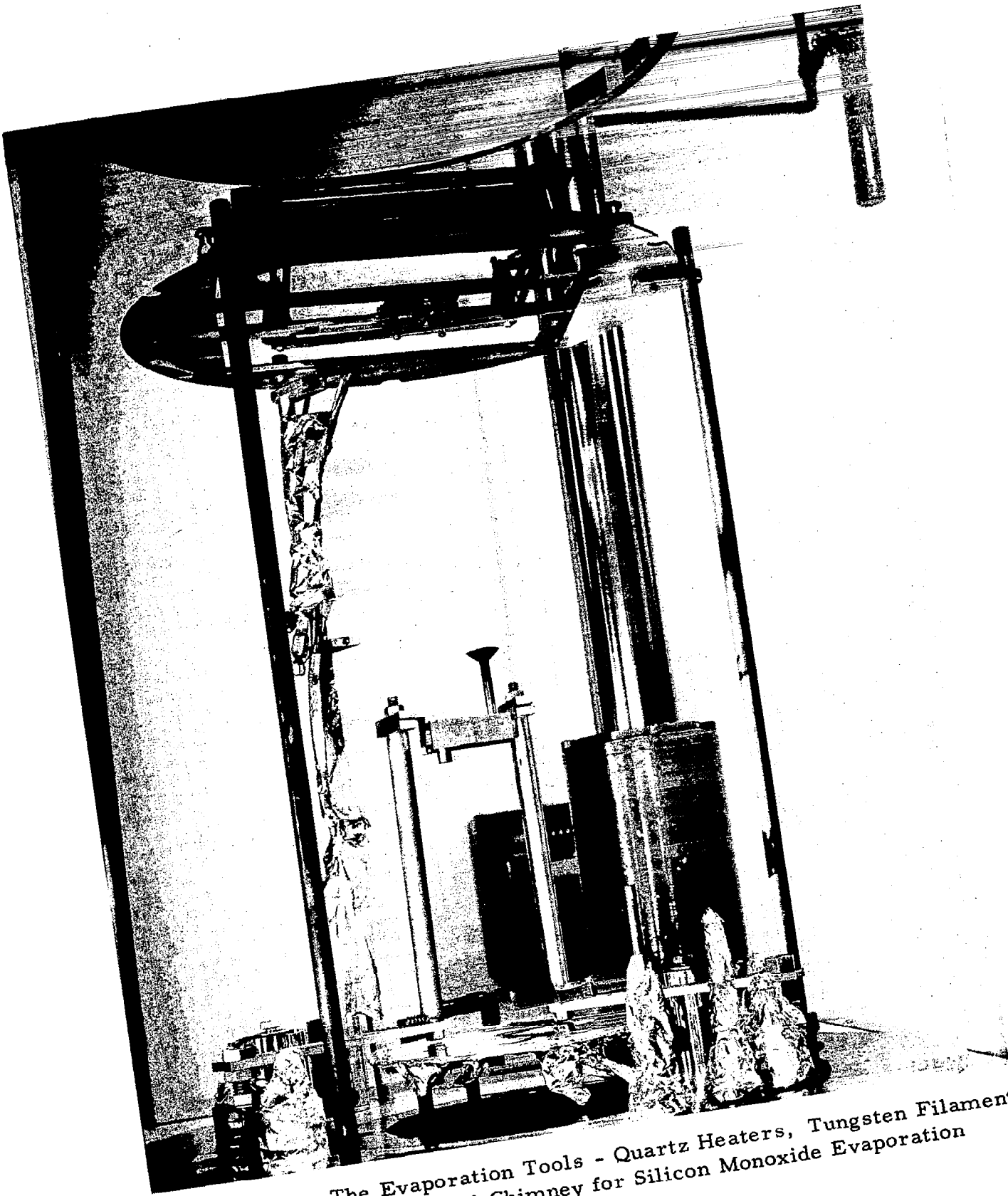

Figure 3-20. The Evaporation Tools - Quartz Heaters, Tungsten Filament Molybdenum Boat, and Chimney for Silicon Monoxide Evaporation onto Silicon

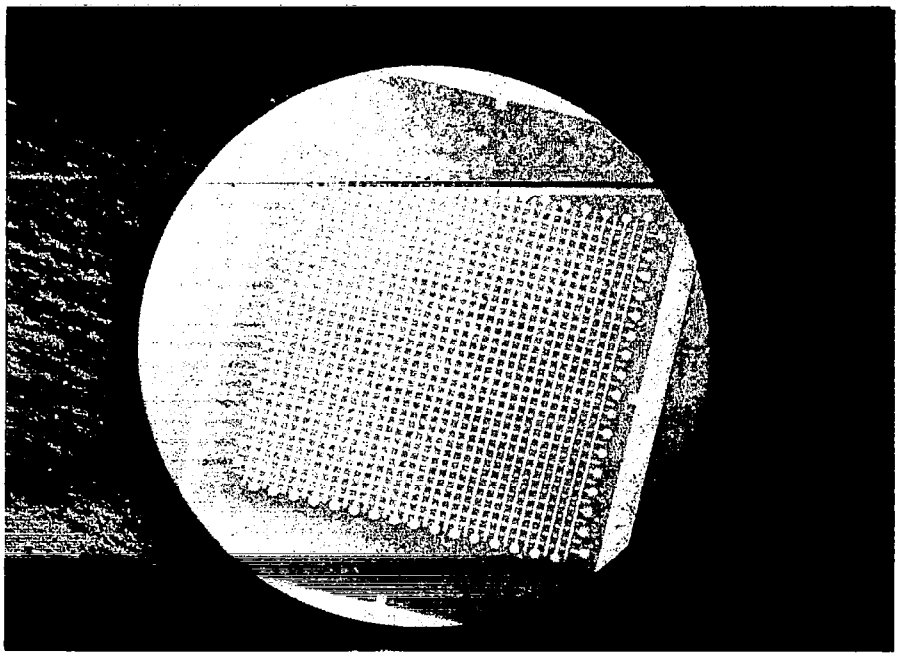

Figure 3-21. Gold Evaporated Pattern on Silicon Defined by the First Mask

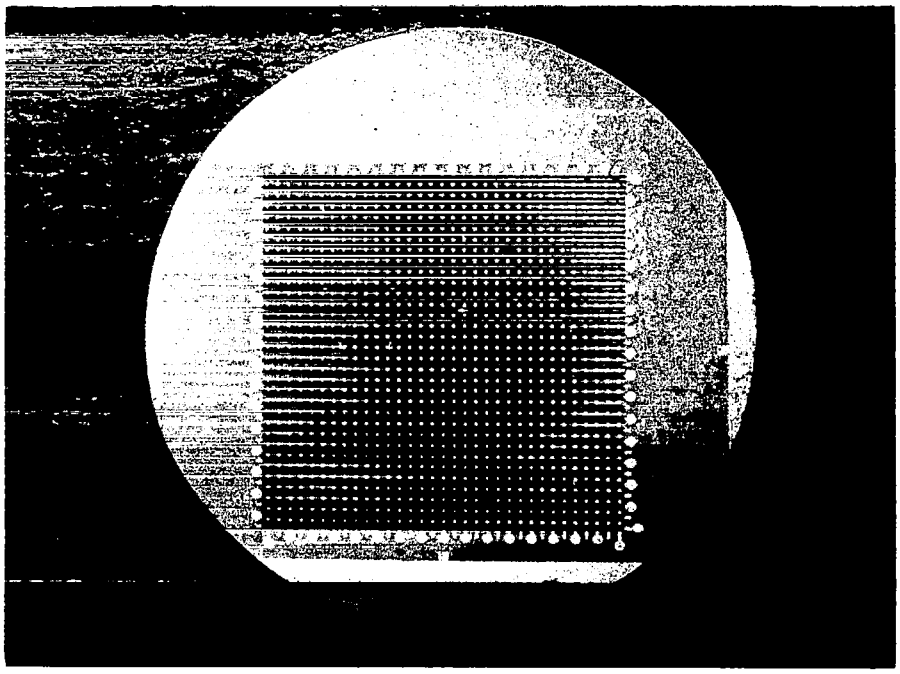

Figure 3-22. Wafer After Second Evaporation - Silicon Monoxide Covering the Long Gold Lines

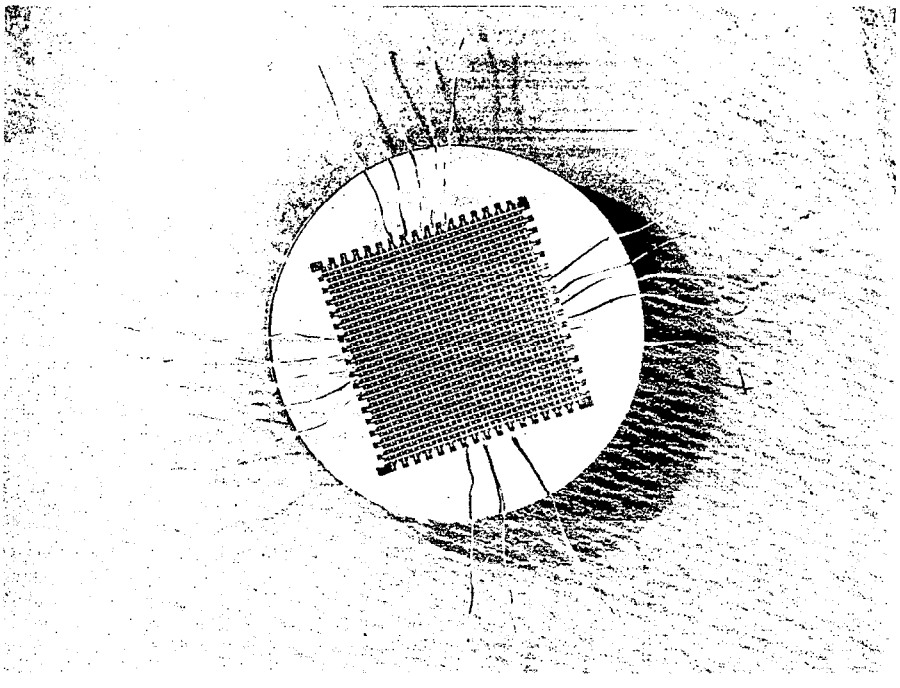

Figure 3-23. Wafer After Third Evaporation - The Previously Discontinuous Conductors Are Joined Over the Silicon Monoxide Strips

attached to the bonding pad. Another ball was formed when the wire was burned into two pieces on both pieces of wire and the operator was ready for the next bond (figures 3-24, 3-25, and 3-26).

A significant advantage of gold-to-gold bonding used here over the standard gold-to-aluminum bonding is that it eliminates the so-called "purple plague." "Purple plague" is a brittle gold-aluminum alloy that tends to propagate from the gold-aluminum junction along both the aluminum and gold connectors. This alloy is a major cause of bonding failure, since it is brittle and after it reaches a sufficient size it breaks easily, causing an open circuit. Since in this case a gold wire is bonded to a gold pad, without aluminum being present, the "purple plague" problem is circumvented.

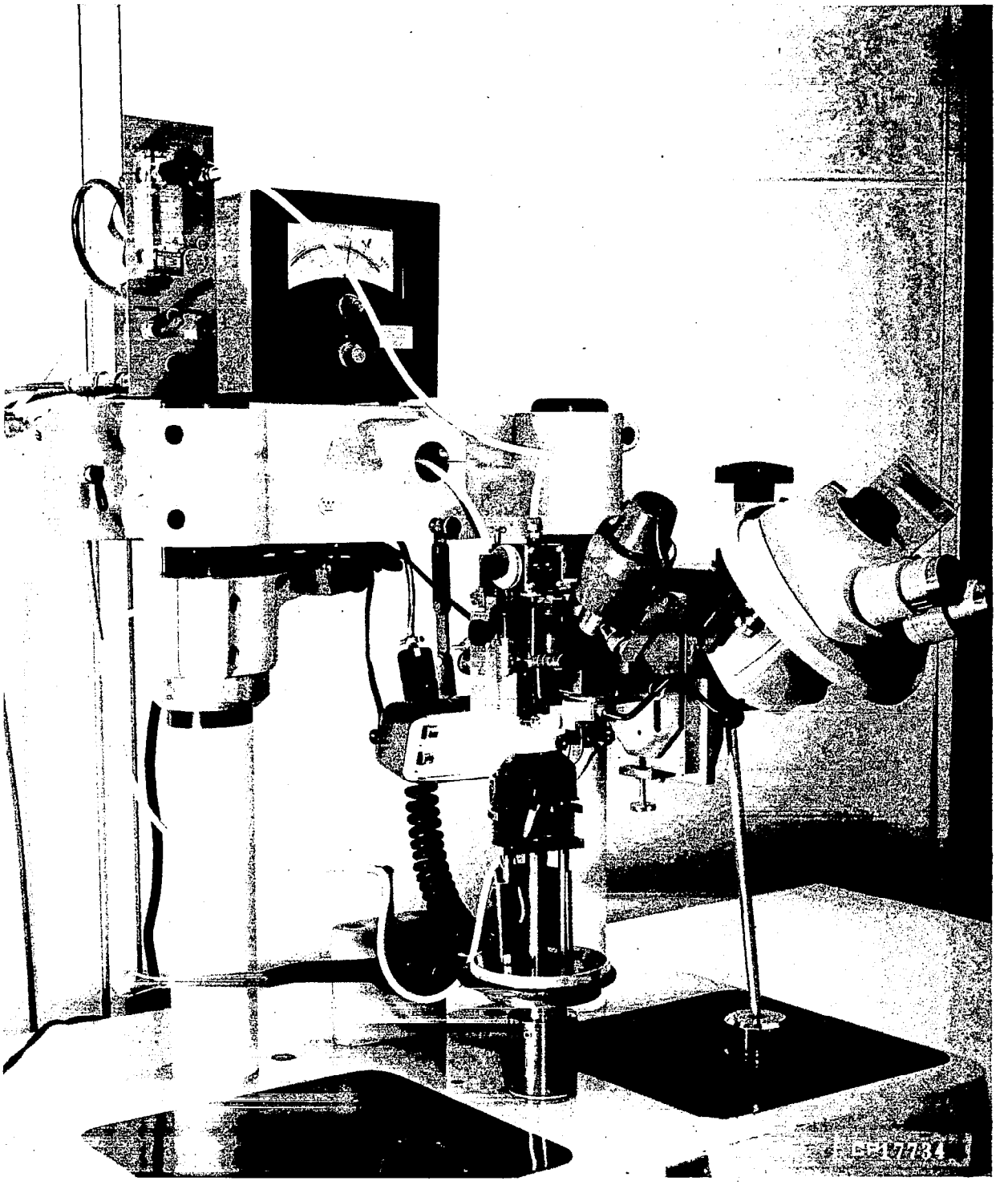

Figure 3-24. Wafer, Capillary, and Spool Ready for Bonding

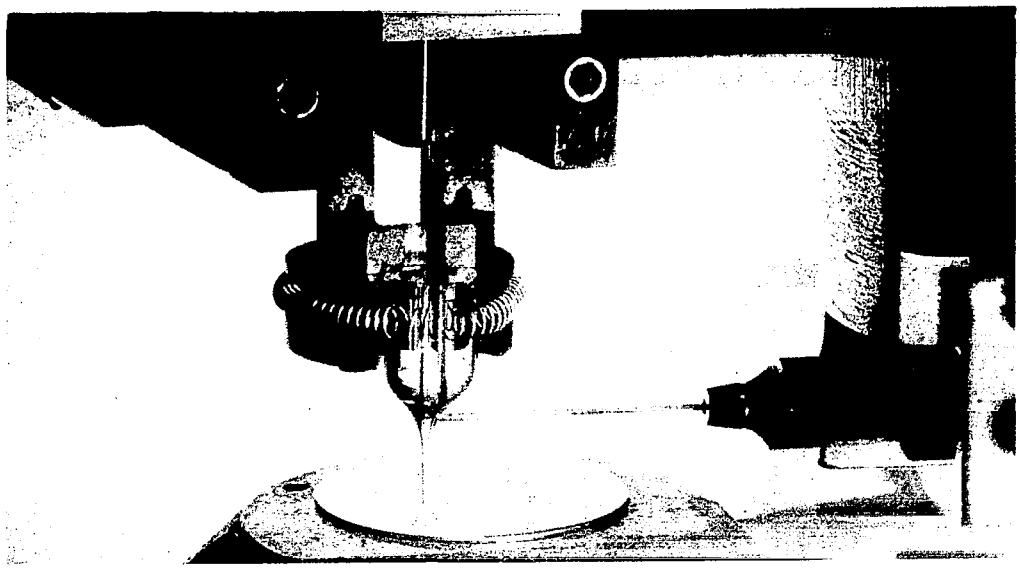

Figure 3-25. Capillary Sliding Up on the Attached Wire After Pressing the Gold Ball to the Hot Wafer

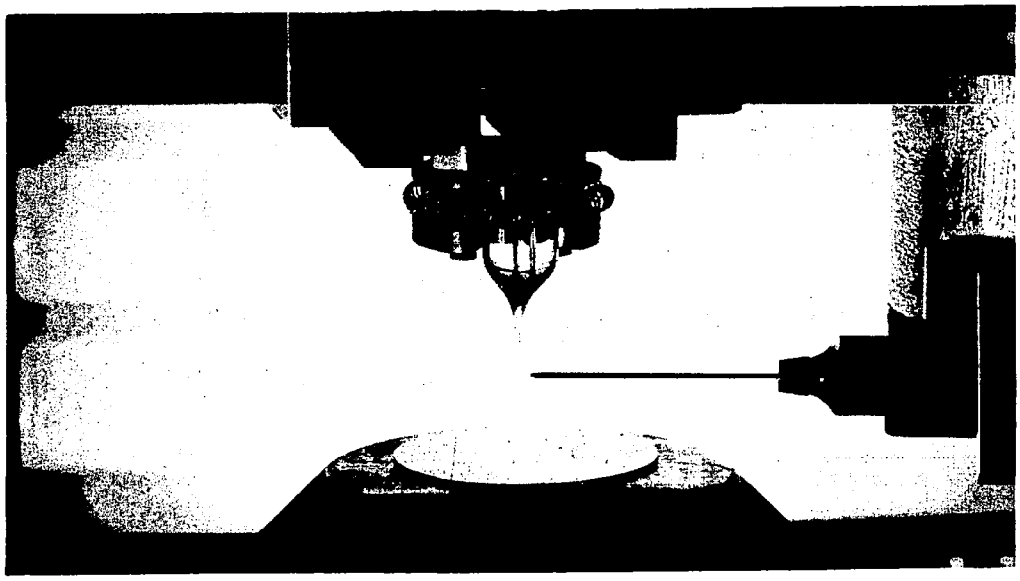

Figure 3-26. Wire Severed and Bond Completed

## 3.6 TESTING

The continuity along the lines and isolation between adjacent lines and lines running perpendicularly with respect to each other were usually checked after bonding. It was found that the resistivity along the 1/2 inch of the lines was usually less than 25 ohms and the resistivity between adjacent lines was usually over 25,000 ohms. This gave a ratio of about 1 to 1000 between the furthest point on the same line to the nearest point on the adjacent line. This is of importance when considering crosstalk between the adjacent lines; that is, when considering the effect of an activated unmonitored line on an adjacent nonactivated but monitored contact. Crosstalk is the amount of signal that will leak from one line to another and it could be considerable if the resistance from the contact to the activation site on the line is comparable to the resistance to the activation site on a neighboring line. As seen above, this ratio was 1 to 1000, substantially minimizing the crossfeed of signals.

Another reason for negligible crosstalk was due to the operation of the detector in a completely depleted mode. The resistance between adjacent lines was, for all practical purposes, infinite, since when operating the unit in a completely depleted mode there are no carriers in the material and the contact lines can be considered isolated from each other by a dialectric. In this manner, the resistance ratio of 1 to 1000 obtained when testing the device without any bias was greatly improved, possibly to a ratio of 1 to 10,000, under the actual conditions of operating at total depletion.

## 3.7 MOUNTING AND POLISHING

After completion of testing, the wafers were mounted onto their headers. These headers were machined in three pieces from aluminum silicate (lava) a naturally occurring mined substance sold by the American Lava Corporation (Chattanooga, Tenn.). After machining, this compound was heat treated; that is, its temperature was slowly raised in air to 1000°C. This gradual temperature elevation prevents the liberated water from fracturing the material. After holding the machined parts at 1000°C for 1 hour the furnace is turned off and the parts are allowed to cool. When machining this material, the tolerances have to take into account the shrinkage of this substance due to expulsion of the water. The machined parts are shown in figure 3-27 and the partial assembly and assembly on figures 3-28, 3-29 and 3-30. When assembling, the header female pins, taken out of tube sockets, were soldered to a 0.020-inch copper lead. These pins were then put into their ceramic holders and were brought out to the periphery of the holder in two levels. The three parts of the header were then fastened together with a bolt and screw. After completion of the header, each one of the female pins had to be opened with a special tool to accept smoothly a 21-pin vacuum tight connector. If the pins were not opened enough, the plugged in connector would not separate from the header. On the other hand, if the pins were opened too wide, the connector and header would insert easily, but several of the 21 pins would not make contact, causing an intermittent contact.

Following the completion of the header, the wafer was attached to the front end. The adhesive used was R-313 resin obtained from C.H. Biggs Company, California. It was mixed in a proportion of 1 gram of resin to 2 drops of hardener. The wires on the wafer were spread sideways into the common plane with the wafer and the mixed resin was spread on the wafer and header both. The two objects were then brought together and allowed to harden. Next the gold wires were bent down and soldered to the respective copper leads on the header (figure 3-31). In addition, a 0.020-inch gold wire (and possibly a spare one) was tied to one of the copper leads, and the thick

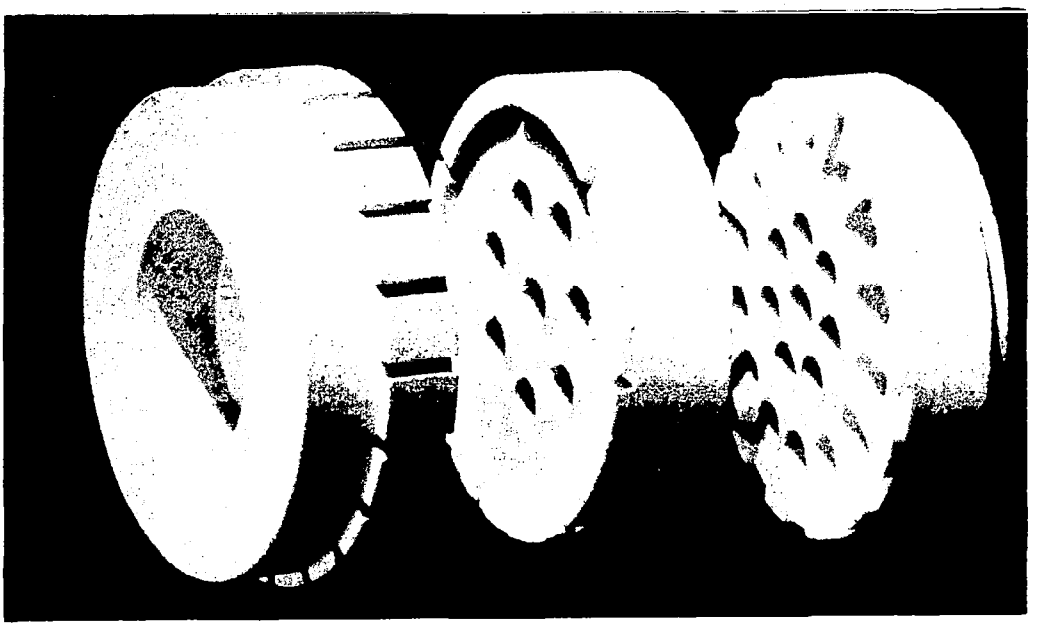

Figure 3-27. The Machined Ceramic Pieces Constituting Parts of the Header

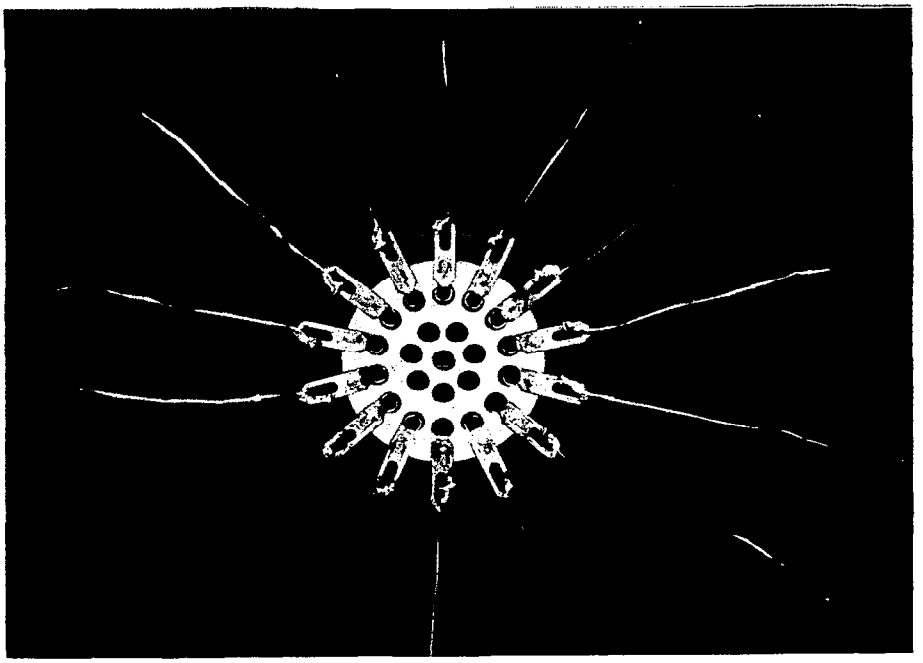

Figure 3-28. Partially Assembled Header (a)

gold conductor was then brought out to the level of the silicon wafer to serve as a ground contact. Mounting of the header was not completed and the unit was ready for potting.

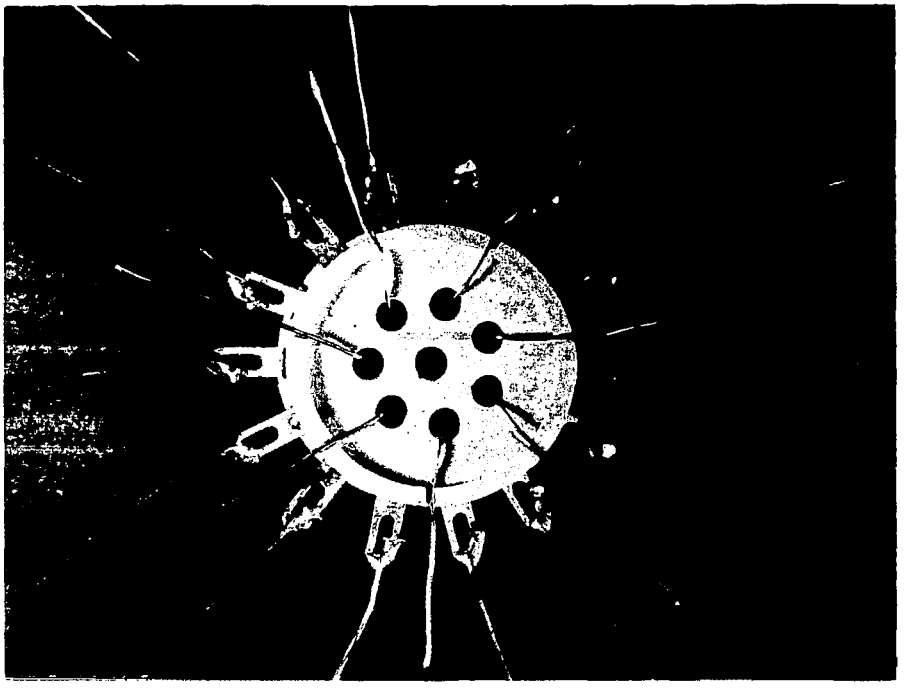

Figure 3-29. Partially Assembled Header (b)

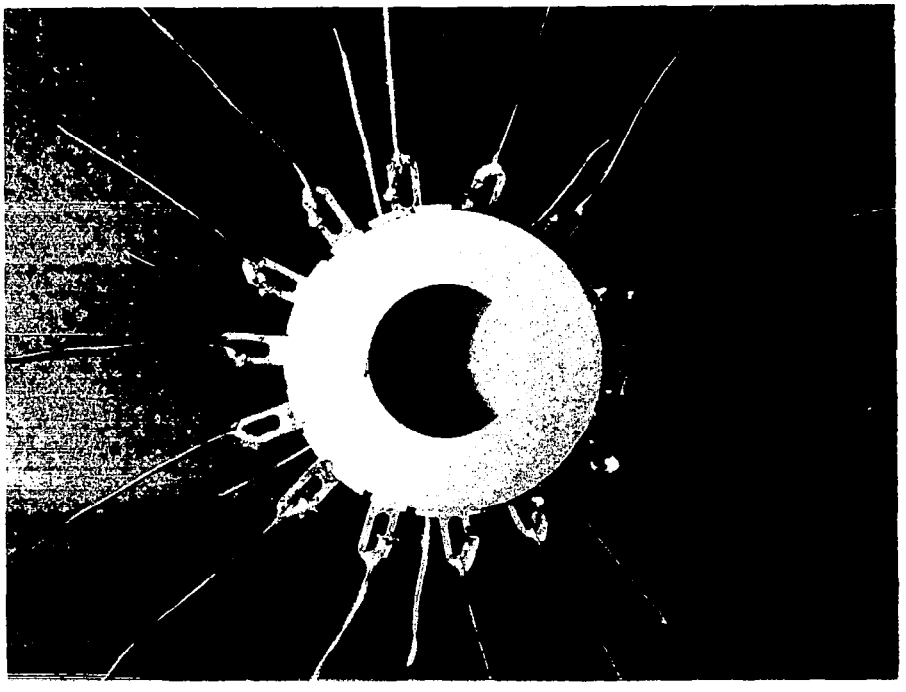

Figure 3-30. Fully Assembled Header

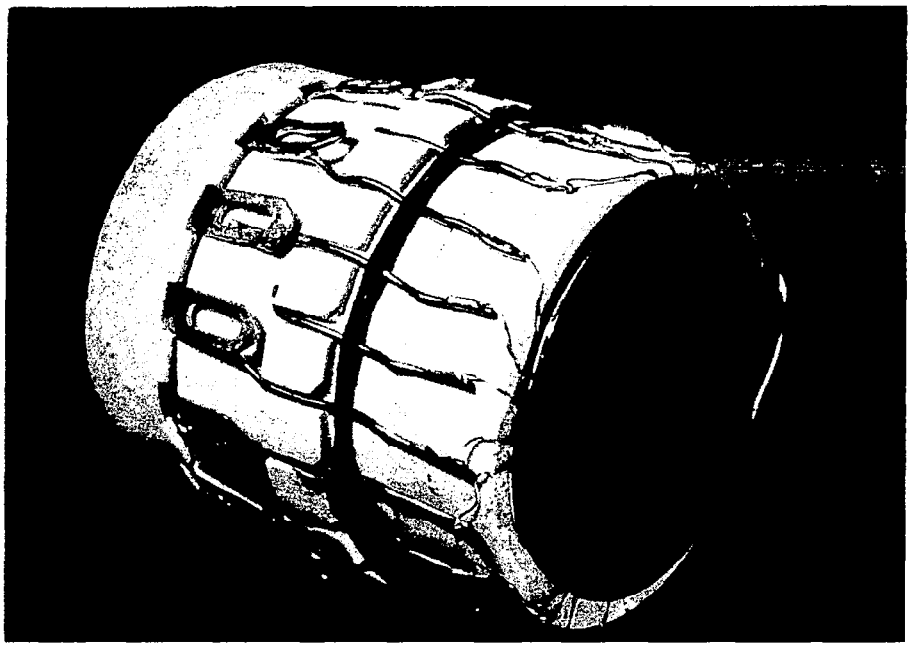

Figure 3-31. Wafer and Header Attached Together and the Gold Wires Soldered to the Respective Pins

When preparing for potting, a 2- by 4-inch glass slide was covered by a transparent sheet of polyethylene. Double coated tape was then put across the polyethylene sheet and the header, with wafer side down, was pressed onto the tape. Two half pieces of teflon mold were then placed concentrically with the header and pressed into the tape. R-313 resin was then allowed to flow between the header and the teflon mold and it was allowed to harden. After hardening the teflon mold was taken off and the polyethylene backed tape was peeled off the front surface. The header after potting is shown in figure 3-32.

The front surface of the assembly was then relapped using 12-micrometer compound until the wafer and the ground contact wire were flat and the whole wafer showed signs of being lapped by the 12-micrometer compound. The header was then carefully washed, followed by a thorough cleanup of the unit using detergent and an ultrasonic cleaner. Following a thorough rinse, another 0.002-inch (approximately) was lapped off the wafer on a glass plate

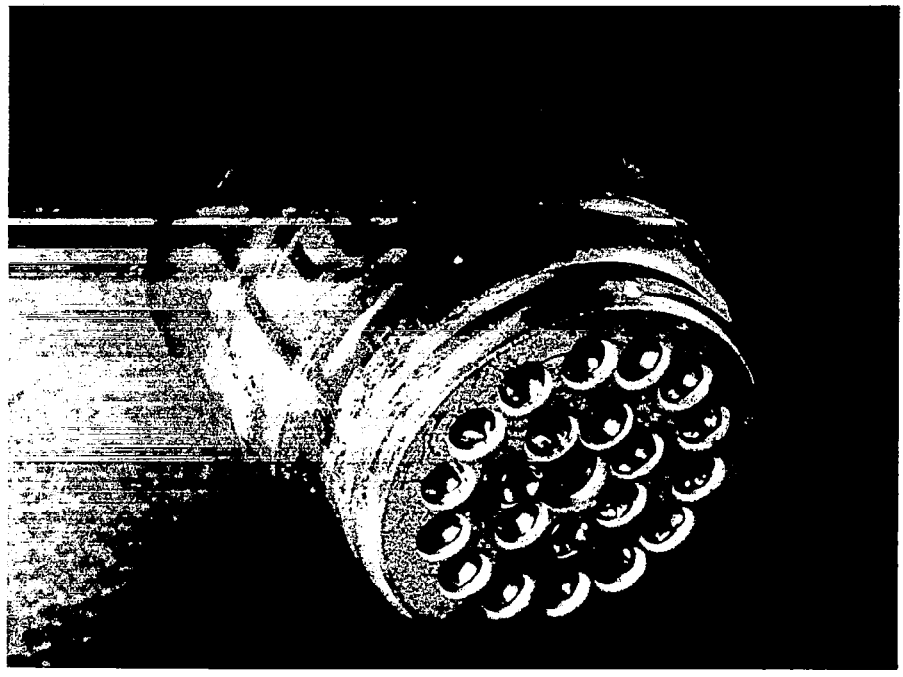

Figure 3-32. Header After Potting

using 3-micrometer compound. After another wash and cleanup, the header was polished on Morris pitch pads using a 1-micrometer compound. With the use of this compound, the front side of the wafer was polished to a mirror finish. After the polish, the wafer was again thoroughly cleaned off, but this time, it was also thoroughly cleaned of traces of detergent and running tap water. The detergent was taken off by repeated ultrasonic cleanings using deionized water. The wafers were then dried with filter paper and stored under an infrared lamp to enhance drying.

## 3.8 ETCHING INVERSION LAYER FORMATION, EDGE PROTECTION, AND EVAPORATION

The etching solution (CP-4) was mixed using 5 parts of concentrated nitric acid, 3 parts of hydrochloric acid, and 3 parts of acetic acid. For every 200 ml of etchant 2 drops of bromine were added. The effect of the bromine was to make the wafer smoother after etch and reduce the number of sharp boundaries and hillocks.

The etching solution was made up in a thoroughly cleaned teflon beaker and was chilled to ice temperature in an ice bath. The beaker containing the ice bath was then placed onto a magnetic stirrer and a thoroughly cleaned teflon-coated magnet was put into the etching solution. The cooled solution was then stirred from beneath without interfering with the immersion of the piece to be etched. After completion of these preparations, the header was immersed into the stirred acid and held there for 3-1/2 minutes. During this time about 0.003 inch of silicon was taken off the surface of the slice. In order to prevent clouding and hazing of the wafer, it was not lifted out of the solution during the etch. After the expiration of the 3-1/2 minutes, the mounted silicon slice was immediately rinsed with deionized water. The unit then was rinsed continuously in deionized water for about 1 hour with the active surface only barely immersed into a full beaker. Incoming deionized water was then rinsing the active area of the unit without washing much of the resin coated side (figure 3-33).

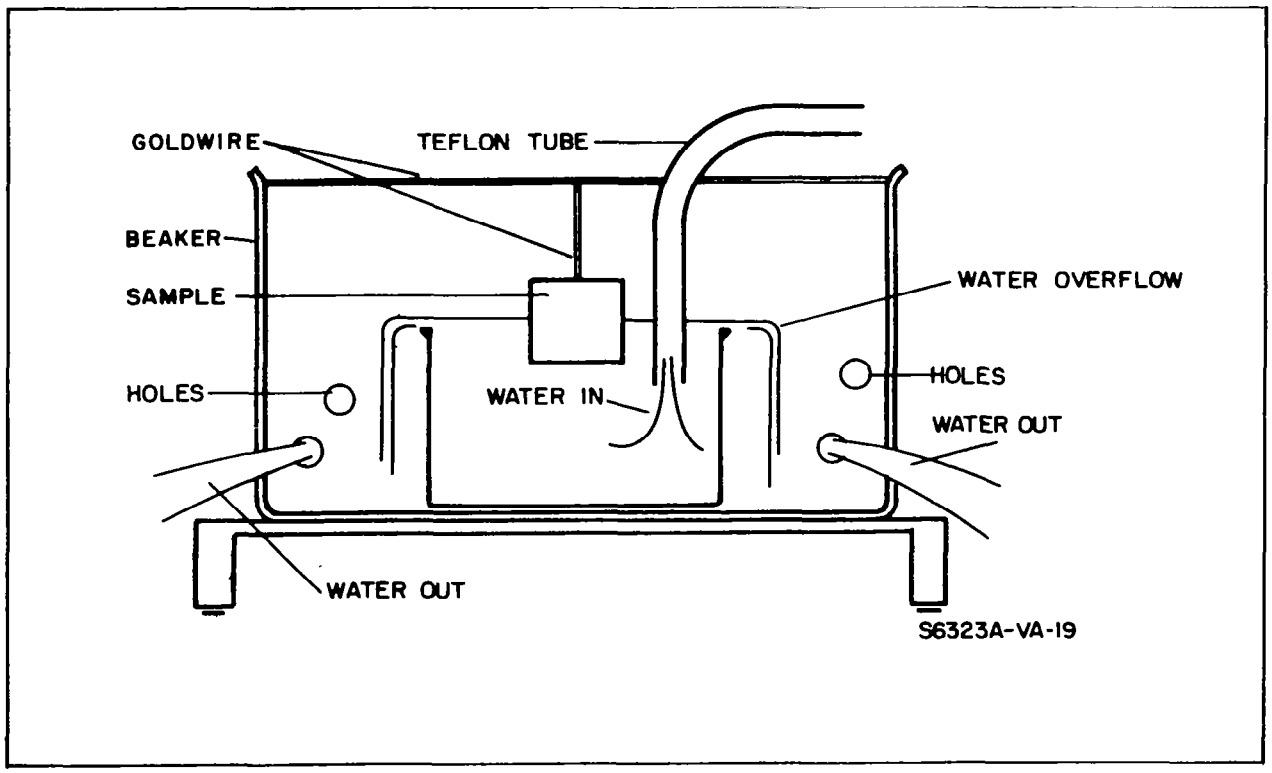


Figure 3-33. Wafer Rinsing in Deionized Water

After the rinse, the unit was tested for hydrophobic contaminants by tilting the header and letting the water run off the wafer. If the surface was free of hydrophobic contaminants the water film that remained on the surface dried slowly and interference fringes were seen at the edge of the film. On the other hand, if the surface was not free of hydrophobic contaminants, the film broke and the water ran off the surface.

After completion of the etching and rinsing procedure, a clean inversion layer was put onto the rinsed off front surface of the wafer. To accomplish this, the boiling water technique was used.[5,6] Following this procedure the header was float boiled in distilled water in quartz beakers for about 30 minutes after completion of the rinse. After a thorough cleaning, four beakers were filled completely with distilled water and the header was immersed in them in such a way that the wafer just touched the surface of the water. Most of the upper part of the header was out of the beaker and the emerging vapors were blown off by the blower of the fume hood. There was no vapor condensation on the side of the header and thus the water did not condense on the side of the unit and it did not run back into the clean boiling liquid. In this manner, the distilled water was kept clean, preventing contamination of the etched surface. This procedure was repeated four times over a 30-minute period with four quartz beakers filled with distilled water. This treatment left a thin p-type inversion layer on top of the high resistivity n-type layer. After completion of this procedure, the side of the header was dried with filter paper and the unit was returned to dry under the infrared lamp.

After a drying period of 24 hours under an infrared lamp at a relative humidity of about 42 percent, an n-type edge-protecting epoxy was applied around the periphery of the wafer. This edge protection covered up the junction between the slice and the hardened R-313 resin (figure 3-34). The edge-protecting epoxy CIBA 502 and its hardener Araldite 951 were obtained

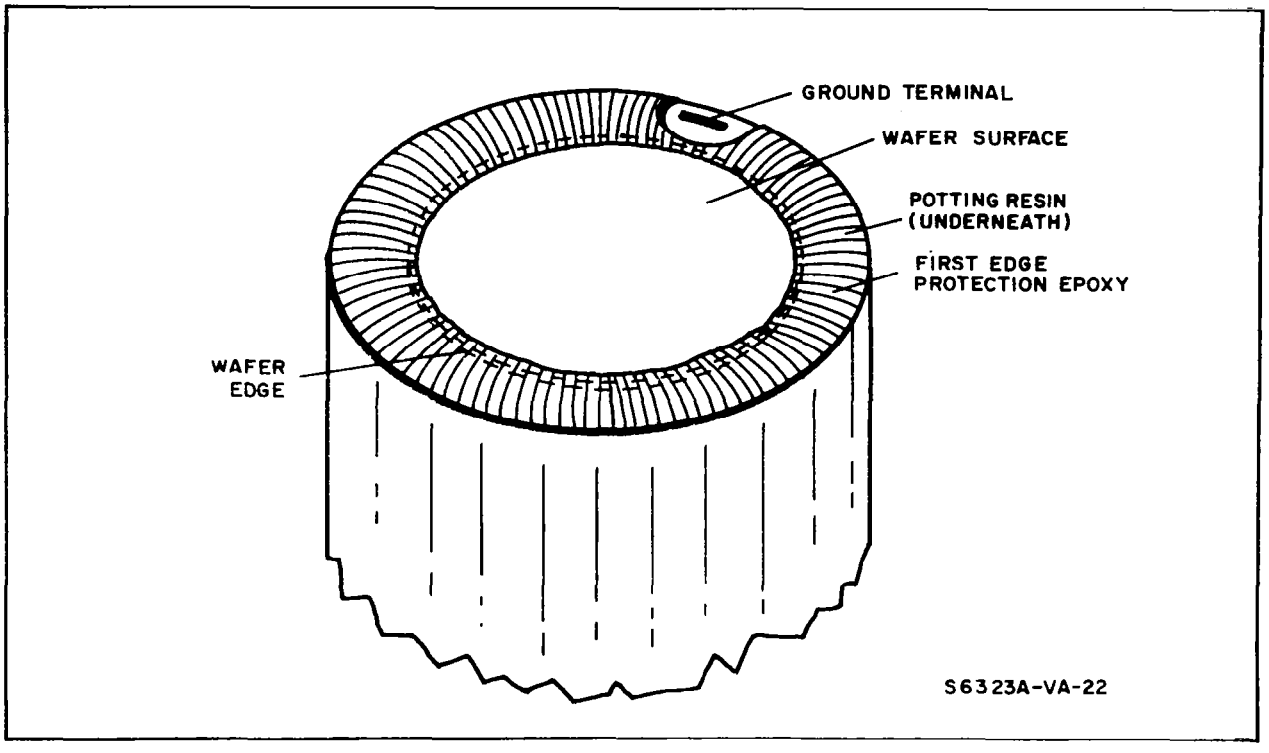


Figure 3-34. Detector After Application of First Edge Protection

from CIBA Products Corporation, Fairlawn, New Jersey. The resin and the hardener were mixed in a ratio of 10 to 1 and then the bubbles originated by mixing the two together were expelled by treatment of the mixture under vacuum for about 20 minutes. This mixture was then applied to the unit as shown on figure 3-35. Araldite 951 is an amine type hardener. Upon applying the mixture containing Araldite 951 to the unit, its surface under the resin covering it was made strongly n-type. This converted the p-type inversion layer back to n-type again. The unit was then exposed to 100° C for 24 hours in a dry atmosphere to thoroughly dry the water out of the epoxy and out of the silicon surface. This drying was done in a quartz tube (2 inches in diameter, approximately 2 feet long) having ground glass male joints at each end. Linde 13X drying compound and a thermometer was placed into one of the ground glass caps fitting onto one end of the tube. The header was

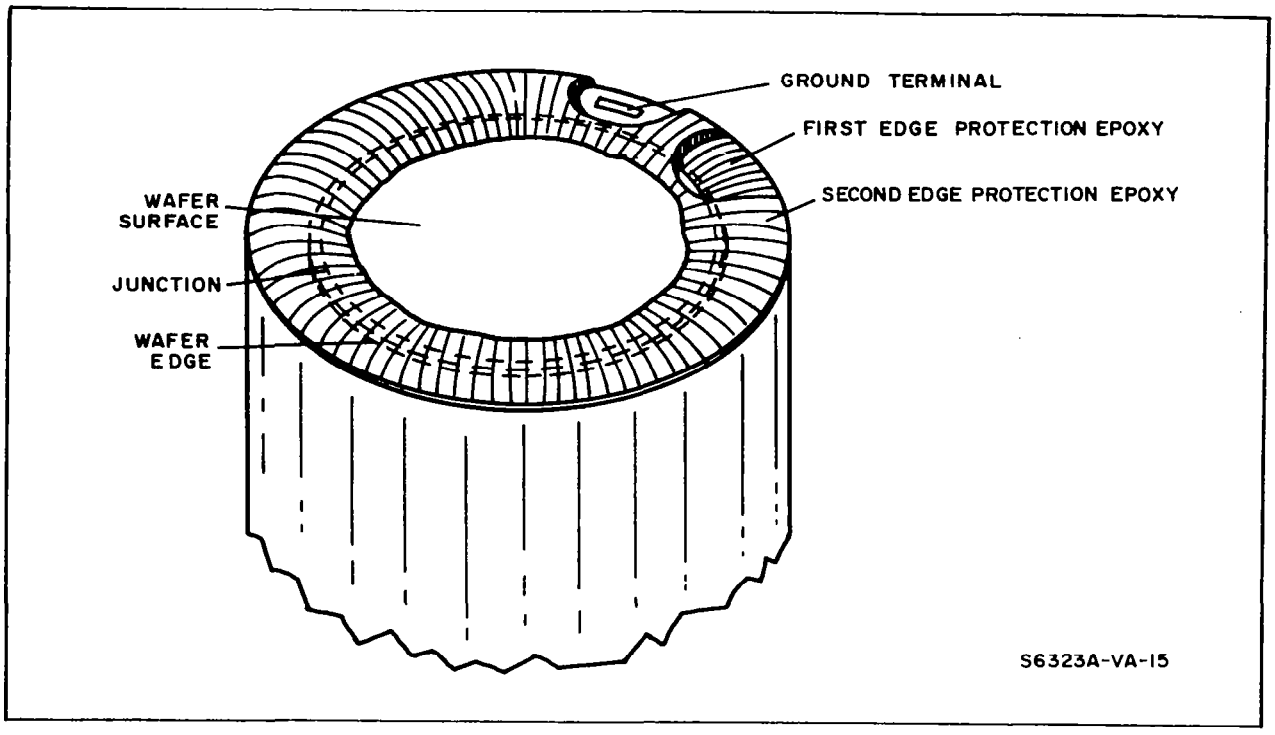


Figure 3-35. Detector After Application of the Second Edge Protection - Note Junction Embedded Between the Two Epoxies

inserted through the other end of the quartz tube. The other cap was then used to hermetically close the tube. A nichrome heater jacket around the tube activated by a variac was then turned on and provided the required temperature of 100°C.

Following the 24-hour drying cycle in the dry atmosphere, the tube was allowed to cool and the header was unloaded. It was then put into the upper level of a dessicator partially filled with a saturated solution of calcium nitrate. The humidity of the enclosed air in equilibrium with the calcium nitrate solution was approximately 51 percent at room temperature. This provided a suitable atmosphere to populate some of the surface states depleted during the previous drying cycle.

After 24 hours at 51 percent humidity, the unit was taken out of the dessicator and a second edge protection was applied. This edge protection,

5 parts of CIBA 502 mixed with 1 part of an amine free hardener (214 obtained from Epoxylite, South El Monte, California) caused the silicon surface underneath it to become p-type. This resulted in a circular junction, positioned at the common boundary between the two epoxies. It was then covered and protected by the second epoxy coating. The purpose of the amine free hardener was to make the epoxy turn the surface under it to p-type. However, this was a marginal process, and in order to ensure the p-type silicon surface under the potting compound, 1 percent iodine was added to the resin before the hardener was mixed in. The iodine in the compound then made it certain that the surface under the resin became strongly p-type. It was convenient to mix the iodine into the CIBA 502 first and chill this mixture on ice while the hardener was added and agitated. The ice bath prolonged the hardening time of the compound and enabled its application to the silicon before setting. The working time of the mixture at room temperature, the time before it sets, was only about 1 minute, and it could not be applied smoothly to the surface of the wafer.

Following the application of the second epoxy at a controlled humidity of 35 percent, the unit was inserted into a quartz tube heated by an infrared lamp. Filtered room air at about 35 percent humidity was then gently blown across the silicon surface for 24 hours. The apparatus for drying and air rinsing is shown in figure 3-36. During this procedure a thermometer placed near the wafer indicated about 65° C. This treatment usually prevented the wafer from discoloration and/or hazing and the slices, when finished, had a resulting bright and shiny surface.

The next and the final step in preparing the units was the evaporation to lay down a film (50 $\mu g/cm^2$) of gold onto the thin (50 Å) porous oxide. This gold film made contact to the inversion layer and connected it over the hardened epoxies to the ground terminal (figure 3-37). This evaporation had to be done under extremely well controlled conditions, since the slightest trace of oil from the pump could be detrimental for the diode. For this reason, a separate evaporation station was built to evaporate only this thin layer of gold.

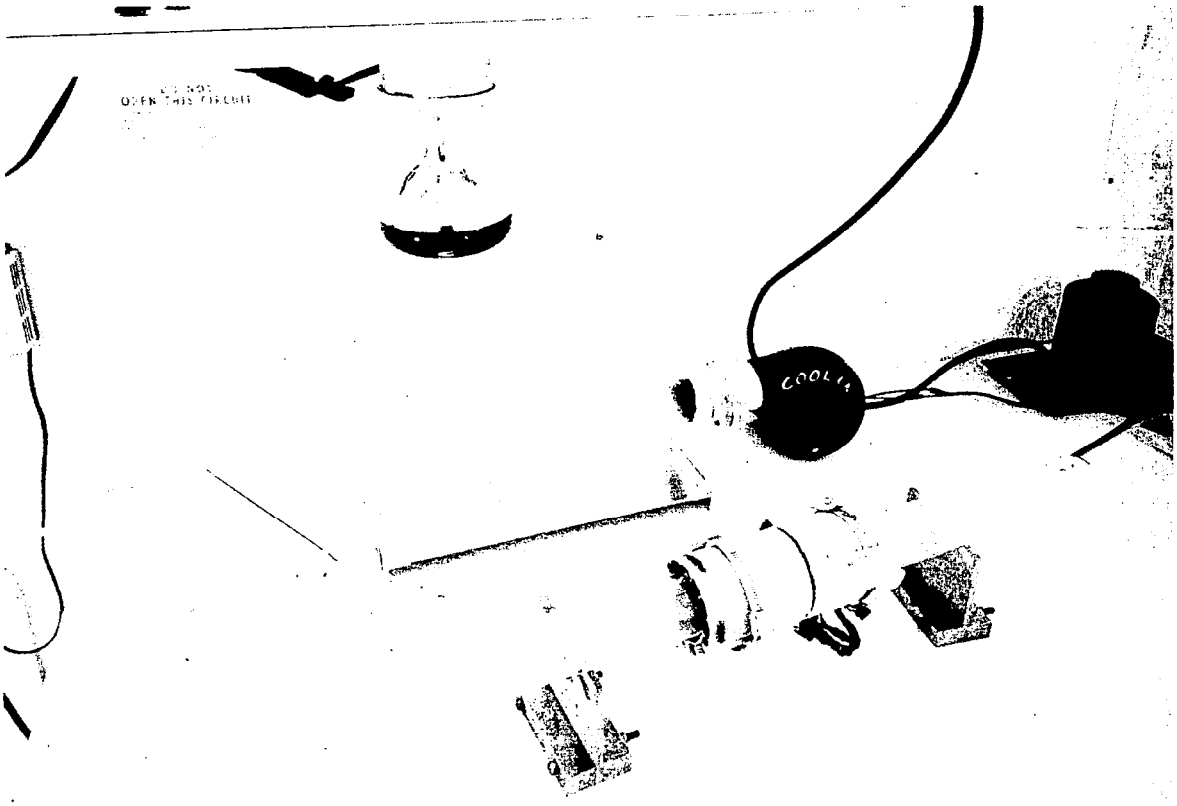

Figure 3-36. Drying Setup to Cure the Second Edge Protection

This evaporator (figure 3-18) differed from conventional units by having in addition to the standard liquid nitrogen cold trap another trap filled with Linde 13X molecular sieve. This molecular sieve could be closed with the help of two vacuum valves. The trap was open only while an evaporation was in progress or while it was baked out. During outbake, lasting for several hours, a tape wound around the outside of the trap maintained the wall temperature of the trap at 300° C. The bottom valve was open at this time so that the moisture generated from the molecular sieve could be withdrawn through the diffusion and forepumps. At the close of the outbake the heater was turned off, the valve was shut, and the trap was allowed to cool down slowly.

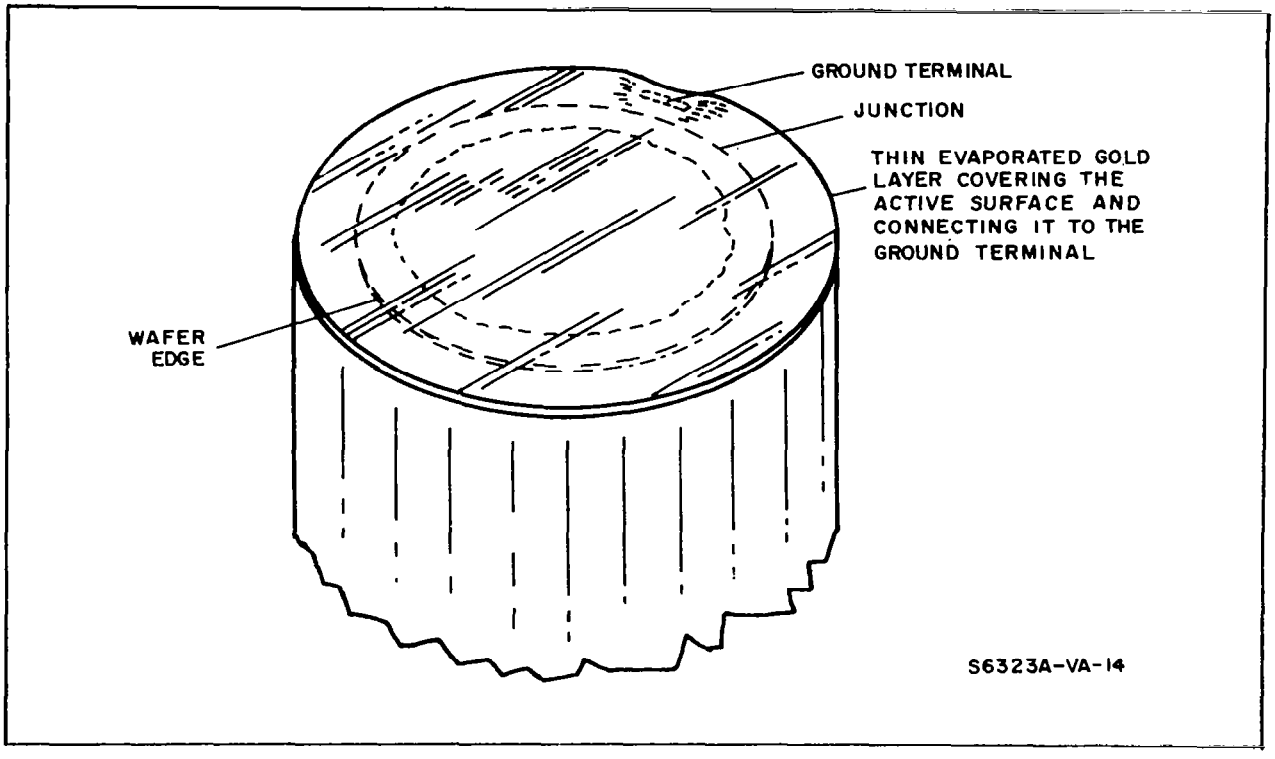


Figure 3-37. Detector After Evaporation - Thin Gold Layer Contacts the Active Area to the Ground Terminal

The evaporation was done at a pressure of about $5 \times 10^{-5}$ Torr or lower using a bright dipped (a chemically etched) and degreased (boiled in trichloroethylene) molybdenum boat. The gold used was 99.999 + pure and about 3 pieces of it each 1/8 inch in diameter and 1 inch long were placed into the boat. Current running through the boat held in copper jaws melted and evaporated the gold. To suppress contamination, a molybdenum shield (figure 3-19) was put over the boat and also over the resistance monitor and over the unit to be evaporated onto. The glass bell jar then fitted over this molybdenum shield. In this way the molten gold was exposed to a molybdenum environment only, with the exception of the sample and the resistance monitor. The above mentioned resistance monitor consisted of a 1- x 3-inch glass piece, with chromium and gold evaporated onto it for contact purposes leaving the middle 1/2 inch of the glass free of evaporant (figure 3-19). Contacts were made to both coated ends of this glass piece.

These two terminals were connected to an external ohmmeter through a feedthrough. Before commencing to evaporate, the ohmmeter resistance read infinite. At the beginning of the deposition the resistance between the two terminals decreased, together with the reading on the ohmmeter. When the resistance reached a predetermined value the evaporation was stopped. The gold thickness aimed at was 50 $\mu g/cm^2$ (about 500 Å), which corresponds to about 7 ohms per square. When the ohmmeter reading recorded 14 ohms (2 squares) the evaporation was stopped, the cold trap was then warmed up, and the detector was unloaded. After aging the unit for about 1 day it was ready for testing.

# 4. TEST APPARATUS AND TESTING

## 4.1 GENERAL

The fabricated units were tested with an Oak Ridge Technical Enterprizes Corporation (ORTEC), 101-102 low noise preamplifier-amplifier system, an Atomic Instrument Company Model 510 pulse height analyzer, and a Berkeley Instrument Company Model 7160 scaler (figure 4-1). A radioactive electron source ($Sn^{113-119}$) was used first to supply 36 keV conversion electrons. Later an electron gun with variable accelerating voltage was employed as the electron source. This source also provided an electron source of variable intensity.

The 101 preamplifier acts as a linear amplifier of the input charge, but does not linearly amplify the input voltage. As mentioned above, when a charged particle enters the silicon wafer, it creates electron-hole pairs and looses energy at the rate of approximately 3.5 electron volts per electron-hole pair formed. The electric field present in the depletion zone separates these charges and drifts them out of the depletion zone to the respective contacts. This charge, induced on the rear contact, causes a decrease in the positive bias relative to a ground potential on the front electrode. In effect, this is a negative pulse at the back contact. The magnitude of the voltage pulse is a function of the total apparent capacitance.

$$V = \frac{Q}{C_{Total}}$$

with Q being the charge "deposited" by some incident particle and $C_{Total}$ being the sum of the effective detector capacitance and all other input capacitances to the preamplifier.

Since the voltage pulse is dependent on the capacitance of the diode and the input circuits, utilization of a charge-sensitive preamplifier input configuration

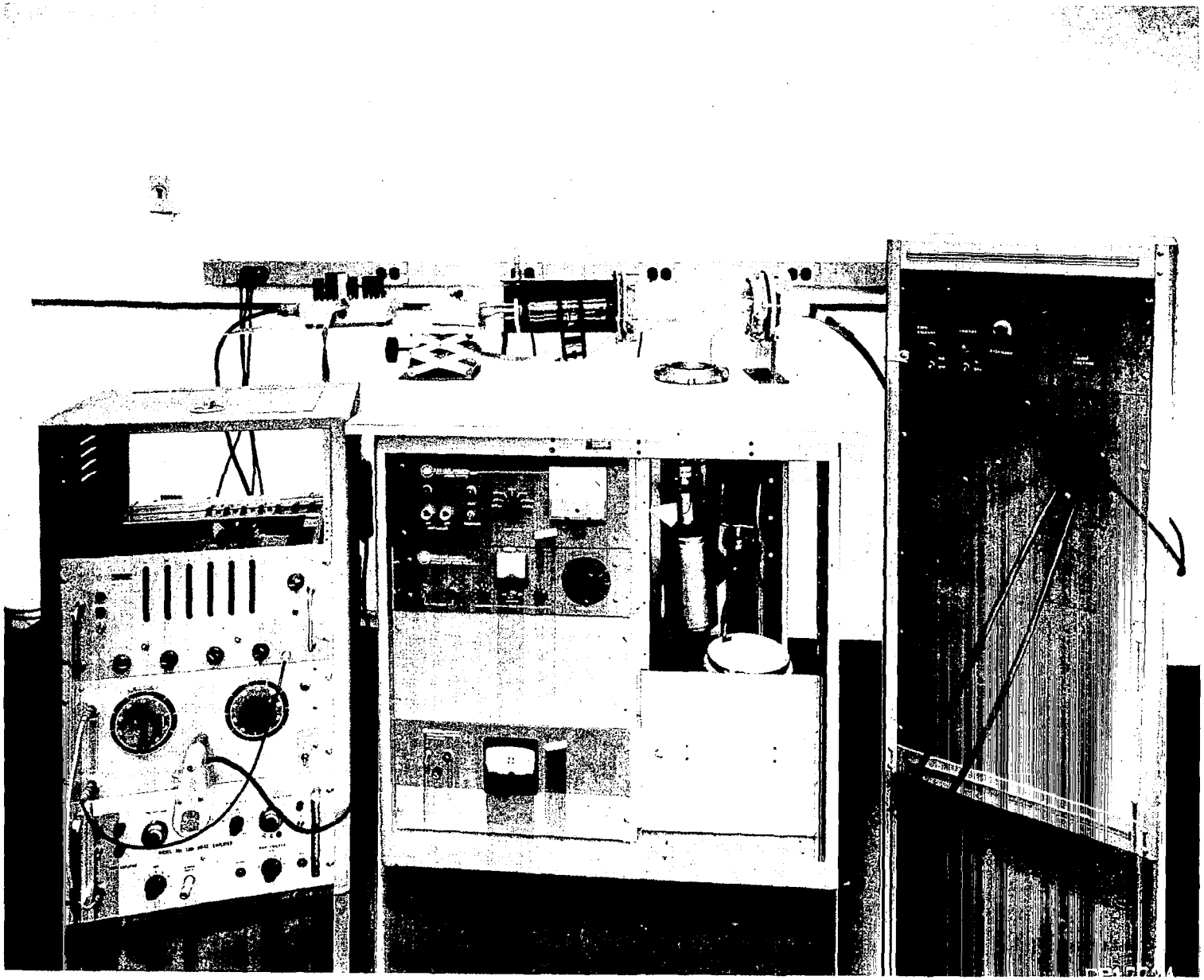

Figure 4-1. Test Setup - ORTEC Preamplifier-Amplifier System, Atomic

is highly desirable. In the Model 101 preamplifier, a voltage amplifier is provided with a negative feedback path via a series capacitor. It then becomes an integrating amplifier or simply a charge-to-voltage transducer. Now, sensitivities may be discussed in terms of voltage output per coulomb of charge deposited. Typical values for the 101 preamplifiers are $1.46 \times 10^{13}$ volts/coulomb which can be restated as 0.67 volts/MeV or 2.45 μV/ion pair for silicon detectors. Utilization of the gains of the main and postamplifiers (16 and 16) provides the maximum charge sensitivity figure of 1.93 volts per keV of particle energy. If a voltage sensitive amplifier were used, the available voltage at the input grid would be

$$\Delta V = \frac{\Delta Q}{C_D + C_{stray}}$$

where $C_{stray}$ includes capacitances due to the signal lead, etc. For a typical detector, $C_D$ may be 20 pF and $C_{stray}$ 25 pF. The ΔV figure becomes

$$\Delta V = \frac{0.457 \times 10^{-19} \text{ C/eV}}{(20+25) \times 10^{-12} \text{ F}}$$

$$\Delta V = 1.02 \times 10^{-9} \text{ volts/eV}$$

$$= 1.02 \text{ millivolts/MeV}$$

subject, of course, to amplification. The important thing to notice here is the effect of the capacitance, and the relative magnitudes of the stray and detector capacitances. Generally, the best signal-to-noise ratios are obtained with high resistivity detectors of small area with large bias voltage applied; great care should be taken to minimize stray capacitances.

As to the circuitry constituting the detection system, the preamplifier consists of a charge sensitive cathode input, second amplifier, and cathode follower output. The pulse shaping in the preamplifier consists of two integrating and two shaping networks. The 201 amplifier consists of two separate units - the main amplifier and the postamplifier. The main amplifier consists of two amplifying stages and a cathode follower. A feedback network limits

its gain to 200 and its rise time to 0.3 μsec. The input can be varied with a step attenuator by 16 in steps of factors of two. The output of the main amplifier has a maximum linear output of 100 volts. The postamplifier will further amplify the pulse by the feedback ratio determined by the gain switch (up to 16). The output is then obtained from a low impedance cathode follower. The bias on this amplifier is adjustable from zero to 100 volts in order to eliminate some of the input noise through the main amplifier from the detector. The maximum output of the postamplifier is again 100 volts.

The Atomic Instrument Company pulse height analyzer accepts the pulses put out by the postamplifier and according to the setting of its base level and width of the window it will select pulses with their tops in the appropriate voltage range. Only these pulses will be registered and for each one of these pulses a 1.5-volt negative pulse is fed by the cathode follower to the scaler.

The Berkeley Division Beckman EPUT Meter then will count the pulses put out by the pulse height analyzer using a decade type flip-flop arrangement. The number of incoming pulses then can be read off of the decade type scale display.

The radioactive source to activate the detector came from Oak Ridge Technical Enterprizes Corporation. It is a $Sn^{113-119}$ isotope deposited on a circular piece of plastic and covered by a thin evaporated film to prevent flaking (figure 4-2). For ease of handling it was held between two circular brass rings. The half life of this isotope is about 115 days and it supplies conversion electrons at 36, 365, and 389 keV. The intensity at each of these energies is shown in figure 4-3. The nominal total activity of this source is 1 microcurie and no Atomic Energy Commission license is required for its purchase.

A more elaborate adjustable voltage and intensity electron source was provided by the electron gun setup. This apparatus was built around a glass T (figure 4-4) with an electron gun fitted into one arm of it, while a movable detector receptable, feedthroughs, baffle, and shield were built into the other one. The vacuum was drawn through the leg of the T.

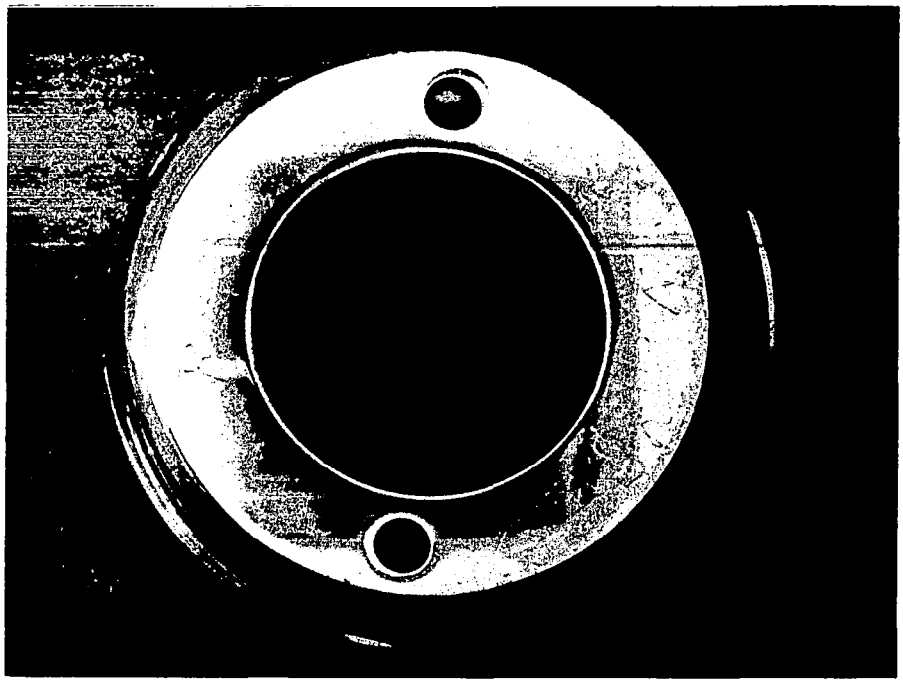

Figure 4-2. The Radioactive Tin Source ($Sn^{113-119}$)

The electron gun (figures 4-5 and 4-6) was constructed in the Electron Optics Technology Laboratory. It consists of a tungsten coiled filament in a stainless steel tube with the tube spot-welded along its seams. A low positive voltage of 22-1/2 volts was applied to a grid by mercury batteries in front of the filament in order to create a space charge reservoir from which these electrons can be drawn toward the front of the gun. At the front of the tube there is a pinhole through which some of the electrons entered the glass envelope. Once in the glass envelope, these electrons were accelerated by about 50 keV toward the detector end of the glass T. At the detector end, these accelerated electrons entered a tantalum shielding tube. At the far end of the tube, the electrons encountered a fixed position baffle with a small pinhole through it. Most of the electrons hit the baffle, but some of them went through the small pinhole and hit the detector behind it. P-3 phosphor was deposited on the baffle around the pinhole to indicate whether or not the particles were approximately on target. When the beam was on target, the phosphor around the pinhole lit up in a vivid green color. A movable detector situated behind

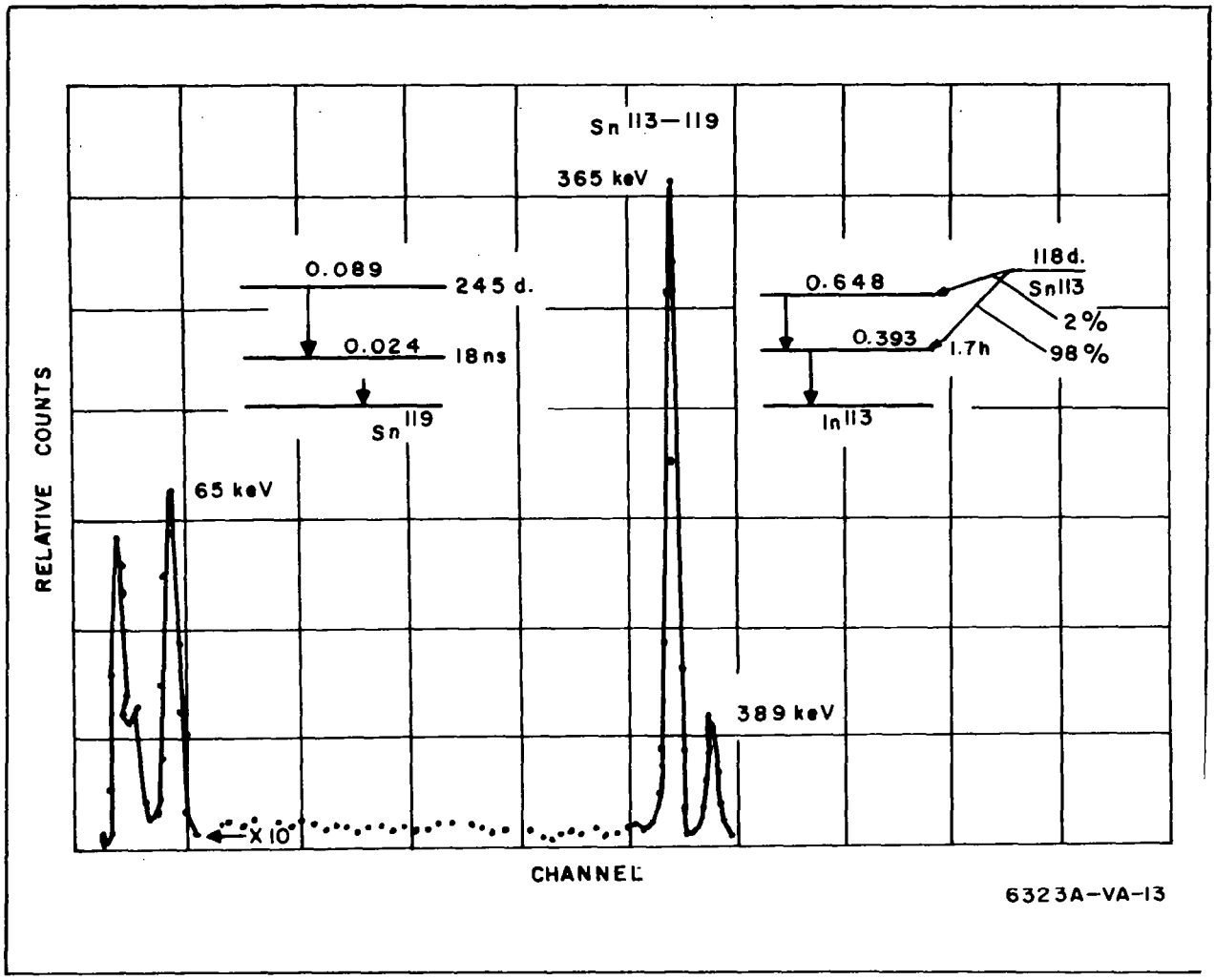


Figure 4-3. Intensity vs Energy Spectrum of the $Sn^{113-119}$ (Tin) Source

this pinhole could then accept electrons over all of its 1/2- x 1/2-inch area b positioning the moving detector so that the appropriate detector region was situated immediately following the pinhole in the baffle.

The receiving end of the glass T has, as mentioned before, a ground glass joint female socket attached to its steel flange. The sealing was done with several transitional glass seals and metal welds (figure 4-7). The sample holder arm (figure 4-8) then fits into this socket. As can be seen from the schematic diagram, the sample to be tested was plugged into the 21-pin vacuum sealed plug of the sample holder arm. The 21 wires were led out from the

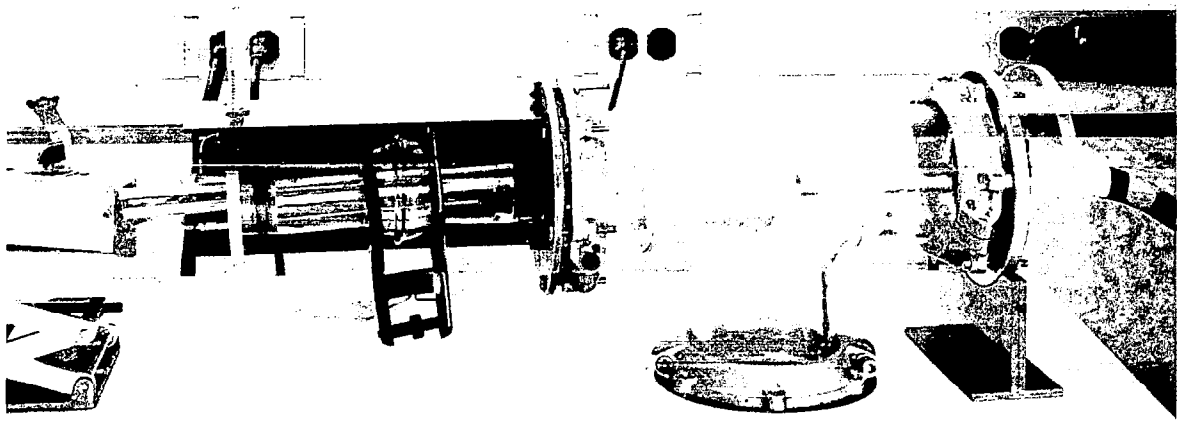

Figure 4-4. The Electron Gun Setup - Electron Gun on the Left-Detector

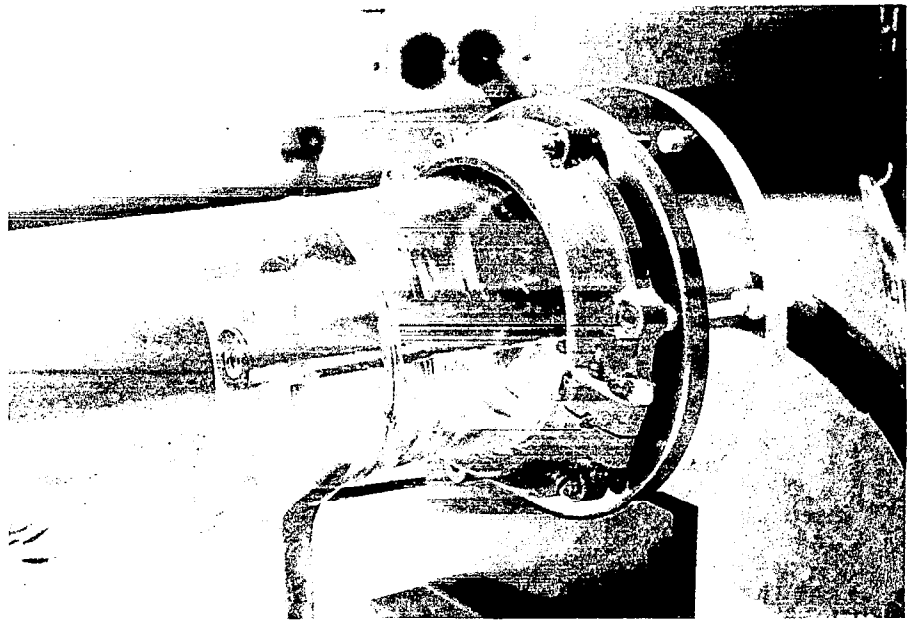

Figure 4-5. Electron Gun

back side of the feedthrough through a metal rod brazed to the feedthrough as shown in figure 4-9. This 21 pin-feedthrough was obtained from Electrical

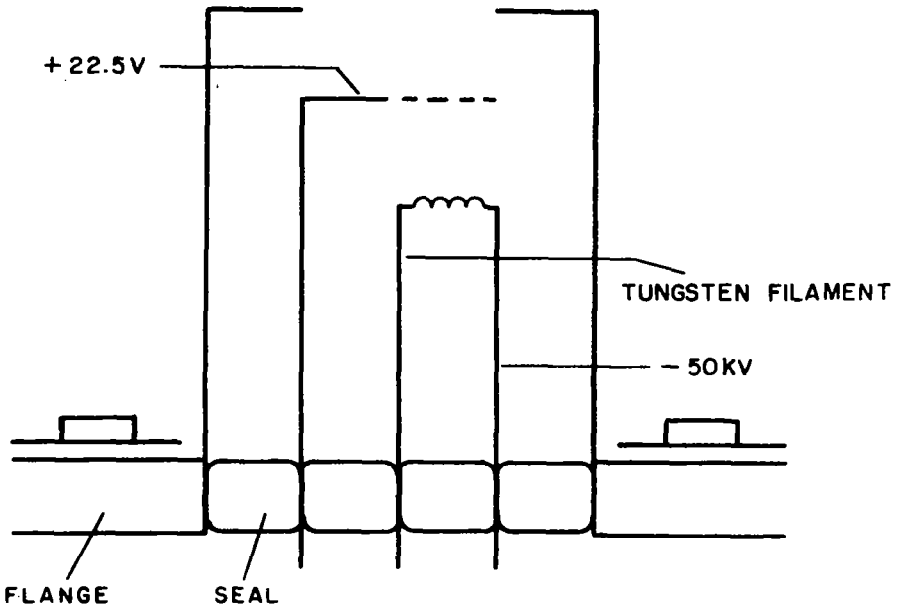


a. THE SCHEMATIC OF THE GUN CONSTRUCTION

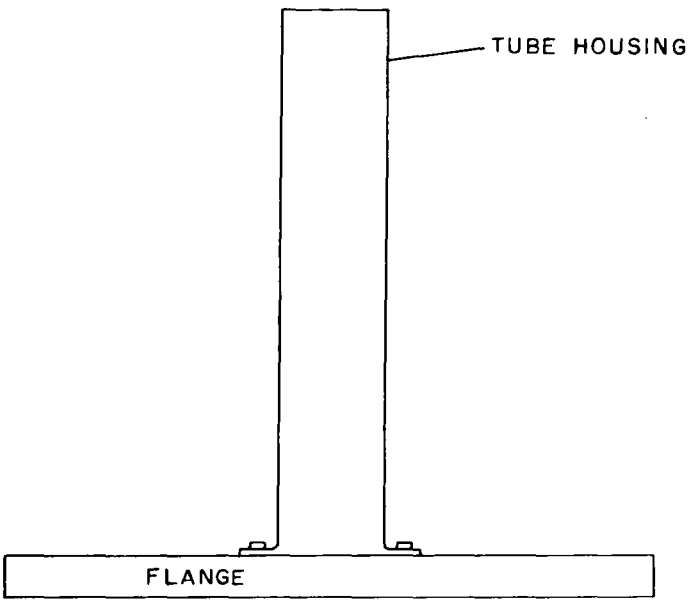


b. THE ELECTRON GUN HOUSING

6323A-VB-34

Figure 4-6. The Electron Gun Schematic

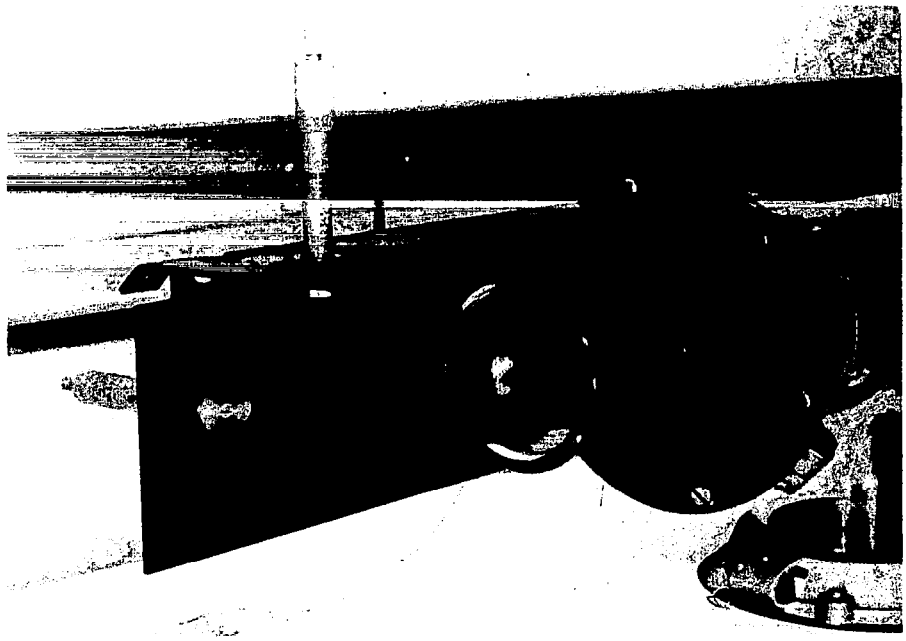

Figure 4-7. Female Ground Glass Joint and Metal End Plate

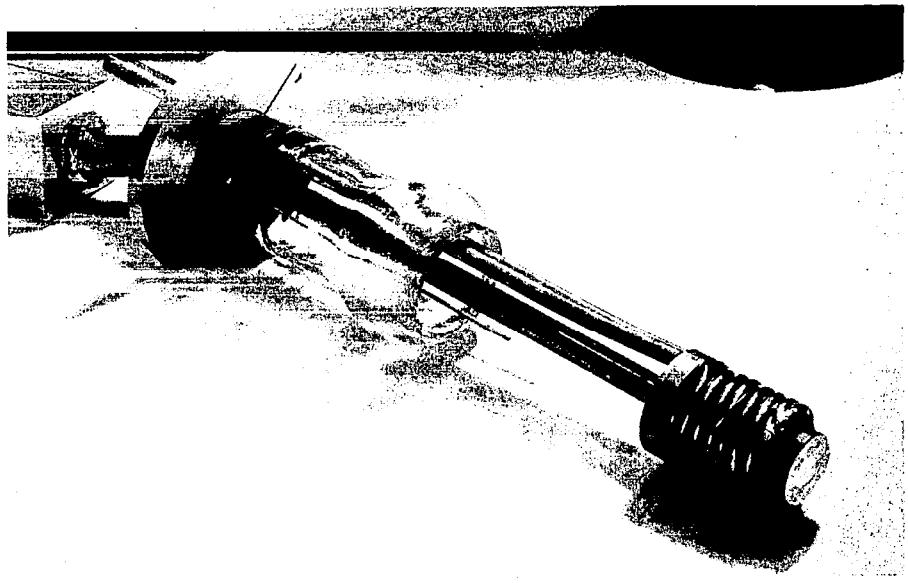

Figure 4-8. Sample Holder Arm

Industries, Incorporated in Murray Hill, New Jersey. It is vacuum tight and can be cooled to liquid nitrogen temperature without damaging it. The tube containing the wires was brazed onto it in hydrogen atmosphere after the

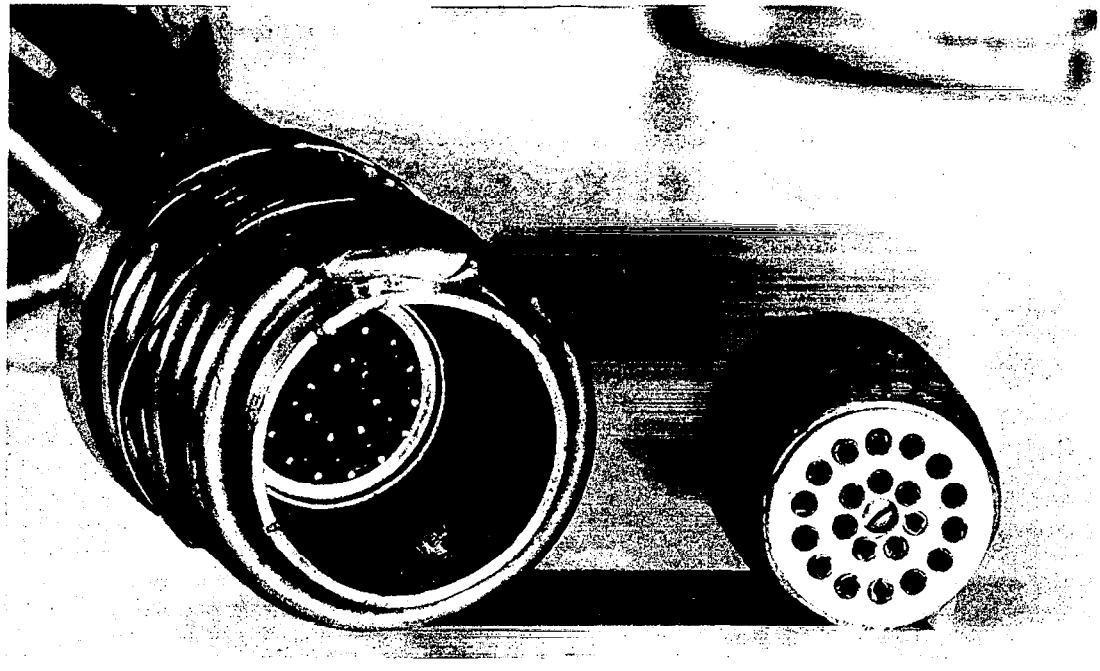

Figure 4-9. 21-Pin Vacuum Feedthrough Inside the Sample Holding Cup

wires were soldered to the individual pins. During this brazing operation, care was taken so that the heat did not spread from the area to be brazed to the solder joints holding the wires to the pins, since this would melt the solder and cause open circuits for several, if not all of the channels.

Cooling of the detector during operation could be provided using copper cooling coils wrapped around the cup containing the sample. The ends of this coil were brazed into two holes on the end plates. Liquid nitrogen could be blown into these tubes from the liquid nitrogen tank. This can be done using compressed air over the top of the liquid in the enclosed can. All welds on the cooling coil and entrance coil were vacuum tight, since the pressurized liquid nitrogen had to be kept outside the vacuum chamber. The two remaining wire feedthroughs on the back plate were for insertion of two thin 0.005-inch copper-constant thermocouple wires into the chamber to monitor the sample temperature.

The sample holder arm (figure 4-8) with the plugged in sample could be pivoted by its ball joint in the socket provided for it. In this manner, by

moving the sample in front of the baffle opening, the electron beam could scan all of the surface of the detector to be tested.

The steel attachment at the end of the arm served to provide X and Y registration of the arm with respect to the end plate to which it is attached. The micrometer travel in both vertical and horizontal positions could be recorded and reproduced. This enabled moving the arm and the sample in it in a prescribed and reproducible manner.

The 21 wires leading out from the feedthrough through the tube were connected to a 21-position selector switch. This in turn supplied pulses to the preamplifier one channel at a time.

The vertical opening (the bottom leg of the glass T) was used to pull the necessary vacuum for the proper operation of the system. The pumping system consists of a Vac-Ion and sublimation pump combination with a sorption pump replacing the fore pump. A Varian Model 921-0013 Vac-Ion pump control unit, a titanium sublimation pump power supply Model No. 922-0006, and a thermocouple control panel Model 972-0006 to control a Hastings thermocouple complete the assembly. The layout and arrangement of the pumping system is shown on figure 4-10.

According to proper operating procedure, the sorption pump was outbaked first using its heating mantle to drive out the excess air from the molecular sieve in the unit. After most of the air was driven to the atmosphere from the sorption container, the unit was closed and cooled to liquid nitrogen temperature. The pump was then kept at this temperature for about 1/2 hour. The valve of the unit to the enclosed vacuum system was opened then and the pressure of the whole system was monitored on the thermocouple gauge meter. When this pressure reached 10 micrometers, the sorption pump was shut off and the Vac-Ion unit was started. Besides the Vac-Ion pump, the system also contained a sublimation pump. This sublimation unit evaporated titanium from a filament inside it onto the walls of the pump enclosure. This atomic titanium then gettered gas molecules thus reducing the residual pressure. The pressure decreased to the vicinity of $10^{-9}$ torr in about 3 hours, if the system was

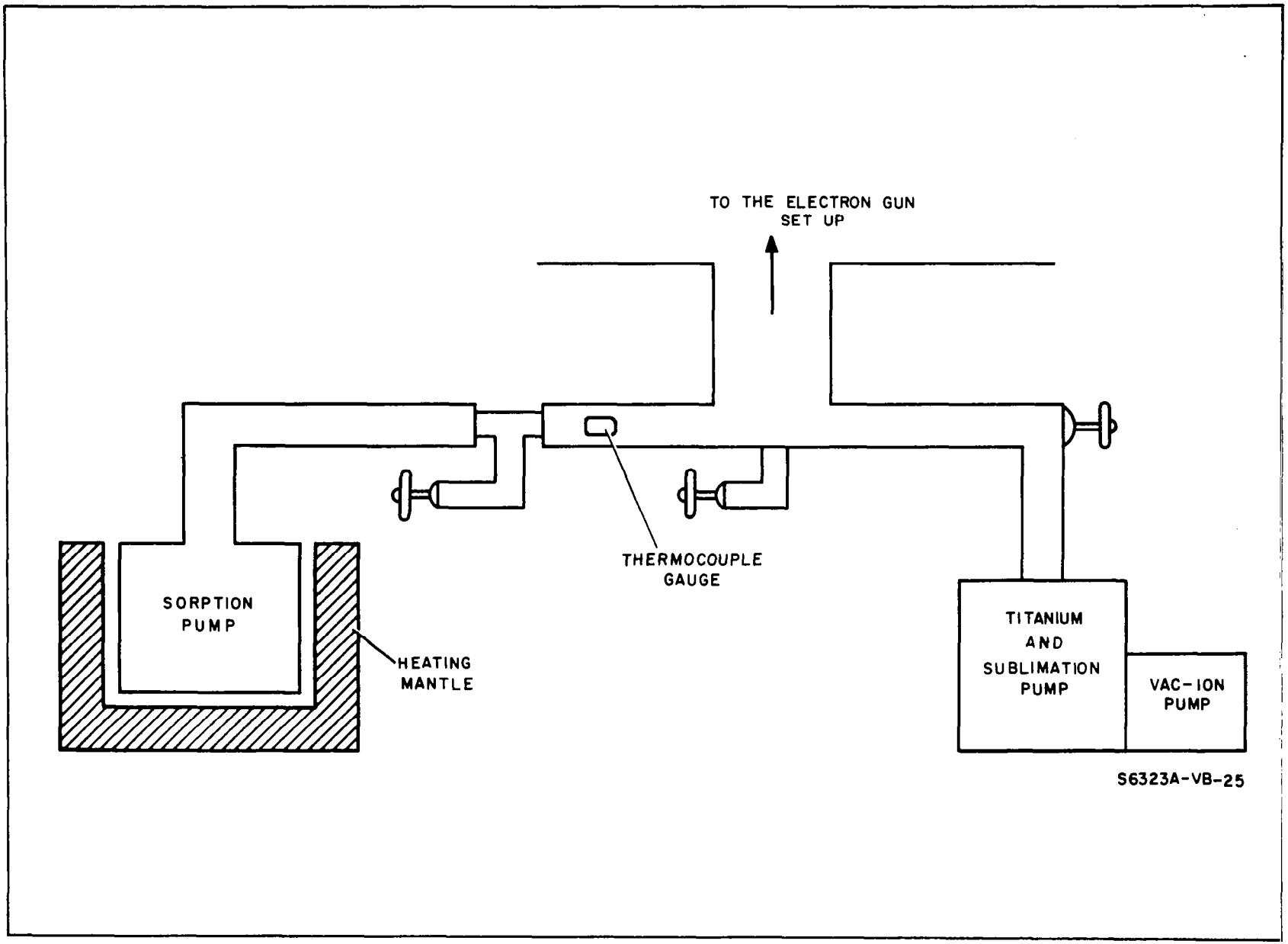


Figure 4-10. Schematic Diagram of the Pumping Unit

operated properly. To reach this pressure the sublimation pump has to work on a decreased duty cycle depending on the pressure. If the pressure was above $10^{-6}$ torr the titanium was sublimed 100 percent of the time. When the pressure was between $10^{-6}$ and $10^{-7}$ torr, the titanium was sublimed only 50 percent of the time. For pressures between $10^{-7}$ and $10^{-8}$, the titanium was sublimed only 25 percent of the time. Below this pressure the duty cycle was still lower, since there was enough titanium evaporated in the brief intermittent periods to getter most gas molecules present. Additional heating then only produced more gas molecules by heating the container walls and outdiffusing from them. This system worked well and efficiently after some initial difficulties were overcome.

The last piece of equipment of this setup is the 50-keV power supply. This supply consists of a 50-keV fixed supply which was varied through a potentiometer. The negative side of the supply has the filament heater winding on it to heat the coiled tungsten filament. After the necessary potting and isolation, the supply delivered about 45 keV, supplying the required low currents in the order of a few nanoamperes. The nanoampere range of current supply at 45 keV was checked for several days using a recorder amplifier and it was shown in a conclusive way that the supply was stable after a sufficient amount of potting and isolation.

The above paragraph completes the description of the testing apparatus. This apparatus worked well and supplied reliable and reproducible data after some of the initial difficulties were overcome.

# 5. CONSTRUCTION OF THE PHOTOSENSITIVE TUBE CONTAINING THE SURFACE BARRIER MOSAIC AND AN S-11 PHOTOCATHODE

The photosensitive tube containing both the surface barrier mosaic and the photocathode was constructed and operated in order to prove compatibility of the semiconductor element with the S-11 (ultraviolet) photocathode in a vacuum envelope at operating temperatures.

This tube was constructed in an H-like pattern (figures 5-1 and 5-2) with one leg of the H housing the UV photocathode, the indicating phosphor, the focusing coils, and the accelerating arrangement. The other leg of the H contained the passivated semiconductor element together with several getters. The two legs of the H housing were joined with a narrow glass tube containing an appendage pump to keep the cesium from migrating onto the sensitive side of the detector, and to keep the hydrocarbons outgassing from the passivated epoxy on the detector from migrating onto the cesium antimony photocathode.

One of the legs of the H housing was about 1-1/2 inches in diameter and had a quartz window attached to its front part with the help of a graded seal. The graded seal was followed by pyrex and uranium glasses, which then joined onto the 7052 glass constituting the body of the tube. After completion of the sealing operation, a mask was placed on the inside center of the front window and an aluminum evaporation followed. The deposited aluminum blocked the sides and the front of the glass cylinder, and the mask defined a 3/8-inch-diameter window in the center of the quartz front plate. This completed, a concentric pyrex cylinder was inserted into the tube. This cylinder had on the inside of it a vapor deposited chromium spiral to serve as the focusing coils. This spiral was made in the Electron Optics Technology Laboratory by coating the inside of the pyrex cylinder with cerium oxide and then using a lathe and scribing tool to erase the cerium oxide in a spiral pattern on the

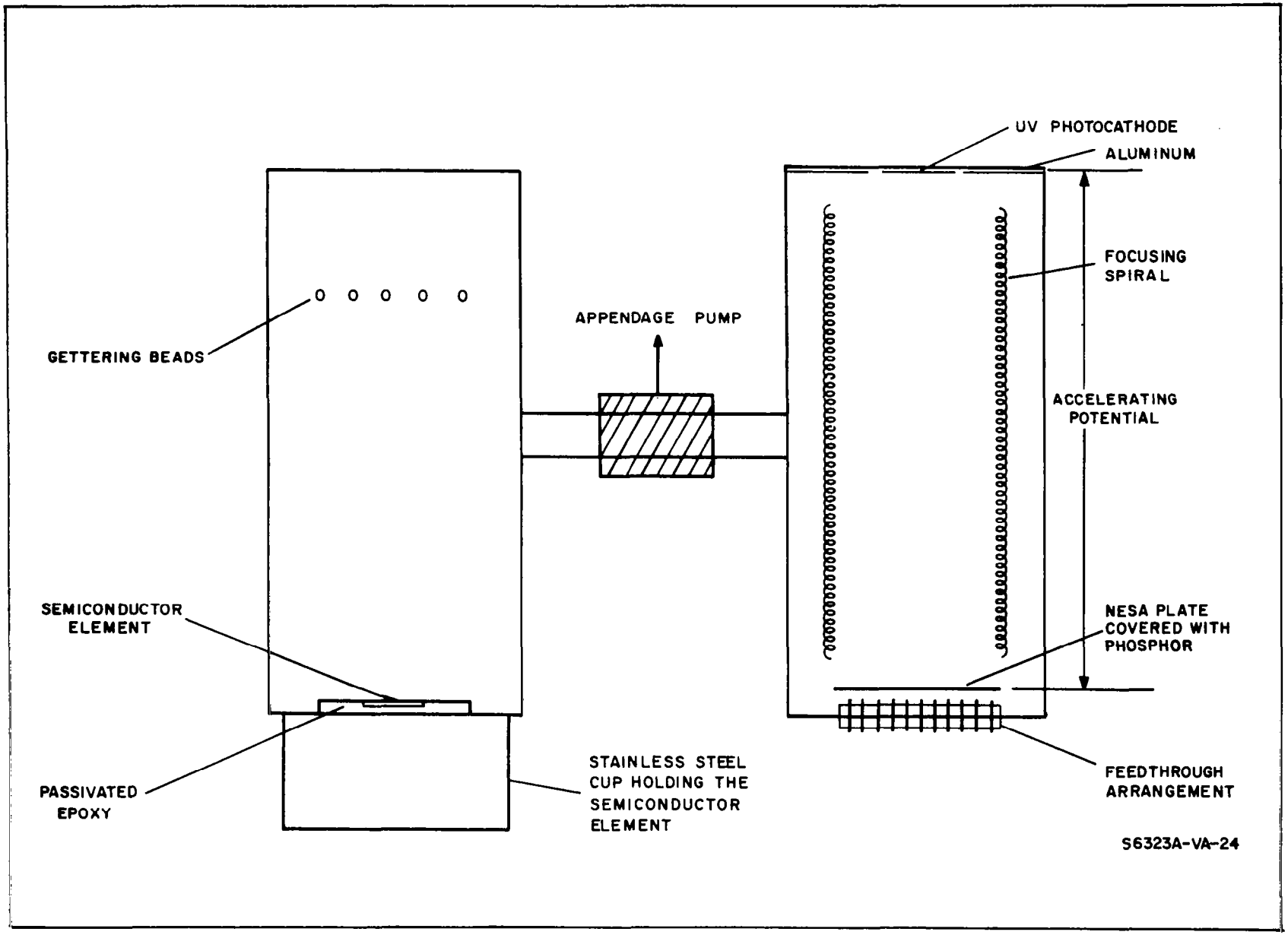


Figure 5-1. Schematic Diagram of the Hybrid Tube

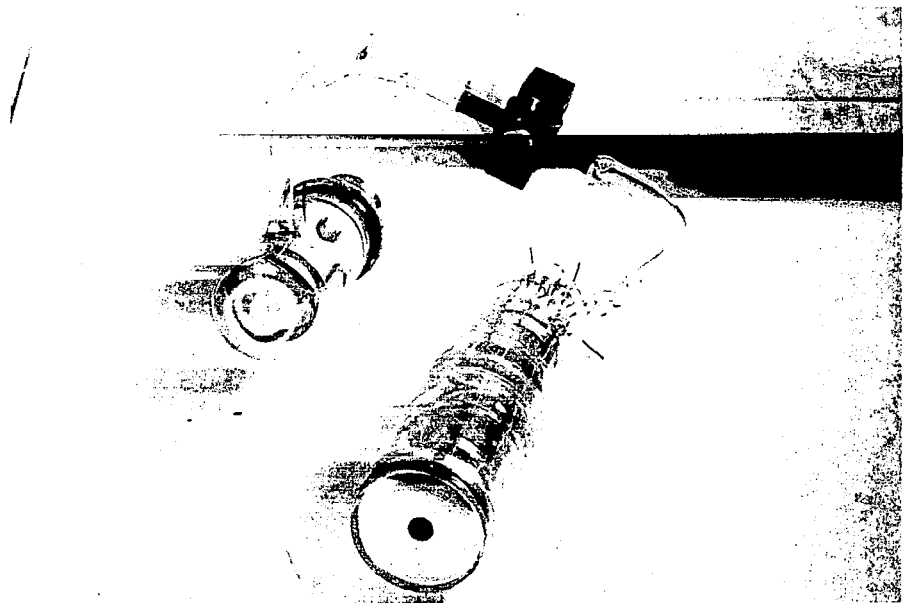

Figure 5-2. The Photon Sensitive Tube

inside of the tube. Following a cleanup of the erased material, sufficient chromium was evaporated onto the open spiral to give a total resistivity of about 2 megohms. The rest of the cerium oxide was then removed leaving a clean adherent high-resistivity chromium spiral well suited for focusing the photoelectrons (figure 5-3).

Next, a pyrex plate coated with a nesa (tin oxide) layer was attached to the bottom of the tube containing the spiral. The thin nesa layer was previously baked onto the plate at about 650°C and then it was sintered. A silver collector ring then was added to serve as an electrode to the conducting tin oxide ring. Next zinc oxide (P-11 type) phosphor was vapor deposited onto this plate and baked at elevated temperatures so that it firmly adhered to the nesa coating. The tin oxide coating had a resistance of less than 100 ohms square in order to enhance conduction and to avoid charging of the phosphor. When finished, this plate was attached to the cylinder containing the

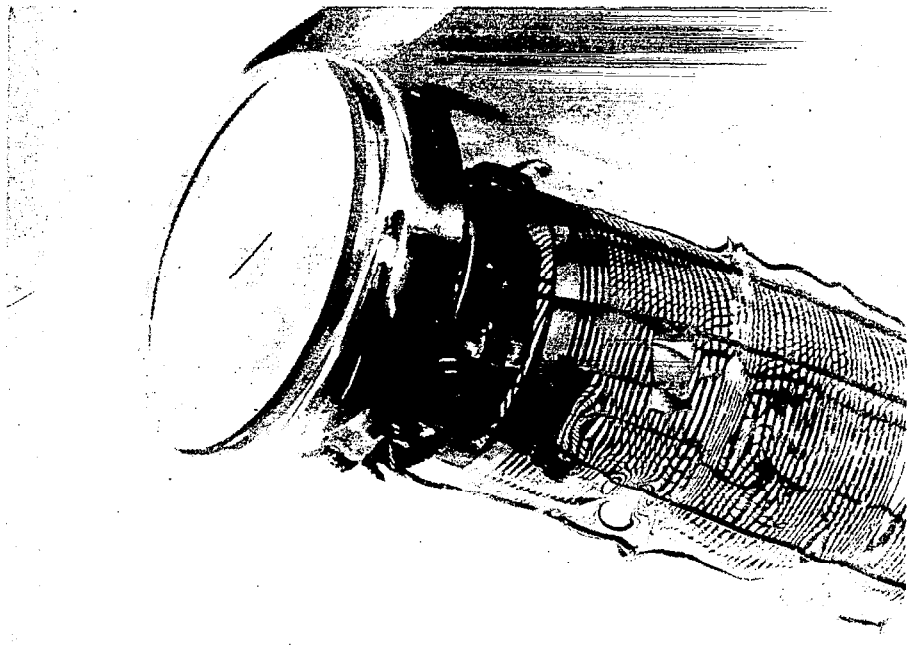

Figure 5-3. Photocathode, Front End of the Tube and Focusing Spiral

accelerating spiral, all connections were finalized and all leads were brought down to a vacuum feedthrough. That is, the collector lead from the nesa coating, the lead from the photocathode, two leads from the focusing spiral, and the various leads from the cesium channel and antimony beads, for use when evaporating the S-11 photocathode, were all brought down to the feedthrough. Following this the feedthrough was sealed to the glass cylinder completing the assembly of the part of the tube containing the photocathode. The above completed two pieces of 7052 stem were attached to the kovar extension of the small appendage pump. The appendage pump was then attached to both legs of the H forming a firm band between the two.

Next, the semiconductor element was prepared for encapsulation. First, it was baked out at 130°C overnight, and then a coat of torr-seal was applied to the epoxy-covered front surface. Torr-seal is a low vapor pressure material made by Varian with its vapor pressure at $10^{-8}$ torr, or lower at

room temperature. This material hardens after mixing the two components, but it is not an epoxy. It is fairly strong after solidifying and can be used for structural purposes. It is also fairly acid resistant. After the first application of torr-seal, the unit was again baked out at 130°C. This procedure then was repeated once more to ensure thorough potting of the epoxy. Next, the unit was plugged into a cuplike holder (figures 5-4 and 5-5) and a flange was tightened onto this holder with its underside first wetted with torr-seal. This arrangement was then baked for 12 hours in air at 130°C. The assembly then was heliarc welded onto the free end of the free second leg of the H. While heliarc welding, circular heat sinks were used to prevent the torr-seal temperature of exceeding 130°C. Actually, the flange was sealed to a cylinder flanged out of a piece of kovar which was previously sealed to the 7052 glass cylinder. Barium beads then were put into this tube for gettering purposes. The end opposite the semiconductor detector was previously narrowed down to fit a vac-ion pump. This vac-ion pump was now attached and the tube was put into a furnace to outbake. The temperature of the assembly was raised to 350°C with the exception of the semiconductor element. This element was just outside of the oven and was kept at 130°C. The outbake continued for several days until sufficiently low vacuum was achieved at the elevated temperatures. The tube then was cooled and sealed off. Immediately following the seal-off, the pressure in the tube was less than $10^{-8}$ torr, and the tube had a good visible and ultraviolet response.

The power for the appendage pump was supplied by six 500-volt batteries. This gave the necessary 3000 volts required for the operation of this pump. The 400-volt accelerating potential between the photocathode and collecting plate and the 1500 volts necessary to focus the photoelectrons also were provided by batteries.

Figure 5-4. Cup-Like Holder With the Semiconductor Unit in It - Front View

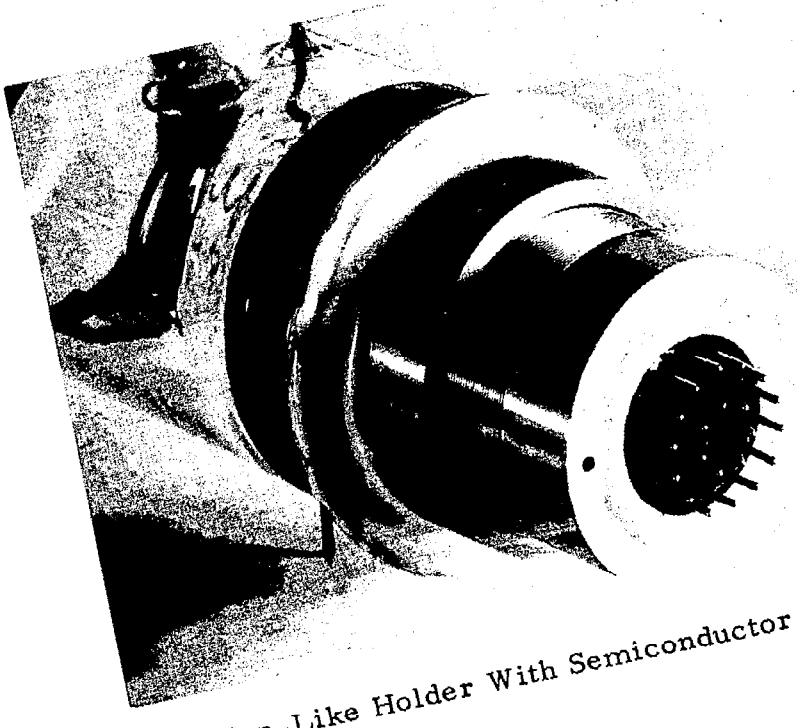

Figure 5-5. Cup-Like Holder With Semiconductor Unit in It - Rear V

# 6. ELECTRONICS FOR THE ELECTRON-SENSITIVE SOLID STATE MATRIX

The effort devoted to the peripheral electronic circuitry for the Electron-Sensitive Solid State Matrix will be considered in two parts. Part I is a discussion and analysis of the circuitry breadboarded and operated to demonstrate the feasibility of its construction and operation in an overall system. Part II is a discussion of the conceptual design of those portions of the electronic system which have not been breadboarded, but which are necessary for a complete working unit. Problems which were encountered in attempts to use off-the-shelf microcircuits are discussed and some possible approaches are outlined.

## 6.1 BASIC CONSIDERATIONS

Initial consideration for the design of the Electron-Sensitive Solid State Matrix electronic system was given to the amplifier design criteria. Since energy spectrum parameters usually measured by conventional nuclear-pulse instrumentation were already known constants and only the presence or absence of signal was required; the design requirements differed in several significant respects from conventional nuclear-instrumentation equipment. For example, the electron energy was predetermined by the sensor design, and in addition, it was not necessary to retain pulse shape. Also, signal-to-noise ratio was not a problem, and counting rate pile-up would not be present since this could be predetermined. However, low input capacity and high voltage gain with good overall stability was required in addition to fast transient response. Serious problems were presented by the low signal levels presented by the detector due to the relatively low energy of the impinging electrons. Also, the capacitive coupling between the inputs of the multiplicity of amplifiers connected to the matrix lines on the back of the sensor wafer also was a source of instability. This requires that actual physical input capacity be

kept to an absolute minimum. Active circuit techniques for reduction of input capacity by feedback are not satisfactory, since unwanted interelement coupling remains and may, in fact, be aggravated by the capacity-reducing feedback loops.

The question of using current- or voltage-mode signal processing was initially considered. Since the signal out of the detector has a duration of about 10 nanoseconds or less, it was felt that a voltage amplification system was desirable. There were several factors which supported this choice. One important consideration was that there was a uniform signal due to a fixed electron energy and it was not pertinent to consider an energy spectrum. In fact, there should be none. A second consideration in the choice was the microvolt signal level from the detector. Therefore, to overcome the problem of noise and extremely low level signal, voltage amplification was felt to be the most desirable mode of signal treatment.

The detector time constant which is the product of the resistance and capacitance shunting the detector terminals was physically small, and the resulting voltage step (which is given by the charge generated by the incident electron divided by the shunting capacity) would not be a factor of importance. The risetime was nearly equal to the duration of the current pulse and essentially independent of the time constant. It was felt that conventional transistor techniques would be capable of coping with the risetime and bandwidth needed. The signal level from the detector ran approximately 300 microvolts for a typical set of conditions. Since the subsequent processing circuitry required a signal level between 1 and 1/2 volt, the gain needed in the amplifier and preamplifier sections was on the order of several thousand.

It was previously noted that signal-to-noise ratio was not important. This statement is true only in the sense that the detailed resolution and width of the energy peaks are not a problem. These are known a priori. However, detecting the low energy signal pulse from a noisy background (in the communication sense) is a problem and does require the use of precautions to achieve a low noise input system. Computations (see paragraph 6.2) show that the voltage appearing on the input line to an amplifier will be below 500

microvolts. Since about 0.75 volts minimum is needed for triggering the subsequent multivibrator serial chain, an amplifier gain of about $10^4$ with a bandwidth of about 50 MHz is needed. The designs available both commercially and described in various publications were analyzed and one was chosen and modified for the specific requirements presented in the Electron-Sensitive Solid State Matrix system.

## 6.2 LINEAR AMPLIFIER STAGES

The input stage consisted of a field effect transistor. This is currently the best available device for the purpose. The advantages are low heat generation (unlike tubes requiring heater power) and a higher gain-bandwidth product as well as no jumps in gain or bias level caused by a thermal cathode. In addition, the requirement for low input capacity and large bandwidth dictated the use of a field effect transistor input section. Current mode amplification was ruled out since the counting rate was known to be low and would be adjusted so that it is low; therefore, there should be no problem with pulse pile-up and pulse tails. The simplicity introduced by using a voltage mode amplification system also was considered to be very attractive since the equipment was to be used in an unattended fashion and also configured in microcircuit structures. Unlike conventional nuclear instrumentation, no gating or other logical type operations need be carried out on the output pulses, and as a result, this simplification makes voltage amplification even more desirable. The optimum situation for a nuclear amplifier is when the decay time constant and the amplifier risetime are approximately equal.

In the case being considered, the shape of the detector current or voltage pulse is not important for the subsequent purpose, the mere presence or absence of the signal is the indication that is being sought. As a consequence, the circuit used consists of a field effect transistor input stage, a following stage consisting of a transmitter emitter follower, an impedance matching network, a grounded emitter amplifier with a local feedback amplifier to correct its impedance and stabilize its gain, and a subsequent emitter follower

which yields sufficient signal at a low impedance to drive the multivibrator serial chain. This is shown in figure 6-1. The 2N3819 was the final choice of field effect transistor for this use and was used in the grounded drain configuration with a 2k load. This configuration resulted in a low-noise, wideband input stage with sufficient gain to get the signal up to a conveniently utilized value. A 2N917 emitter follower stage with a 10k emitter was direct coupled to the source output of the FET. This resulted in almost negligible resistive or capacitive loading on the FET. A bias adjusting voltage divider allows the output potential to be set to allow dc coupling to a 2N917 amplifier stage with local feedback to its emitter from the 2N917 stage which also acts as an output stage. A zener diode acts as a voltage level shifter for the local feedback signal, and a 2N918 acts as an output emitter follower and could be used for feedback to the input bias resistor of the FET if this is desired. Under the particular conditions which were present, it was found that the feedback, which was usually of value in reducing the input capacity, contributed little because the capacity was already very low and did not present any problem such as would be found in a long cable line from detector to input amplifier. Signal gain was sufficient to trigger the multivibrator series chain. In the evaluation of the system, three amplifiers were built and had the inputs intercoupled to assess the problem of coupling. No problems resulted; however, there is a significant distinction in the coupling instability between three amplifiers and 128 amplifiers.

Calculations for the stages follow: Voltage amplification $A_V$ is given by

$$A_V = \frac{g_m R_L}{1 + R_L g_o}$$

where

$g_o$ = output conductance

$g_m$ = transconductance

$R_L$ = load resistance

typically $R_L g_o$ is much less than unity for the 2N3819.

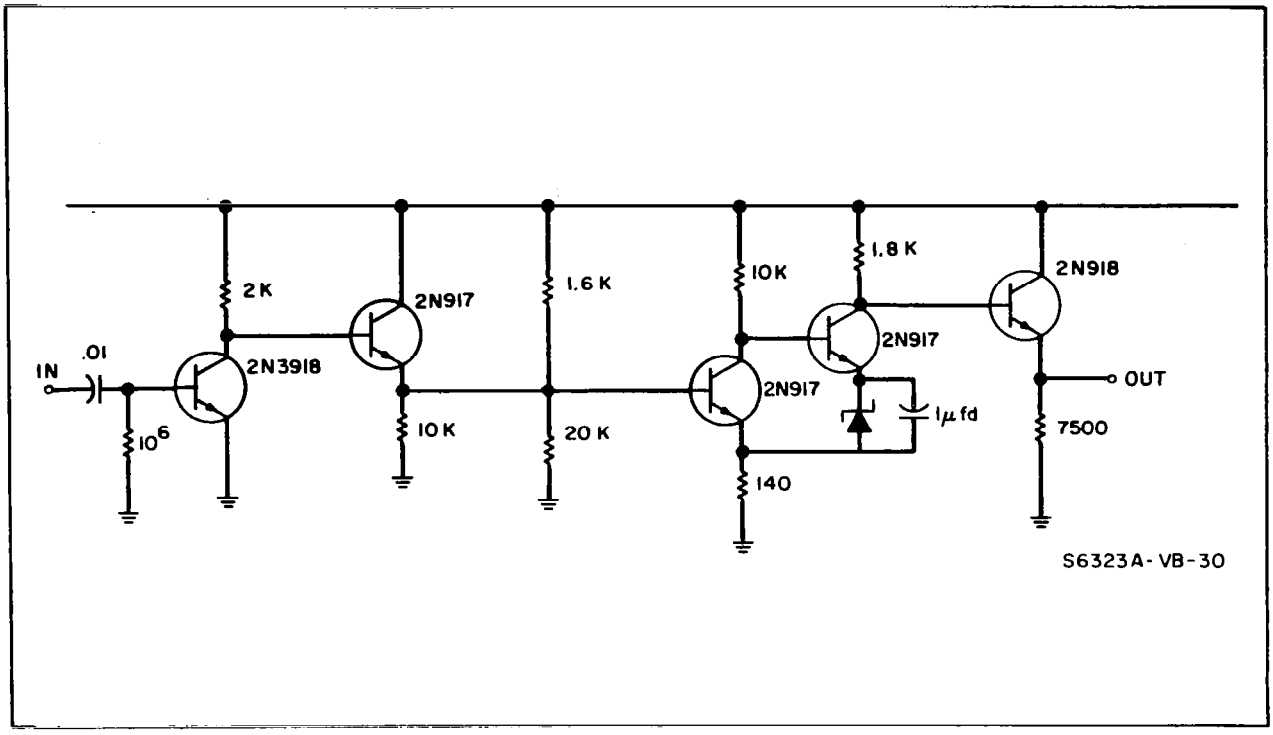


Figure 6-1. Circuit Diagram of the Amplifier

Simplification to

$$A_V \simeq g_m R_L$$

yields an approximation good to within a few percent. The output impedance is given by

$$R_o = \frac{R_L}{1 + R_L g_o}$$

again, as above, the approximation $R_o \cong R_L$ holds very closely. The 2N3819 has a

$$g_m = 3000 \times 10^{-6} \text{ mho}$$
$$g_o \leq 500 \times 10^{-6} \text{ mho}$$
$$R_L = 2 \times 10^3 \text{ ohms}$$

by substitution

$A_V \simeq 6$ for the input stage

The subsequent stage consisting of a 2N917 emitter follower working into a composite load of

$$Z_L = \frac{\frac{1.6k + 20k}{1.6k + 20k} \times 10k}{10k + \frac{1.6 \times 20k}{1.6 + 20k}} = 1.29k$$

This value set was dictated by the attempted simulation of the SA20 amplifier. The basic local feedback amplifier gain is evaluated by making certain simplifying approximations.

The feedback emitter composite resistance can be approximated by

$$R_E = \frac{R_{e_{ext}} (R_{b_{int}} + R_{b_{ext}})}{R_{e_{ext}} R_{e_{in}} + R_{b_{int}} + R_{b_{ext}}}$$

$$= \frac{140 (50 + 25 + 1000)}{140 + 50 + 25 + 100} = 122$$

the voltage gain of the composite stage can be expressed as

$$A_{V_{Total}} = \left(\frac{R_L}{R_{e_{ext}}}\right) \left(\frac{R_E}{R_e + R_{e2}}\right) \frac{R_M}{R_E}$$

$$= \left(\frac{104}{140}\right) \left(\frac{122}{122 + 50}\right) \left(\frac{1.8 \times 10^3}{122}\right) = 800$$

The exact solution of this circuit follows and it can be seen that the result is rather complicated and unwieldy to use. Figure 6-2 shows the equivalent circuit and transistor configuration.

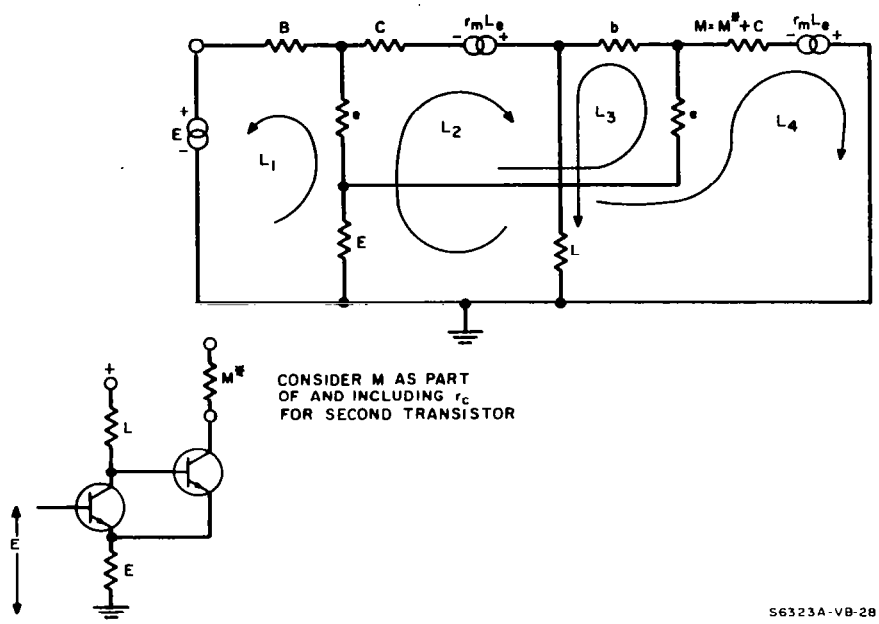


Figure 6-2. Circuit for Analysis of Feedback Pair

Voltage gain of the amplifier is given by the following:

$$
\begin{aligned}
A_V = {} & ME\Big\{ (e+E-r_m)\Big( [E+f-r_m] - [f+b+L+E]\Big) - \Big( [C+L+E+e-r_m]\ [E+f-r_m] - E^2\Big) \\
& + \Big( [C+L+e-r_m]\ [f+b+L+\epsilon] - E^2\Big)\Big\} \Big\{\Big(B+e+E\Big)\ \Big( [C+L+\epsilon+e-r_m]\ [(f+b+L+\epsilon)\ (f+M \\
& +\epsilon-r_m) - (E+f)\ (E+f-r_m)] - [E^2]\ [(f+M+E-r_m) - (E+f-r_m)] + [E^2]\ [(E+f) \\
& - (f+b+L+E)]\Big)\ (-1)\ (e+E-r_m)\ \Big( [E+e]\ [(f+b+L+E)\ (f+M+E-r_m) - (\epsilon+f-r_m)\ (E+f)] \\
& - [E^2]\ [(f+M+E-r_m) - (E+f-r_m)] + [E^2]\ [(E+f) - (f+b+L+\epsilon)] \\
& + (E)\ ([E+e]\ [E]\ [(f+M+E-r_m) - (E+f-r_m)] - [E]\ [(C+L+\epsilon+e-r_m)]\ [(f+M \\
& +E-r_m) - (E+f-r_m)]\Big) - (E)\Big( [E+e]\ [E^2]\ [(E+f) - (f+b+L+\epsilon) - (C+L+\epsilon \\
& +P-r_m)\ (E\ \{E+f\} - \{f+b+L+\epsilon\})]\Big)\Big\}^{-1}
\end{aligned}
$$

## 6.3 POSITION INDEXING CIRCUITS

The monostable multivibrator shown in figure 6-3 is comprised of two 2N917 transistors in the conventional cross-coupled configuration, in which the right side base is returned to B+ through a 120-kohm load and comprises the normally ON side. The coupling and speed-up capacitors are 0.001 μF. The normally OFF base is returned to a -1.5-V bias through 22 k and to the normally ON collector through a paralleled 0.001 μF and 120 kohm resistor. Both transistor collectors have 10-kohm loads. The normally OFF collector load is split, and at the junction of the two 5-kohm resistors, a 1 μF coupling capacitor couples the trigger from the previous stage. The 1-kohm emitter load resistor of the normally OFF side is used as the trigger source. This minimizes loading of critical points in the multivibrator and allows a low impedance drive which reduces any tendency for reversed triggering. The emitter of the normally ON side feeds a complementary transistor emitter follower which has a 4.4-kohm split emitter load. Amplifier triggering is sent to this emitter follower by a 0.001 μF coupling capacitor. The 4.4-kohm resistor is split and goes to the common bus which feeds the counter that is fed in parallel from all the multi-multivibrators. This common line is fed from a split resistor via a 0.001 μF and a 1N3070 diode and a 50-kohm resistor to ground. Waveform improvement may be achieved by insertion of diodes in the appropriate location; however, this was not deemed necessary since satisfactory operation was obtained without them.

Calculations[7] for the stage follow, based on circuits shown in figure 6-4: Let

$V_o$ be the quiescent charge on $C_T$

$V_{CC_1}$ be the collector emitter saturation voltage

$V_{b_2}$ be the instantaneous base emitter voltage

The loop equation may be written as

$$V_{ec}(s) - R_1 I(s) \frac{1}{c_1 s} I(s) - q(0+) - V_{ce}(sat)(S) = 0$$

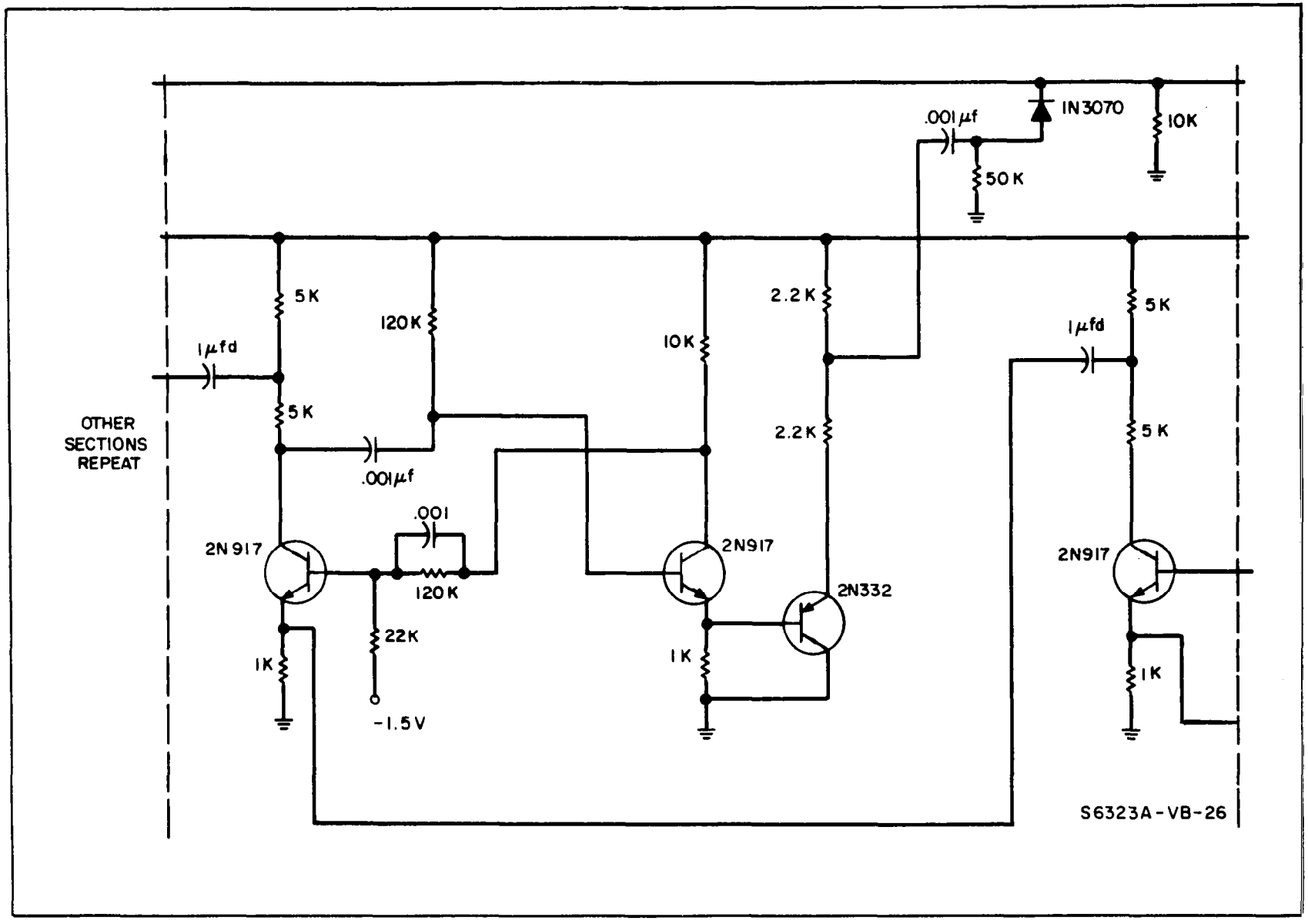


Figure 6-3. Circuit Diagram of Multivibrator

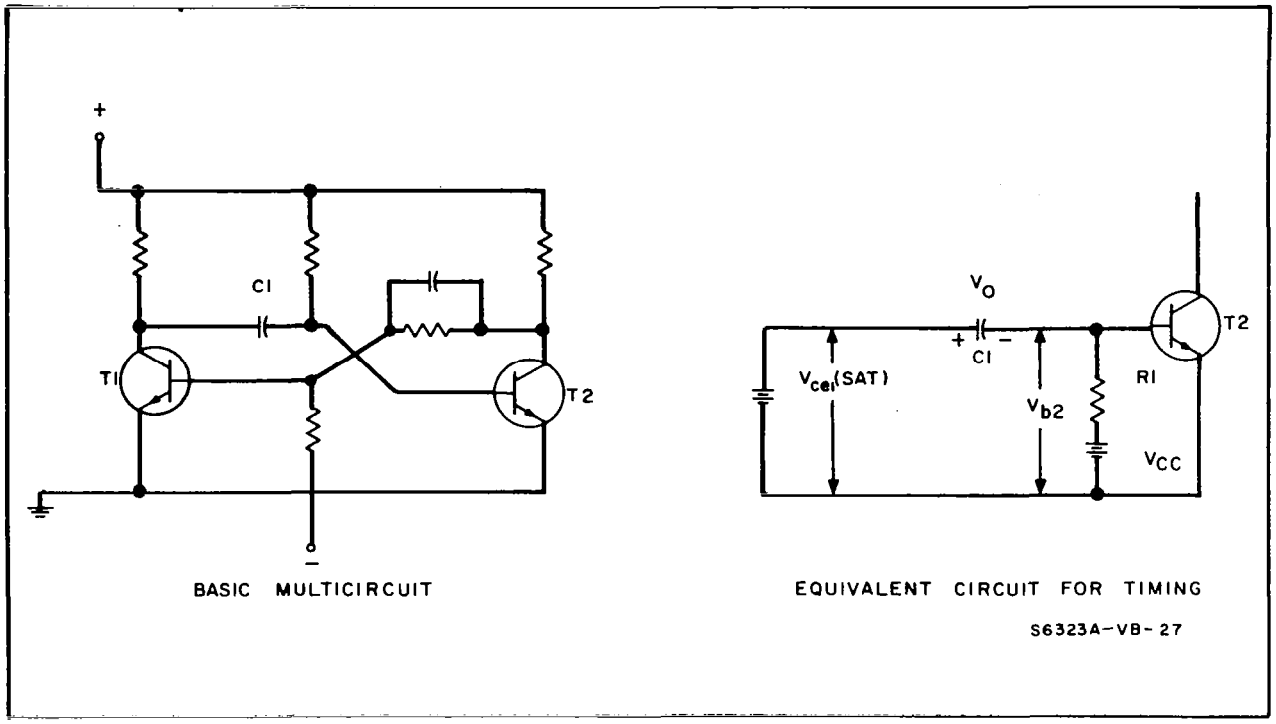


Figure 6-4. Circuits Used for Multivibrator Analysis

This can be rewritten and expressed as

$$I(S) = \frac{V_{cc} + V_o - V_{CP1}(sat)}{R\left(S + \frac{1}{R_1 C_1}\right)}$$

also

$$V_{b2}(S) = V_{cc}(S) - R_1 I(S) = \frac{(V_{cc}/R_1 C_1) - S V_o - V_{Cel}(sat)}{S\left(S + \frac{1}{R_1 C_1}\right)}$$

rewritten as

$$V_{b2}(S) = K\ A/S + B/S + \frac{1}{\tau}$$

where

$$R_1 C_1 = \tau$$

and

$$V_o - V_{Cel}(sat) = K$$

Solving the above for the pulse width $T_p$

$$T_p = \tau \log_\epsilon \frac{K + V_{cc}}{V_{cc} - V_{bec}}$$

or

$$T_p = R_1 C_1 \log \frac{V_{ec} + E - V_{be3} - V_{be2} - V_{cel}(sat)}{V_{cc} - V_{be2}}$$

Simplify to

$$T_p = R_1 C_1 \left(\frac{E}{V_{cc}}\right)$$

This is linear with E and can be used to set the desired width of the output pulse.

6.4 STORAGE AND PROCESSING EQUIPMENT

The following equipment such as the counter and storage have not been mechanized, but will be considered in the light of currently mechanized equipment of a similar nature.

Since the number of amplifiers and lines is an integral power of two, the binary system is desirable, if not almost mandatory. For maximum utilization, a serial binary ripple counter may be used. The multivibrator chain consists of a sequence of 64 monostable multivibrators with conventional cross coupling. Each of these is triggered by a pulse amplifier independent of all of the others which are fed from one line of the matrix. When the multivibrator is triggered, it triggers the subsequent multivibrators which are in series with it. Each of these will then yield a single pulse delayed in time from the previous, and the total pulse count corresponds to the numerical position of the line of the matrix which is initially excited. These pulses are put into a counter, and the location corresponding to the count is then made available in the memory. The number of times that a particular line number is excited is stored in the memory and retained as a measure of the intensity of

illumination at the particular intersection on the wafer. While signal processing is taking place, the detection system will not be available for new inputs. This downtime should be a small portion of the total time, and in addition, a statistical evaluation may be made to account for the missed signals.

In addition, the rate at which the information is being fed into the system is low and therefore there should be a very small loss of information. The number of stages "n" will be given by the maximum number of lines desired expressed as $2^n$; i.e., 64 lines will have n = 6. This binary number can be parallel-gated from the counter into the appropriate memory location which is an accumulator of the requisite bit capacity. The capacity will have been predetermined by a previous mission analysis. A count content of $2^{13}$ should be ample; this would call for 13 stages of accumulator. The accumulator is the ideal element for this purpose, since it does both adding the unity and storing the total.

In brief, the photon impinging upon the sensitive surface of the silicon wafer will excite one each of the x and y coordinate lines. These will excite the serial x and y multivibrator chains, and while pulses are on the bus to the counter, an inhibit circuit will prevent transfer of any signal to the accumulator bank. Simple control circuitry can be included to prevent synchronizing conflicts. Only when the lines to the counters are cleared and the counters have a content will the proper accumulator bank location be activated, a single pulse fed to the accumulator, and the counters cleared and the multivibrators reactivated. This will prevent erroneous counts, pile-ups, and other undesired signals from entering the counter and accumulator bank. For readout of the contents of each accumulator, the readout equipment will feed pulses to each accumulator bank location, and when the accumulator content has reset to zero, the final overflow pulse will be routed out to a common bus line to stop the filling of the particular location and move to the next. The filling of the location also resets it to zero. The number of pulses fed

in also goes to a tape recorder or transmitter and appears as the complement of the number stored in the accumulator to the particular counter modulo.

## 6.5 OFF-THE-SHELF DEVICE PERFORMANCE

Several commercially procured items were tried, and the results were unsatisfactory. The initial specifications of the SA20 Sylvania integrated circuit amplifier were very interesting and apparently suitable for use as the amplifier. However, when these elements were connected in the configuration to be used, it was discovered that they were unstable and oscillated at both 20 and 40 MHz under broadband termination conditions. Since it is necessary to use this amplifier as a broadband amplifier, it was not possible to apply it in the form that it was delivered. As a result, experiments were carried out to see what modifications would be necessary to stabilize this element.

It was discovered after a period of time that the addition of pole shifting capacitance would make it stable; however, the bandwidth was greatly reduced and was insufficient as a result. This SA20 device consisted of a grounded emitter stage with feedback to the emitter from an output emitter follower which had an amplification stage inserted in between. It was found that the gain of the system was satisfactory; however, the oscillation could not be tolerated. This amplifier was breadboarded with separate components in a similar circuit configuration and tested. The tests showed that this configuration was marginally useful even in this form, and as a result, it was necessary to diverge rather widely from the structure exemplified in the SA20. This indicated that the conventional off-the-shelf microcircuit amplifiers were not usable at this time for the equipment that was under construction. Since the varying B+ shifted the frequency, a series of networks to stablilize the amplifier was tried. Those which did stabilize the SA20 resulted in a bandwidth of under 1 MHz. As a result, no more attempts to use the SA20 were made. However, since the circuit configuration seemed good, an attempt to establish the particular reason for the instability was carried out.

The SA20 was simulated with separate components, whose performance was equivalent as far as possible to those elements in the SA20. This circuit showed good performance and was stable. This indicated, as a first possibility, that the interelement capacitance was the source of trouble. Small capacitors composed of bits of insulated wire were placed in various locations in the breadboarded amplifier, and several configurations were observed to behave as the original SA20. It was not possible under the limited time and effort that could be devoted to this problem to definitely establish the particular source of trouble, but microscopic observation of the SA20 indicated close physical proximity of an input resistor and output load resistor.

A similar problem was discovered with the Sylvania logic block, the SUHL62. This particular item appeared overly complex for the purpose for which it was to be applied; however, it was the only commercial one that appeared usable. When the device was put into use, it was found that the triggering sensitivity was extremely poor, and it was necessary to use an external set of components to set the timing. As a result, it was decided to use completely external components for this purpose, and a conventional two transistor monostable multivibrator was developed with successful triggering and satisfactory sensitivity.

## 6.6 TEST BED PERFORMANCE

A demonstration unit consisting of 3 multivibrators and amplifiers to drive them were constructed, and the various triggering operation modes were demonstrated in a successful manner. The structure performed as predicted with one, two, and three pulses resulting from the multivibrators when the appropriate lines 1, 2, or 3 were triggered. It was found necessary in the multivibrator circuit to introduce additional decoupling diodes and to take the signal from the least sensitive loading points. The two emitters were provided with 1000-ohm load resistors, and the signal was taken from these points for triggering subsequent amplifiers and for driving the common bus line to the counter. A standard external counter was used to demonstrate the counting

ability of the system. An oscilloscope was also used to view the presence or absence of these pulses upon triggering. While the storage system for equipment was not breadboarded, a conceptional design for a portion of the equipment was established. In this portion of the system, it was necessary to develop a method of identifying the coordinates of the location where the photoelectron impinged for determining the number of times a photoelectron impinged on the tube in a period of time.

## 6.7 ANTICIPATED DESIGN PROBLEMS

Various problems present themselves in a study of configuring this equipment in the form of microelectronic circuits. There are also a number of inherent problems which are independent of the fact that microelectronic circuit configurations are required. One serious problem is the coupling between the large number of broadband amplifiers which are confined to a small volume and which have a significant interelement coupling capacitance. When it is considered that approximately 128 broadband amplifiers are used, all of whose inputs have approximately a 1/2 inch of wire overlapped, the severity of the coupling between the input stages becomes apparent. Not only would crosstalk between the input stages of the various amplifiers be a serious problem, but also, there could possibly be enough capacitance coupling between the stages to cause a serious oscillation problem and the isolation and stabilization of these amplifiers could be a significant difficulty.

Shielding of noise and triggering from the subsequent multivibrator stages will cause difficulty with the higher level stages. The decoupling of the various high signal stages will probably cause serious difficulty with the grounding situation; because, the intercoupling of ground signals in the ground leads will be very difficult to deal with. Amplifier input capacity, due to the physical configuration, will probably be relatively small. It may even be small enough so that it will not be necessary to have a negative capacitance feedback system which is usually used in the amplifiers introduced into the system. However, temperature stabilization and environment conditions under which these elements will be used can cause serious problems. Since transistors are

sensitive to temperature, the gain and stability of the various stages will have to be carefully examined in the final detailed design.

To prevent loss of performance, consideration of the memory design indicates that a special purpose memory is probably most suited for this equipment. A conventional random access memory is probably more complex than is necessary, and a counting type system is probably best for this system. A set of accumulators, each one of which will correspond to the intersection point on the diode matrix for detection, is probably the simplest and most desirable configuration. In this mechanization, each pulse which impinges at a given point on the matrix will be recorded into a counter which is matched to that intersection point. The use of the accumulator simplifies the circuitry greatly and makes a redundant system possible where the failure of some portion of the equipment will not affect any other portions of the equipment. The capacity of such an accumulator can be made quite large and would give the maximum economy in the use of the digital system. Thermal stability of the transistor elements in the amplifiers and multivibrators as well as in the memory will prove to be a serious problem over wide temperatures. Therefore, careful design of the equipment in the form of separate components and evaluation of the most sensitive elements will be necessary as a first step.

Subsequent development of these elements in microcircuit form will require the inclusion of positive and negative temperature coefficient elements to compensate for wide temperature changes. Transistors usually exhibit a doubling of leakage current for every 8°C temperature rise. Therefore, a suitable network will have to be included to prevent or to balance this leakage. There are a number of limitations on the values available for use in microcircuit elements. As a result, some of the equipment will no doubt be built in hybrid form. This is where coupling capacitors and other elements which are not available in the microcircuit values are needed.

# 7. SUMMARY AND CONCLUSIONS

During the course of this effort, several types of surface barrier diodes were fabricated. First, a diode with a single contact on its back was made, then a unit with two contacts on its back was prepared. The next detector fabricated had on its back a 10 by 10 grid, and this was followed by a unit having 32 lines running in each of the two perpendicular directions on its insensitive side. Masks were prepared and it was demonstrated that a 64- by 64-line unit can also be made with this technique on a 1/2- by 1/2-inch piece of silicon.

In addition, a detector was enclosed in a vacuum envelope together with an S-11 photocathode demonstrating compatibility of the semiconductor element with a cesium antimony photocathode. Also, a discrete element transistorized circuit was constructed consisting of a preamplifier, amplifier, and scaler showing a detection arrangement whereby the number of output counts indicates the channel number activated by the incoming particle.

The results and potential of this study compare favorably with those of electronography concerning sensitivity and speed. Resolution of the electronographic approach can also be matched by the semiconductor approach by using a suitable and possibly interchangeable optical arrangement in front of the hybrid tube.

## 7.1 DETAILED DESCRIPTION OF RESULTS

During the first phase of the contract, several single contact detectors were made. These were tested with the tin ($Sn^{113-119}$) radioactive source at energies less than 50 keV and showed a pattern illustrated on figure 7-1. It is believed that the first peak was due to an electron emission of the $Sn^{113-119}$ source at about 37 keV, and that the second lower and wider hill is due to the electron emission intensity kink and tail following this kink at about 40 keV (figure 7-2). The large half width of the first peak is due to the lack of

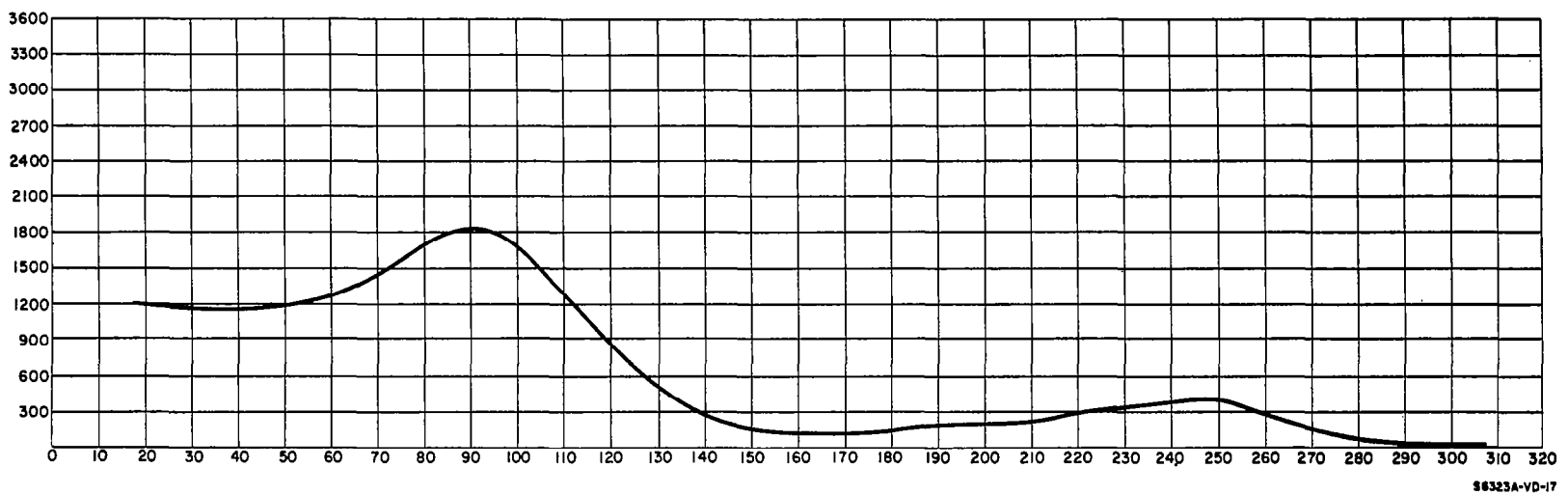


Figure 7-1. Count vs Energy Graph for a Surface Contact on Its Insensitive Side

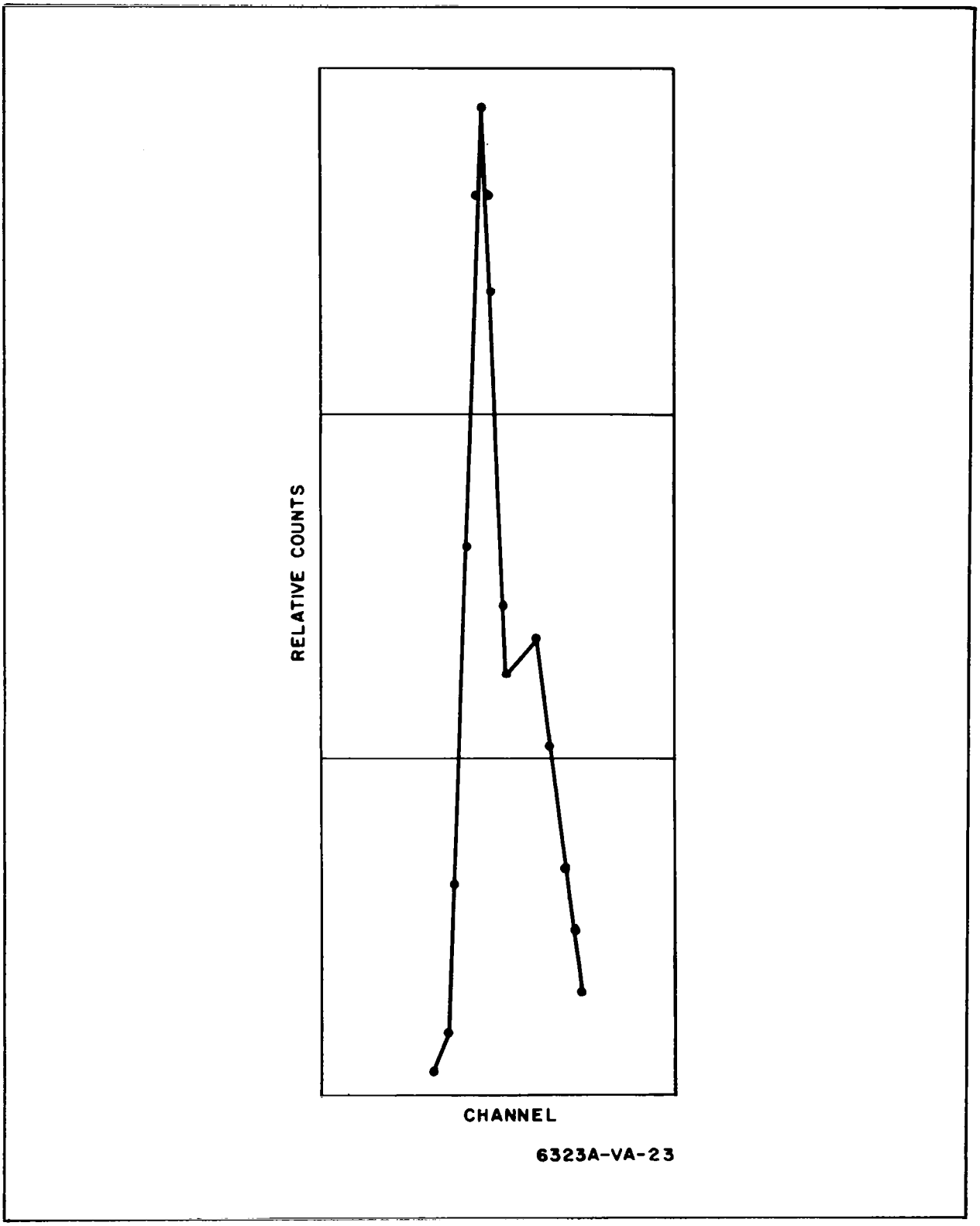


Figure 7-2. Enlarged First Portion of the Electron Emission vs Energy Curve for $Sn^{113-119}$

ability of the single channel pulse height analyzer to define a narrow window. The weakness of the source to give a sufficient and reproducible count pattern within a reasonable time also contributed to the widening of this peak.

During the following contractual period, several detectors were fabricated with two round contacts on their backs. These contacts were situated about 1/2 inch from each other on the reverse side of the unit. When tested, these samples were completely depleted and thus they were isolated from each other showing the characteristics of essentially two units on two chips.

The units with ten perpendicular lines each way on their reverse sides were tested both with the radioactive source and with the electron gun setup. When using the radioactive source to test the unit, the detector was plugged into the testing arm (figure 4-8) but was not inserted into the electron gun setup. With this arrangement, only a very few counts over the background noise count could be detected. This was due to the low activity of the source and due to the blocking action of a thin plate with an approximate 1/8-inch hole in it. This plate was used in an attempt to select one single channel and activate it while leaving the adjacent channels inactive. The results of testing using the radioactive source and the plate were thus quite inconclusive. This again was due to the low activity of the source, due to the substantial noise of some of the channels, due to the lack of electrical shielding ability resulting in pickup noise, and due to the lack of ability to orient the shielding plate with respect to the testing arm and with respect to the unit to be tested. Also, since the energy of these electrons is quite low, a substantial number of them were absorbed by the air, by the thin p-type inversion layer of the detector itself, and by the thin plastic coating, serving to prevent flaking of the radioactive material off the mounting substrate.

As a next step, units with ten perpendicular lines each way on their insensitive side were tested with the electron gun setup. When tested, only 5 lines out of the 20 possible lines exhibited low enough noise so that changes could be observed on them. The rest of the 15 lines had a noise count of 2000

counts per second or higher. Some of the less noisy channels counted as low as 40 counts per second without the electron beam activating the line. This count increased to 600 or over, depending on the intensity of the beam when it was activating the channel. All low noise channels showed the same increase in the number of counts indicating that they were equally sensitive. (That is, a channel with a background noise of 40 increased the count rate to $640 \pm \sqrt{640}$ when the beam activated it, while a channel with a background count of 800 increased its counts to $1400 \pm \sqrt{1400}$ when it was in the line of the beam.)

Interaction between channels did not seem to exist, since when the beam was moved only slightly off a channel the scaler did return to indicate the background count observed before activation. Also, while the beam was on-channel displaying activation on that channel, the line adjacent to the activated one did not show an appreciable increase in counting rate. This confirmed the conclusion that when the unit was back-biased by about 50 volts the individual channels were completely isolated. This was expected, since 50 volts reverse bias completely depletes the 0.006-inch width of the 2000 ohm-cm material converting it essentially to an insulator. It then appears as if the adjacent lines were deposited onto an insulating substrate.

Concluding, insulation between lines should be sufficient even if the slice is not completely depleted, since the resistance along a single line is less than 50 ohms in all cases and the resistance between the lines is always larger than 1000 ohms. This ratio even without depletion is at least 200 to 1, and signals from the line can be differentiated from signals coming from an adjacent strip.

Units having 32 perpendicular lines in each direction on their insensitive side were also checked using the electron beam source. One of these finished units is shown in figure 7-3. It was found that only about 10 percent of the lines had a low enough noise count to distinguish whether or not the electron beam was on or off. However, some of the low-noise lines were completely noiseless; that is, their background count was exactly zero at a pulse height

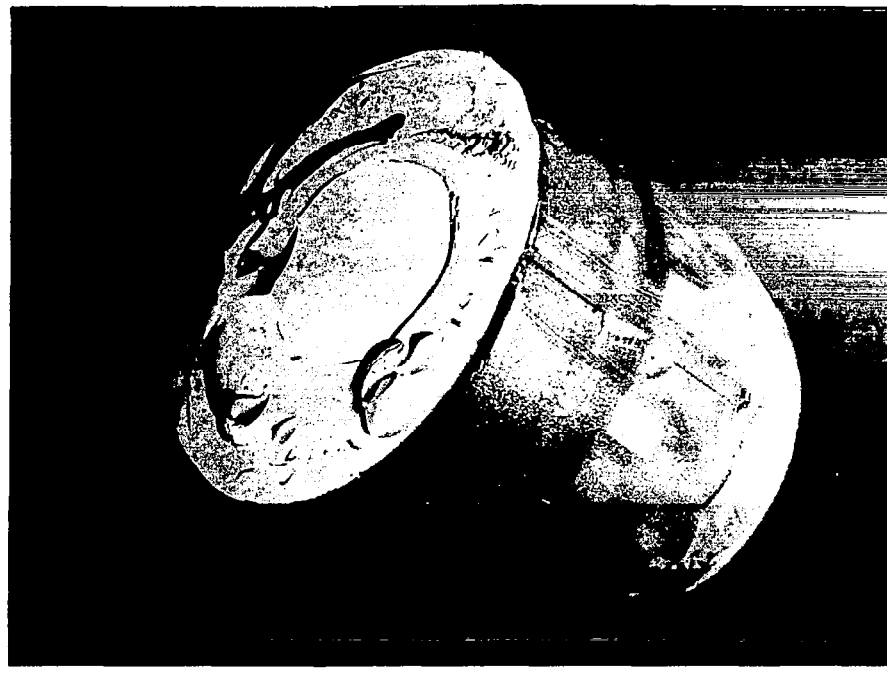

Figure 7-3. The Completed Low-Energy Electron Position Detector

analyzer window setting of about 35 keV. When activated, these units were again at least as sensitive as some of the more noisy ones, indicating that noiseless sensitive channels can be made though they are somewhat difficult to prepare. Here again, it was demonstrated that crosstalk between activated and inactivated channels was nonexistent if a sufficient back bias was applied. In this case, the reverse bias was about 50 volts, but it occasionally decreased to 35 volts, depending on the exact thickness and resistivity of the wafers.

Testing of hybrid tubes (containing the photocathode and the semiconductor element) involved checking the current day after day following the completion of the tube. A Spectroline Model SL-3660 longwave black light lamp was used as the ultraviolet source and it was positioned about 18 inches in front of the tube. The curve of activity versus time elapsed is shown in figure 7-4. It is evident that during the past month the activity of the tube decreased to about 30 percent of the original activity. This is probably due to contamination of the photocathode, since the glassware was only baked out at 350°C instead of

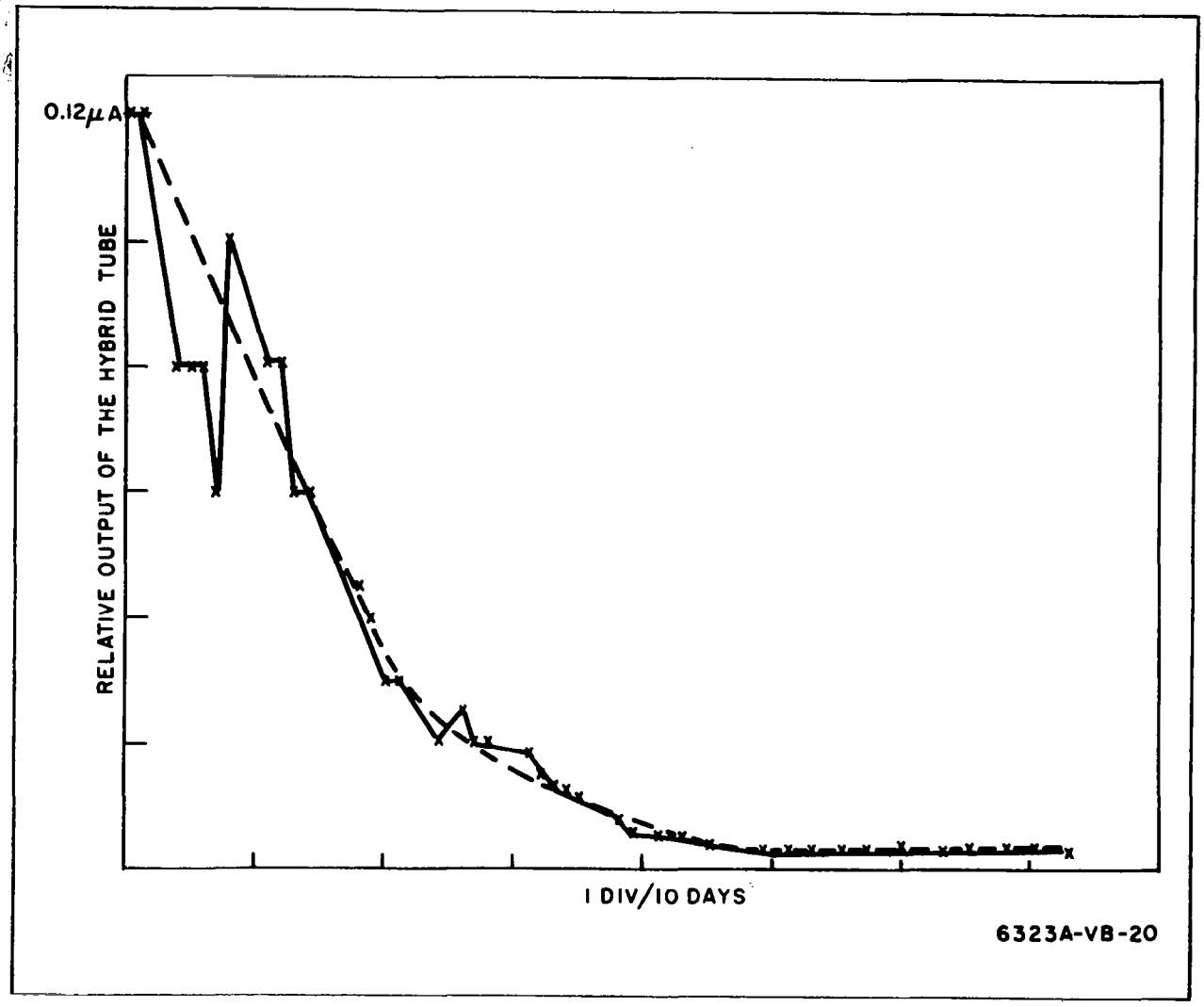


Figure 7-4. Ultraviolet Response of the Hybrid Tube

the required 450°C. It was not possible with the present arrangement to heat the glassware to 450°C and keep the detector temperature below 150°C. The gradual loss of the current response was also due to the fact that hydrocarbons from the epoxy probably leaked to the surface slowly through the torr-seal. In addition, the gold plated surface of the silicon and the flange containing it were only baked out at 100°C, and they probably contained some water vapor and other surface contaminants, which eventually got onto the photocathode and poisoned it.

When testing the transistorized electronic amplifying and designating system, it was found that it was working satisfactorily after correcting some of the initial difficulties. Pulses in the 50-microvolt range, the size expected from the detectors, were fed into the input of the preamplifier. These pulses were then amplified by the preamplifier and amplifier to obtain a gain of several hundred thousand. This increased the pulse size to approximately 1 volt (the pulse size for which the self-tripping multivibrators were designed). When a pulse having this approximate size was fed into the first of the three multivibrators from the first channel, it tripped the first, second, and third multivibrators in succession and indicated a count of 3. If a pulse from channel 2 or 3 entered the second or third multivibrator, the system delivered a count of 2 or 1 respectively. Thus, the activated channel was designated by the number of counts obtained from the self-tripping multivibrators.

After several adjustments and alterations, this electronic arrangement was made to work satisfactorily, and all intermediate waveforms were well defined and clearly conformed to the design principles.

## 7.2 COMPARISON OF THE HYBRID TUBE DETECTOR WITH THE ELECTRONOGRAPHIC SYSTEM

Before attempting to make a comparison between the Hybrid and the Electronographic Tubes the meaning of the term electronography (or photoelectronography) should be made clear. Electronography is concerned with amplification of the effects of photons in a photographic emulsion. For this purpose, a tube is prepared with a sensitive photocathode on its front part to convert the photons to electrons with a reasonable efficiency (possibly 25 percent). These electrons are then focused and accelerated toward a photographic emulsion, and they imbed themselves into this material. Also, a gain can be obtained exposing the emulsion to energetic electrons instead of photons. The magnitude of this gain is the topic of considerable discussion and ranges from a factor of 10 to possibly 40, depending on the density of the photoelectrons per unit area of the emulsion, the grain size, type of the emulsion, the exposure time, and other parameters concerning the development of the film. These development

parameters include the time and temperature of development and the types and concentrations of solutions used. Concerning photoelectronography, another parameter of importance is the preparation of the tube. The problems of preparation are substantial, since the emulsion is usually a high vapor pressure material and these vapors, as in the case with the hybrid tube, do effect the sensitive photocathode and cause deterioration.

In addition, the operation of this (Lallemand's) tube in an atmospheric environment is fairly complex. Photocathodes are prepared in small evacuated glass capsules and loaded into the system. The system containing the electron optics and the film container is then evacuated. Just prior to the exposure, the glass capsule is broken inside the system with a magnetically operated slug enabling the photoelectrons to leave this enclosure. At the same time, a film is put into the path of the accelerated electrons. Using this method, the photocathode is not degraded substantially by the "dirty" vacuum, since it is exposed to it for only a short time during the exposure of the film.

The electrons emitted by the photocathode are accelerated by the electron optics and hit the film blackening several grains of it. After the picture is completed, the system is disassembled, cleaned, outbaked, and a new capsule containing another photocathode is loaded into it. It is then sealed off again and is ready for another exposure.

In space, some of the difficulties of this camera would be alleviated and some of them increased. Gaseous contamination is, of course, no difficulty. However, the film would have to be developed in space, and it has to be scanned either optically or electronically before the information can be telemetered back. To develop the picture in space and to maintain some of the stringent conditions of development for this type of a film are hard enough; however, to scan the picture (either optically or electronically) and to maintain the inherent film resolution are almost impossible. This follows from the fact that the smallest diameter scanning beam available is many times larger then the resolution of the film. This difficulty degrades resolution, one of the inherent advantages

of this method, and makes the realization of this approach somewhat less than feasible.

Linearity also seems to be a problem, since when considering this approach some of the additional factors such as quantum efficiency, the product of quantum efficiency and exposure, and the speed gain are highly nonlinear as illustrated in figures 7-5, 7-6, and 7-7. Finally, it should be noted that the sensitivity of this device is not over 40 times of that obtained using nonvacuum photographic methods, but it is closer to 10 times that of the standard photographic sensitivity. It seems that the sensitivity of the ordinary photographic methods was under estimated, when making this comparison.

An inherent advantage of photoelectronography is resolution, since by using a photographic emulsion 40 or more line pairs per 0.001 inch can be obtained. This feature of photoelectronography is of course unequaled by the hybrid-tube approach; however, as pointed out above, this advantage of the electronographic approach is partially negated when data has to be recovered for telemetry by scanning the developed film. Also connected with the use of film is the fact that there is a limited amount of it available in the craft, and once it is used up, the apparatus will become useless. On the other hand, the hybrid-tube approach does not require film, and its picture taking activity is limited only by the available power. It is possible that this type of device could send back informative photon counting statistics for several years.

In summary, it is evident that, concerning sensitivity and speed, photoelectronography is far behind the semiconductor approach. Also when considering readout, it is apparent that the photoelectronographic approach requires external scanning, while scanning is an inherent part of the hybrid-tube method and is provided automatically.

Essentially, in the case of the hybrid tube, the scanning is equivalent to counting individual photons by sensing single electrons which are in a one-to-one optical correspondence with the ultraviolet quanta originating them. It is this counting of the single photons and the accumulation of individual quantum statistics that

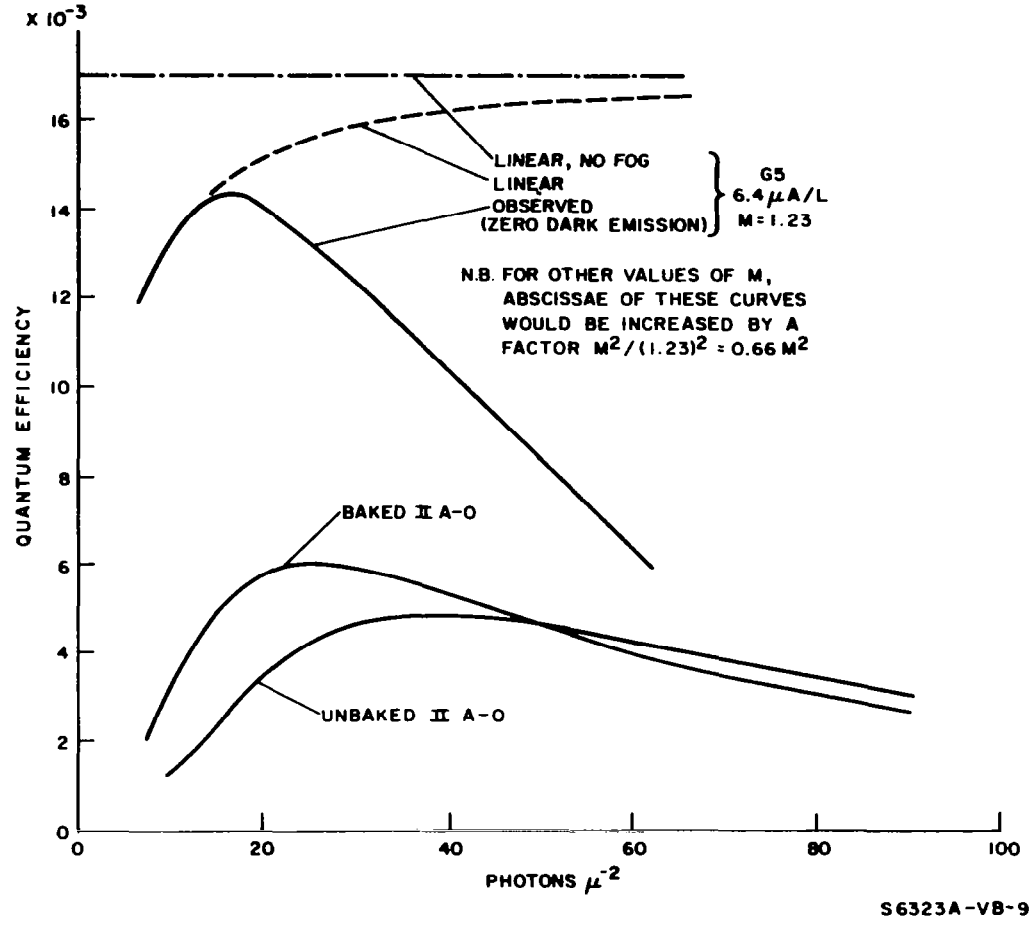


Figure 7-5. Quantum Efficiency vs Photons per Micrometer Square

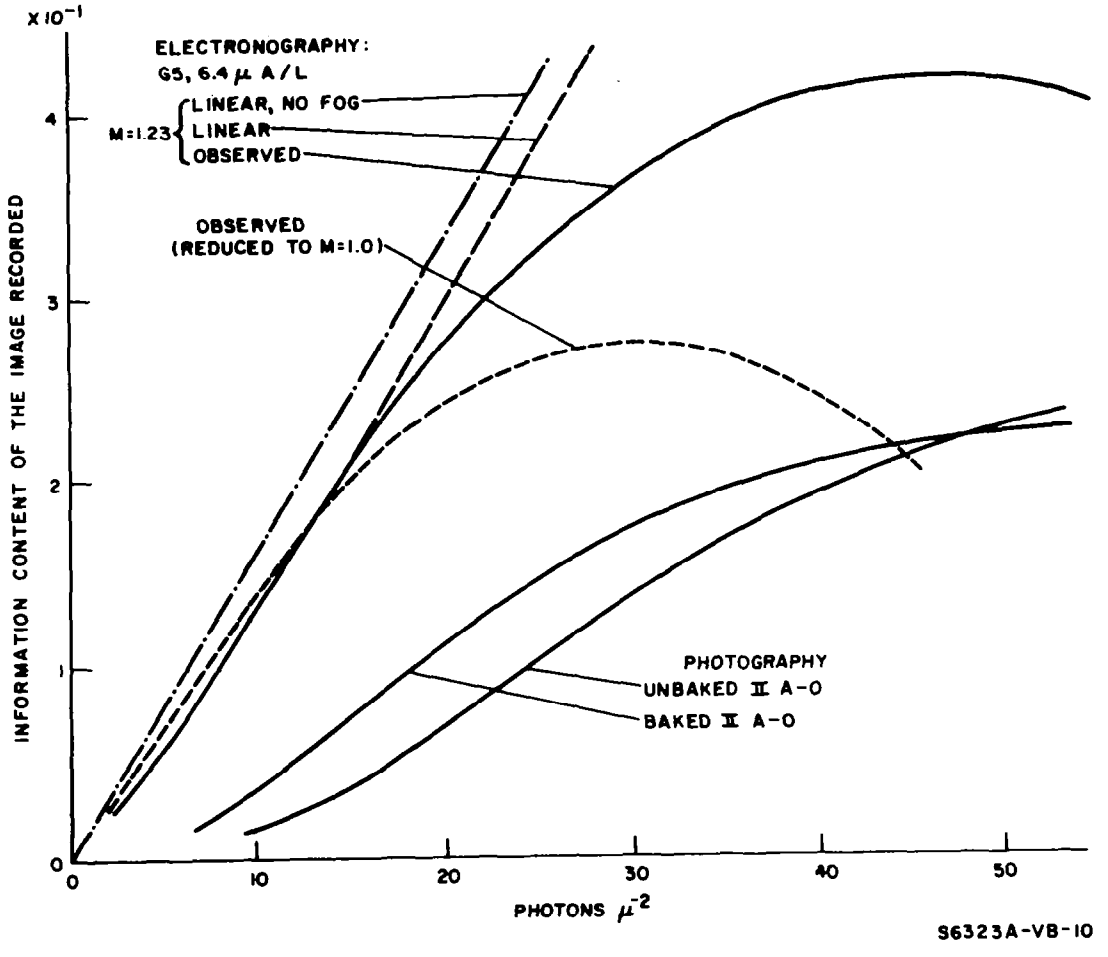


Figure 7-6. Information Content of the Image Recorded vs Photons per Micrometer Square

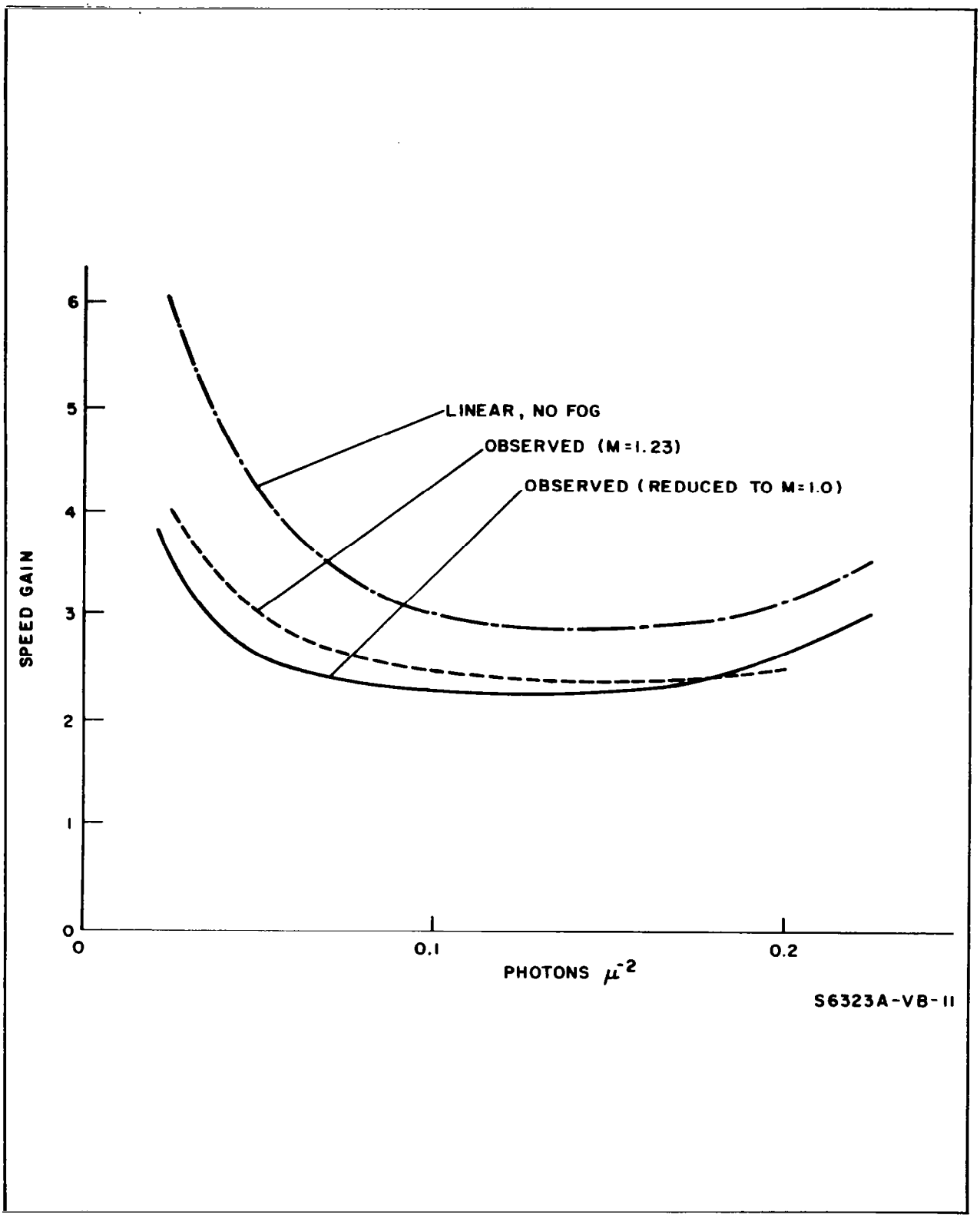


Figure 7-7. Speed Gain vs Photons per Micrometer Square

makes the hybrid tube especially attractive for exploring extremely low intensity ultraviolet sources. In this case, these sources are the presently unknown (dark) domains of space, which cannot be reached by any other means.

In addition from the hardware point the fabrication difficulties connected with the electronographic tube and reproducibility of this method seem to require a process control that is more sophisticated than that required for preparation of the semiconductor tube. It seems that the only advantage electronography offers is in the resolution, but even this advantage is negated by the necessity of scanning. When using the hybrid tube, additional resolution can always be obtained by the use of an appropriate and possibly interchangeable optical system in front of the photocathode.

It seems then that, by proper preparation, the performance characteristics of the semiconductor approach surpasses electronography in all aspects. In addition, the handling and economy considerations also favor the hybrid-tube system over the electronographic approach.

## 8. REFERENCES


1. Werthier, C. K. "Semiconductor Nuclear Particle Detectors," National Academy of Science, Washington, Publication 871, p. 128.
2. Dearnaley and A. B. Whitehead, A. E. R. E. Rep. R-3666.
3. Klingensmith, R. W., "Solid State Radiation Detectors," Institute of Radio Engineers, New York, N. S. 8 No. 1 (January 1961) p. 112.
4. Curtis, O. L., et al., J. A. P. 28 (1957) p. 1161.
5. Klema, E. D., Nuclear Instruments and Methods, Vol. 26 (1964) p. 205.
6. Klema, E. D., Proceedings of 11th Nuclear Science Symposium, Vol. NS12 (1965) p. 288.
7. Wong, H. R., Electronic Engineer, (1966), p. 950.
8. Baum, W. A., Science, Vol. 154 No. 3745 (1966) p. 112.

*"The aeronautical and space activities of the United States shall be conducted so as to contribute . . . to the expansion of human knowledge of phenomena in the atmosphere and space. The Administration shall provide for the widest practicable and appropriate dissemination of information concerning its activities and the results thereof."*

—NATIONAL AERONAUTICS AND SPACE ACT OF 1958

# NASA SCIENTIFIC AND TECHNICAL PUBLICATIONS

TECHNICAL REPORTS: Scientific and technical information considered important, complete, and a lasting contribution to existing knowledge.

TECHNICAL NOTES: Information less broad in scope but nevertheless of importance as a contribution to existing knowledge.

TECHNICAL MEMORANDUMS: Information receiving limited distribution because of preliminary data, security classification, or other reasons.

CONTRACTOR REPORTS: Scientific and technical information generated under a NASA contract or grant and considered an important contribution to existing knowledge.

TECHNICAL TRANSLATIONS: Information published in a foreign language considered to merit NASA distribution in English.

SPECIAL PUBLICATIONS: Information derived from or of value to NASA activities. Publications include conference proceedings, monographs, data compilations, handbooks, sourcebooks, and special bibliographies.

TECHNOLOGY UTILIZATION PUBLICATIONS: Information on technology used by NASA that may be of particular interest in commercial and other non-aerospace applications. Publications include Tech Briefs, Technology Utilization Reports and Notes, and Technology Surveys.

*Details on the availability of these publications may be obtained from:*

SCIENTIFIC AND TECHNICAL INFORMATION DIVISION

NATIONAL AERONAUTICS AND SPACE ADMINISTRATION

Washington, D.C. 20546